INTERACTION BETWEEN RIVER MORPHOLOGY AND INTRA-GRAVEL FLOW PATHS WITHIN THE HYPORHEIC ZONE

A Dissertation
Presented in Partial Fulfillment of the Requirements for the
Degree of Doctor of Philosophy
with a
Major in Civil Engineering
in the
Collage of Graduate Studies
University of Idaho

by
Daniele Tonina

September 2005

Major Professor: John M. Buffington, Ph.D.

AUTHORIZATION TO SUBMIT

DISSERTATION

This dissertation of Daniele Tonina, submitted for the degree of Doctor of Philosophy (Ph.D.) with a major in Civil Engineering and titled "Interaction between river morphology and intra-gravel flow paths within the hyporheic zone," has been reviewed in final form. Permission, as indicated by the signatures and dates given below, is now granted to submit final copies to the College of Graduate Studies for approval.

Major Professor _____ Date _____
John M. Buffington

Committee Members _____ Date _____
Alberto Bellin

_____ Date _____
Peter Goodwin

_____ Date _____
Klaus Jorde

Department Administrator _____ Date _____
Sunil Sharma

College of Engineering Dean _____ Date _____
Charles L. Peterson

Final Approval and Acceptance by the College of Graduate Studies

_____ Date _____
Margrit von Braun

ABSTRACT

The hyporheic zone is a saturated band of sediment that surrounds the river and forms a linkage between the river and the aquifer. It is a rich ecotone where benthic, hyporheic, and groundwater species temporarily or permanently reside. The exchange between surface and subsurface water, known as hyporheic exchange, is a crucial mechanism for delivering nutrients, oxygen and other solutes to the sediment, and for washing away waste products.

Hyporheic exchange has been extensively studied in sand-bed channels having two-dimensional dune-ripple morphologies, but few studies have examined hyporheic flow in pool-riffle channels, which are characterized by coarser sediment, steeper slopes, and three-dimensional bed forms that strongly influence surface flow. These channels are particularly important habitat for salmonids, many of which are currently at risk worldwide, and which incubate their offspring within the hyporheic zone.

Hyporheic exchange in gravel pool-riffle channels was assessed with a pumping transport model that accounts for spatial variations in total near-bed pressure resulting from flow over three-dimensional bedforms. A series of laboratory experiments were conducted to test the model across a range of discharges and bedform amplitudes. Results show good agreement between predicted and observed hyporheic exchange, indicating that the major mechanism for exchange in pool-riffle channels is bedform-induced advection.

The model was used to evaluate the relative importance of some key factors in hyporheic flow: river discharge, depth of alluvium, bedform amplitude, hydraulic conductivity of the sediment and mean groundwater flow velocity. Results demonstrate that sediment permeability, bedform amplitude, and flow regime are important factors, while depth of alluvium is significant when it is less than the hyporheic depth. Moreover, mean groundwater flow velocities higher than 10^{-4} $m \cdot s^{-1}$ reduce both hyporheic volume and hyporheic residence time.

Finally, the model was used to examine the effect of redd formation on hyporheic processes. When salmon build their redds (nests) they alter sediment size and conductivity, and create macro-scale bed topography. Simulations comparing hyporheic

exchange in a pool-riffle channel with and without redds show that redd formation changes not only the river hydraulics, but also the local areas of upwelling and downwelling, enhancing the flow velocity and dissolved oxygen content through the egg pocket and, thereby, potentially enhancing the survival of salmonids incubating within the streambed gravels.

ACKNOWLEDGEMENT

I would like to first acknowledge the help of the people who supported me during this research. I would like to thank my supervisor John M. Buffington for making this research possible and for his advice. Without his passion in this field and his help in supporting the project, this work could not have been possible.

I would like to mention my committee members, Alberto Bellin, Peter Godwin and Klaus Jorde. Special thanks go to Alberto Bellin who inspired me to follow this career and advised me in seizing the opportunity to study at the University of Idaho.

It was a pleasure to work with the staff of the Saint Anthony Fall Laboratory. I would like to mention Jeff Marr for coordinating my stay and Sara R. Johnson for helping with the flume experiments and enjoying the laboratory; also, Chris Ellis and Brett Otteson for their technical support.

I would like to mention the grants, which funded the research. This work was supported in part by the STC Program of the National Science Foundation under Agreement Number EAR-0120914, by the USDA Forest Service Yankee Fork Ranger District (00-PA-11041303-071), by the US Department of Education Fund for the Improvement of Postsecondary Education (Award Number P116Z010107), and by the USDA Forest Service Rocky Mountain Research Station (03-JV-11222014-060).

DEDICATION

Ai miei Genitori, mio Nonno Renato e Zia Maria

Table of Contents

List of Tables

List of Figures

Chapter 1.

HYPORHEIC FLOW

Rivers are dynamic systems that are connected to the groundwater and surrounding riparian areas through the hyporheic zone, where river water percolates into the sediment in near-bed high-pressure areas, mixes with groundwater and re-emerges into the river in near-bed low-pressure areas. Hyporheic flow is driven by pressure variations along the streambed, which at reach and subreach scales are modified by bedforms and other flow obstructions, such as logs, boulders, beaver dams, and salmon redds. Mechanistic study of hyporheic flow requires coupling the surface and subsurface flow fields, with the hyporheic flow modeled as a Darcy flow.

1.1. Overview

Hyporheic exchange is a process that mixes river water with pore water by bringing surface water and solutes into the sediment. My study focused on identifying the major mechanisms that drive intra-gravel flows in gravel-bed rivers having a pool-riffle morphology [e.g., *Montgomery and Buffington,* 1997]. Previous research has studied this process at large to medium scales, with models that tend to overlook the detailed mechanics of the exchange [e.g., *Bencala and Walters,* 1983; *Bencala and Harvey,*

1993], or at small scales with simplified two-dimensional models that have predominantly been applied only to sand-bed rivers with dune-like bedforms [e.g., *Elliott and Brooks*, 1997b, a; *Packman and Bencala*, 1999; *Packman et al.*, 2000; *Marion et al.*, 2002]. My research built from these later studies, developing a three-dimensional model that captures the process mechanics for solving hyporheic flow and exchange in hydraulically complex channels. Additionally, this model can be applied in different fields to solve a wide range of problems that depend on hyporheic flows. For example, in modeling solute transport in rivers, in identifying surface-subsurface interactions, in simulating tracer-laden river water flowing within the hyporheic zone, in investigating chemical reactions, and in assessing ecosystem function and condition.

My research focused on hyporheic exchange in pool-riffle channels, which are a common morphology of headwater rivers [*Montgomery and Buffington*, 1997; *Buffington et al.*, 2003a], and important habitat for threatened and endangered salmonids [*Montgomery et al.*, 1999; *Buffington et al.*, 2003b]. I first conducted a series of laboratory experiments examining surface and subsurface flows through pool-riffle channels, and then compared observed hyporheic flow to numerical simulations from computational fluid dynamics (*CFD*) software (Fluent 6.1 [*Fluent*, 2003]). Comparison between predicted and observed values showed that my proposed three-dimensional model for hyporheic flow predicts solute exchange accurately for a wide range of water discharges and bedform amplitudes and is superior to previous two-dimensional models [*Elliott and Brooks*, 1997b, a]. Furthermore, I used the model and laboratory measurements to investigate the effects of physical channel characteristics on the nature of hyporheic flow in pool-riffle channels.

Additionally, the model was used to analyze the effects of salmonid redd construction on channel hydraulics and hyporheic flow to better understand biophysical interactions in mountain channels used by spawning salmonids.

The dissertation is composed of four chapters, three of which are separate papers that address the above issues:

- Chapter 1 presents an overview of hyporheic flow and groundwater fluxes. It summarizes previous research and discusses the processes of salmonid redd

construction and the dependence of salmonid spawning habitat on hyporheic exchange.

- Chapter 2 describes the laboratory work conducted at the National Center for Earth Surface Dynamics, Saint Anthony Falls Laboratory, University of Minnesota. This chapter discusses the pool-riffle geometry and the measurements conducted in the flume experiments. The chapter also presents a three-dimensional pumping exchange model modified from the work of *Elliott and Brooks* [1997b, a], and a comparison of predicted and measured hyporheic exchange.
- Chapter 3 uses the above numerical model to examine the relative importance of several key factors governing hyporheic exchange: river discharge, bedform topography, sediment permeability, mean groundwater flow velocity, and depth of alluvium. From this analysis, two relationships were developed to predict the storage exchange coefficient and storage area, fundamental parameters for the widely used Transient Storage Model [*Bencala and Walter*, 1983], which estimates solute transport in rivers by linking surface and hyporheic flows. The proposed relationships allow application of the Transient Storage Model without the need for site- and discharge-specific calibration of these two parameters, providing a significant improvement over standard application of this model.
- Chapter 4 examines the effects of salmonid redds on river hydraulics and hyporheic flow using numerical simulations. Two scenarios for a pool-riffle reach, with and without redds, were studied to evaluate the effects of redds on intra-gravel flow velocity and dissolved oxygen concentrations, and to examine implications for survival of salmonid embryos incubating within redds.

1.2. Hyporheic zone

1.2.1. Definition

Figure 1.1 shows typical hyporheic flow and the extent of the hyporheic zone in a two-dimensional flume experiment. Red dye is injected near the sediment surface at the stoss side of the riffle. The bedform shape interacts with the river flow, modifying water

depth and flow direction. These changes generate a high-pressure zone upstream of the riffle crest, where in-stream water and red dye are driven into the sediment. On the downstream side of the riffle, a complimentary low-pressure zone occurs due to shallower water, faster velocities, and/or flow separation over the riffle crest. In this location, the dye is drawn out of the sediment and re-enters the river flow. In the same manner, other solutes carried by rivers are transported into the sediment or removed from the pore interstices. More complex flow paths are present in three-dimensional experiments Figure 1.2, but the mechanism responsible for this flow remains the same (Chapter 2) and has been termed pumping exchange [*Elliott and Brooks,* 1997b].

Figure 1.1: Hyporheic flow path generated by a dune-like bedform constructed in a teaching flume at the Saint Anthony Fall Laboratory (photo by Tonina). The hyporheic flow is visualized by red dye injected at the upstream edge of the riffle, known as the pool tail.

In two-dimensional systems, hyporheic flow is fairly simple, predominantly having a two-dimensional flow path in the vertical and longitudinal directions, and is readily evidenced by dyes (Figure 1.1). However, in three-dimensional systems, hyporheic flow is substantially more complex, with stronger lateral motion and potential interaction with the riparian and floodplain zones (floodplain hyporheic flows) [*Edwards,* 1998] (Figure 1.2). Consequently, tracer visualization is impossible and, thus, numerical simulations are required, as done in my research.

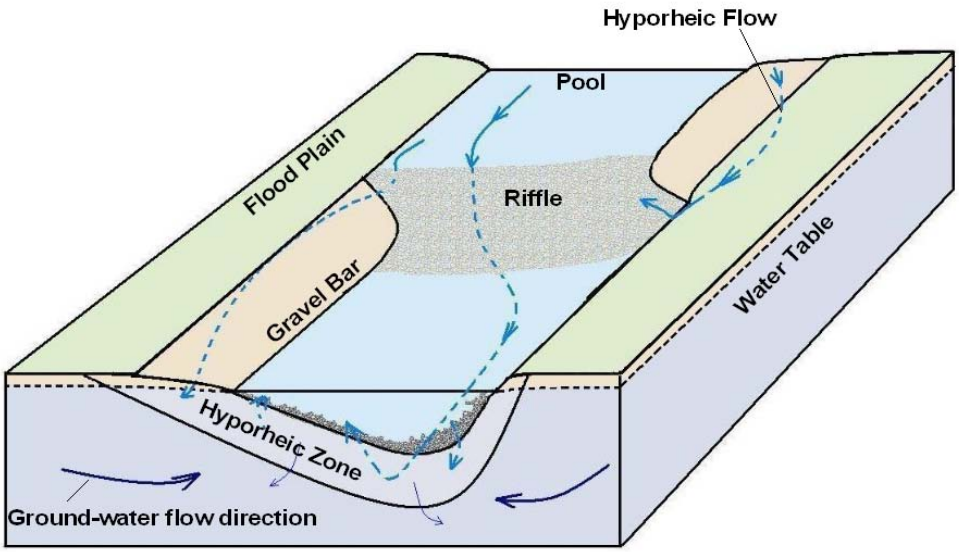

Figure 1.2: The hyporheic zone of a typical pool-riffle channel, showing both hyporheic flow and groundwater flow (modified from *Winter et al.* [1998]).

1.2.2. Importance of the hyporheic zone

Physiochemical processes that depend on advective transport of water and solutes through the hyporheic zone necessarily depend on the intensity and extent of the hyporheic flow (Figure 1.3). Solutes and surface water transferred into the sediment modify stream solute concentrations [*Bencala and Walters,* 1983] and groundwater habitat, with local ecosystems affected by the amount and type of solutes delivered [*Kim et al.,* 1992]. Furthermore, upwelling water brings reduced elements and transformed solutes into the river [*Triska et al.,* 1989; *Nagaoka and Ohgaki,* 1990; *Triska et al.,* 1993a]. Hyporheic flow mixes groundwater and surface water and exposes in-stream water to the groundwater environment, generating physical and chemical gradients. For example, the solid matrix of the sediment influences water temperature and filters the fluid, while biofilms and organisms uptake solutes and release their waste products). Fish and other organisms are sensitive to these physiochemical gradients. For instance, hyporheic flow is a source of nutrients and algal cells to streams that are recovering after a flood event. A study of the ecology of Sycamore Creek in Arizona showed that the algae that grew on the first layer of the streambed sediment were the quickest to recover following storms in areas where hyporheic upwelling occurred [*Valett et al.,* 1994]. It was found that the concentrations of dissolved nitrogen (an essential element for algae growth) were higher in upwelling areas than in areas where downwelling was present.

This example shows the importance of modeling hyporheic flow accurately for predicting not only its intensity and duration, but also its location and extent.

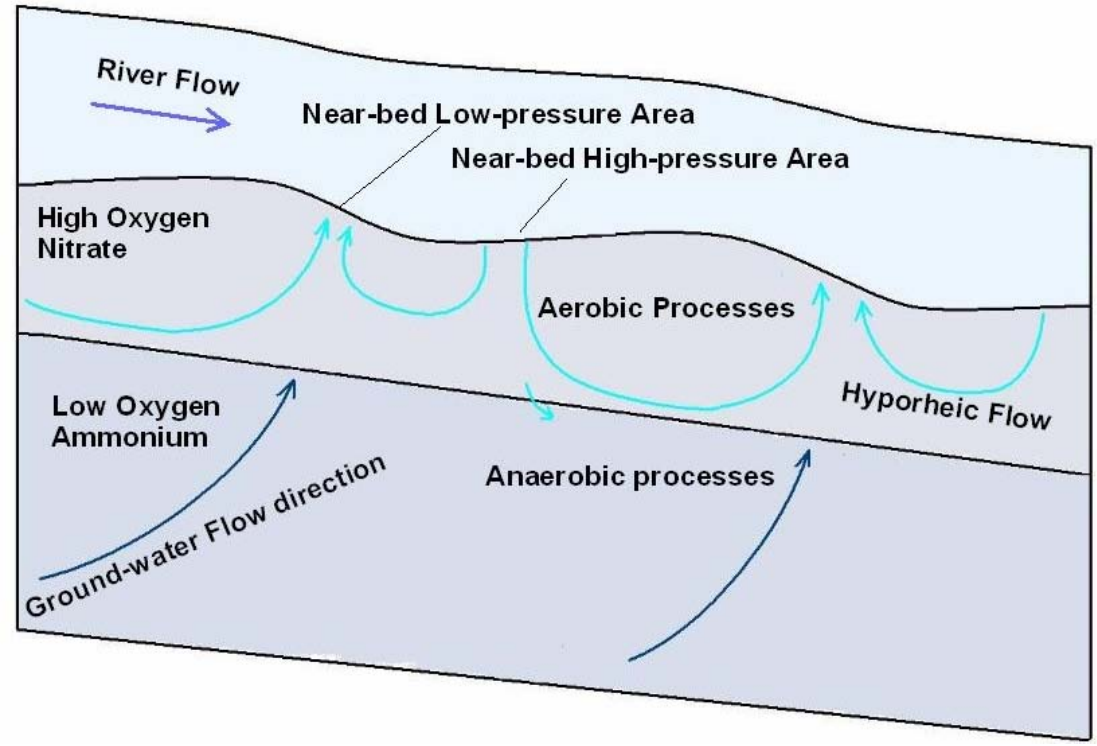

Figure 1.3: Cartoon of typical flow paths and processes linking river flow, hyporheic flow, and ground-water flow at subreach scales in an alluvial river (modified from *Winter et al.* [1998]).

1.2.3. Process scale

River-groundwater interactions may be studied at different scales (Figure 1.4). At watershed scales (hundreds to thousands of kilometers) and stream-segment scales (tens to hundreds of kilometers), the groundwater surface-water exchange is analyzed from a regional point of view, in which the fine scale details are lost [*Edwards,* 1998]. At the reach-unit scale (tenths to tens of kilometers), valley topography, knickpoints, and bedrock outcrops define the river geometry, and their dimensions and location affect the hyporheic exchange [*Bencala and Harvey,* 1993; *Wagner and Harvey,* 1997; *Baxter and Hauer,* 2000]. However, it is at the channel-unit scale (that of individual pools and bars; tenths to hundreds of meters) that the hyporheic flow can be appreciably observed and mechanistically modeled [*Cooper,* 1965; *Vittal et al.,* 1977]. At this level, the hyporheic flow depth is a function of river morphology and size of the individual topographic elements (riffles, bars and pools) [*Elliott and Brooks,* 1997b, a; *Marion et al.,* 2002].

Obstacles, such as boulders and bars govern the vertical and longitudinal extent of the hyporheic flow.

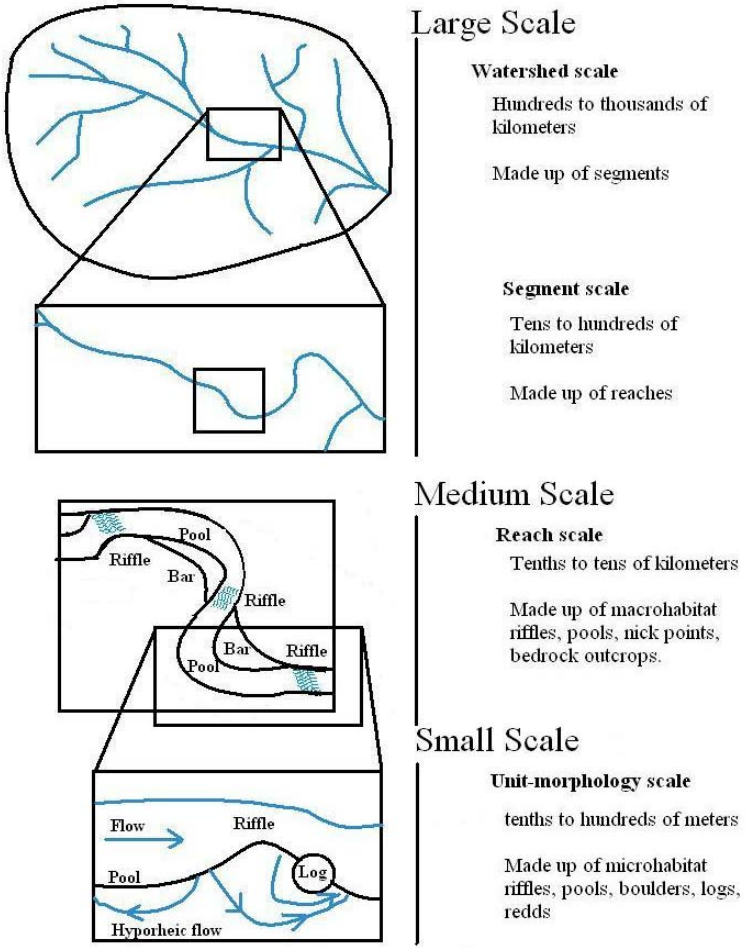

Figure 1.4: Scales of hyporheic flow (modified from *Winter et al.* [1998]).

1.3. Subsurface flow

Hyporheic flow occurs within sediments that form a porous medium, which is a solid matrix with voids. The ratio between the volume of voids and the bulk volume defines the porosity, which for natural formations, is a function of grain size and arrangement. Sediments composed of sands and gravel (those relevant for pool-riffle channels) typically have porosities ranging between 0.3 and 0.34 [*Ghetti*, 1980], and in my project I used a value of 0.34.

1.3.1. The energetic status of the ground water

In the study of flow in porous media, the heat energy of the fluid is neglected, excluding exceptional cases (for instance the study of geysers) because temperature gradients are gradual and of small magnitude. Hence the energy terms are:

$$\begin{aligned} E_k &= \frac{1}{2}mv^2 && \textit{Kinetic energy} \\ E_p &= mgz && \textit{Potential energy} \\ E_{fes} &= m\frac{p}{\rho_w} && \textit{Energy due to the external surficial forces} \end{aligned} \qquad \textbf{(1.1)}$$

where m indicates the mass, v the velocity of the water parcel, g the gravitational acceleration, z the elevation of the parcel with respect to a datum, and p and ρ_w are the pressure and the water density, respectively. Furthermore, velocities are usually very small, therefore the kinetic term can be neglected, leading to the following definition of total energy:

$$E_t = gz + \frac{p}{\rho_w} \qquad \textbf{(1.2)}$$

At this point, it is important to define the physical quantity h

$$h = \frac{E_t}{g} = z + \frac{p}{g\rho_w}, \qquad \textbf{(1.3)}$$

which represents the energy of an infinitesimal parcel of fluid expressed in meters of water. The last quantity in (1.3) is usually indicated with the symbol ψ or h_p and was measured in the experiments with a mini-piezometers installed at the sediment surface, while z represents the vertical position from the bottom of the flume. It is important to understand that the flux is governed by both terms, position and pressure, and not by each one separately [*Dear*, 1972]. Movement of water occurs only if an energy gradient is present and not if z and h_p vary without changing h.

1.3.2. Darcy's law

Darcy's law can be used to model hyporheic flow as long as the flow is laminar or has small Reynolds numbers, Re≈1, [*Hassanizadeh and Gray*, 1987]. Otherwise, inertial accelerations or non-uniform flow conditions would arise, requiring modification of

Darcy's law [*Dagan,* 1979]. This law is based on a linear proportionality between energy gradient, *h,* and discharge, *Q*

$$Q = -kA\frac{\Delta h}{\Delta x} \qquad \textbf{(1.4)}$$

The negative sign in equation (1.4) indicates that the direction is opposite to the energy gradient. *A* is the surface orthogonal to the direction of the flux, while *k* is the hydraulic conductivity, which has the dimensions of velocity (length per time) and depends on the characteristics of the porous medium and the fluid.

Porous media can be classified as heterogeneous, if *k* changes point-by-point, and anisotropic if *k* has preferential directions. Otherwise, the medium is homogeneous (i.e. *k* is spatially constant) or isotropic (i.e. *k* does not change with directions). I chose a medium characterized by the last two properties for my experiments in order to keep the system controlled and simplified.

Furthermore, hydraulic and geometric properties of porous formations become stable and steady only when their volumes are greater than a threshold size [*Dagan,* 1989], known as the representative elementary volume, R.E.V.[*Hassanizadeh and Gray,* 1979]. At the R.E.V scale, the medium is considered homogeneous, with the constitutive properties of the flow given by Darcy's law. Therefore, the discharge per unit area that passes through a volume is equal to the specific discharge assessed by Darcy's formula, only if the volume is larger than the R.E.V. If flow properties (e.g. velocity, and discharge) were determined for volumes smaller than the R.E.V., Darcy's law would not hold. Even though the sediment used in my analyses is homogeneous, the pore dimensions and sediment size determine the smallest dimension of the finite element volume, which needs to be larger than the R.E.V. and particular care was devoted in choosing the right grid size for my numerical model (Chapter 2).

1.4. Previous studies of hyporheic flow

Over the last few decades, several studies have examined the hyporheic zone from a variety of perspectives (e.g., ecological, fisheries, engineering). The major objective of these studies was to characterize the role of mixing and transport of contaminants and solutes, such as nitrogen, phosphorus, and organic carbon. Results of these studies

demonstrate that the hyporheic zone plays an important role in the N, C and P cycles [*Triska et al.,* 1989; *Wondzell and Swanson,* 1996].

Most researchers have focused on solute transport in rivers, and they have analyzed the hyporheic zone for its capacity to temporarily store passive tracers and to transform biodegradable solutes. Numerical and field studies include those of *Bencala and Harvey,* [1993] and *Choi et al.* [2000]. Other research has focused on the hyporheic zone as a remover of solutes or a place for chemical reactions to occur [*Triska et al.,* 1993b, a; *McClain et al.,* 1998]. Some studies have examined the influence of local topography, but these analyses were primarily focused on the role of the hyporheic zone for water quality issues at the segment scale [*Bencala and Harvey,* 1993]. All of these studies are at large and medium scales (Figure 1.4), where local variations in physical characteristics are not examined and are averaged over the reach length. Hyporheic exchange through bedforms and the near-surface alluvium is a small-scale process that at the reach scale can be parameterized without mechanistic modeling [e.g., *Bencala and Walters,* 1983]. However, quantifying the smaller-scale, subreach exchange through bedforms and surficial alluvium may be important for understanding biophysical interactions that structure riverine ecosystems.

In ecology and habitat studies, local processes are important, and starting from the early laboratory work of *Cooper* [1965], hyporheic flow began to be studied at the small-scale (unit-morphology scale, Figure 1.4). More recently, studies in engineering and water quality have examined the hyporheic zone at the unit-morphology scale to understand the mechanisms that generate hyporheic flow. *Bencala and Harvey* [1993] showed that the local river morphology creates an interaction between the hyporheic zone and the underlying aquifer, which is superimposed on the regional groundwater flow. The small-scale topography does not change the regional water balance, but it creates preferential areas of upwelling and downwelling (Figure 1.4). At the channel unit scale, hyporheic flow affects solute mixing processes and determines the extent and amount of the vertical and horizontal penetration of solute-laden surface-water into the riverbed. At this scale, perturbations of the near-bed pressure due to bedforms and other flow obstructions can change both the amount and path of these fluxes. Some researchers have analyzed hyporheic flow through dunes, simplifying the bed topography to a two-

dimensional sinusoidal feature [*Shimizu et al.,* 1990, *Mendoza and Zhou,* 1992; *Packman and Bencala,* 1999]. In particular, *Elliott and Brooks* [1997a, b] proposed a physically-based pumping exchange model in which pressure variations at the bed surface generate upwelling and downwelling hyporheic fluxes through the riverbed. The model, which was developed for sand-bed rivers with two-dimensional bedforms, is modified here for use in mountain gravel-bed rivers with bedforms and channel hydraulics that are strongly three dimensional.

1.5. Salmon redds

While benthic species usually do not change either the geometry of riverbeds or hydraulic characteristics of channels, fish, such as salmon and trout, are big enough to modify channel topography and bed material characteristics during construction of their egg nests, called redds. Mass spawning and repeated spawning over many years in the same location may lead to production of persistent bedforms with maximum dune heights as much as 1.5 m [*DeVries,* 1997], and long-term alteration of sediment characteristics and hydraulic conductivity [*Gottesfeld et al.,* 2004]. Salmonids (salmon, trout and charr) females construct egg nests in streambed gravels (Figure 1.5). The female uses her tail to redirect and accelerate the flow toward the streambed, carving out a depression by undulating her body (Figure 1.5b.). She then deposits thousands of eggs (roe), while one or more males fertilize them. After that, the female moves a slight distance upstream and begins excavating a second depression, the spoils of which cover the downstream egg pocket (Figure 1.5c.). The spawning activity tends to winnow fine grains from the streambed, resulting in relatively coarser and more porous sediment than the undisturbed bed material [*Crisp and Carling,* 1989; *Kondolf et al.,* 1991].

Hyporheic flow is sensitive to local variations of bed topography and sediment hydraulic conductivity. Consequently, spawning activity and redd formation may alter local hyporheic patterns. In a pioneering paper, *Cooper* [1965] presented a set of laboratory experiments in which dye tracers showed that redd-shaped bedforms induced hyporheic flow. In a subsequent investigation, *Alonso et al.* [1988] developed a two-dimensional finite-difference model to predict solute and fine particle intrusion into egg pockets through hyporheic advection. This model lacked real interaction between redd

characteristics (topography and conductivity) and river hydraulics. Moreover, three-dimensional effects were not captured by their approach. In my research, I investigated the interaction between redd formation and river hydraulics in a pool-riffle channel, and the development of redd-induced hyporheic flow (Figure 1.5c.) using the numerical model developed in Chapter 2. The model predicts the flow field within the redd and is able to quantify the intra-gravel velocities, dissolved oxygen concentration and, thus, the effects of spawning activities on water quality and the potential survival of eggs incubating within the redd (Chapter 4).

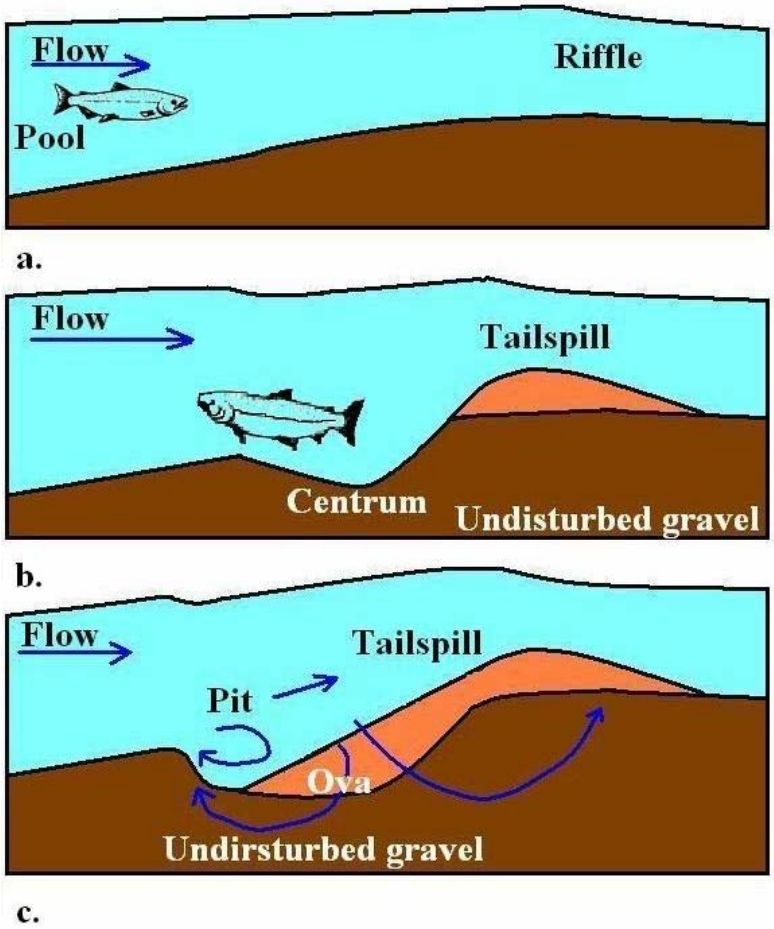

Figure 1.5: Longitudinal view of a typical salmonid spawning area (pool tail) and stages of redd construction: a. undisturbed pool-riffle formation; b. creation of the egg nest; c. the redd is covered and a second pit is created. Flow paths of redd-induced intra-gravel flow are shown (modified from *Bjornn and Reiser* [1991]).

References

Alonso, C. V., F. D. Theurer, and D. W. Zachmann (1988), *Tucannon River Offsite Study: Sediment intrusion and dissolved-oxygen transport model*, U.S. Department of Agriculture, Agricultural Research Service Hydro-Ecosystem Research Group, Fort Collins.

Baxter, C. V., and R. F. Hauer (2000), Geomorphology, hyporheic exchange, and selection of spawning habitat by bull trout (*Salvelinus confluentus*), *Canadian Journal of Fisheries and Aquatic Sciences, 57*, 1470-1481.

Bencala, K. E., and J. W. Harvey (1993), The effect of streambed Topography on Surface-Subsurface Water Exchange in Mountain Catchments, *Water Resources Research, 29*(1), 89-98.

Bencala, K. E., and R. A. Walters (1983), Simulation of solute transport in a mountain pool-and-riffle stream: a transient storage model, *Water Resources Research, 19*(3), 718-724.

Bjornn, T. C., and D. W. Reiser (1991), Habitat requirements of salmonids in streams, *American Fisheries Society, Special Publication*(19), 83-138.

Buffington, J.M., R.D. Woodsmith, D.B. Booth and D.R. Montgomery (2003a), Fluvial processes in Puget Sound Rivers and the Pacific Northwest. In D.R. Montgomery, S. Bolton, D.B. Booth and L. Wall (eds.) *Restoration of Puget Sound Rivers*. University of Washington Press, Seattle, WA, pp. 46-78.

Buffington, J. M., D. J. Isaak, and R. F. Thurow (2003b), Hydraulic Control on the Spatial Distribution of Chinook Salmon Spawning Gravels in Central Idaho: Integrating Reach-Scale Predictions via Digital Elevation Models, *In* Proc. *AGU Fall Meeting*. *Edited by* EOS. AGU, 84, San Francisco.

Choi, J., J. W. Harvey, and M. H. Conklin (2000), Characterizing multiple timescales of stream and storage zone interaction that affect solute fate and transport in streams, *Water Resources Research, 36*(6), 1511-1518.

Cooper, A. C. (1965), The effect of transported stream sediments on the survival of sockeye and pink salmon eggs and alevin, in *Bulletin 18*, International Pacific Salmon Fisheries Commission, New Westminster, B.C., Canada.

Crisp, D. T., and P. A. Carling (1989), Observations on siting, dimensions, and structure of salmonid redds, *Journal of Fish Biology, 34*, 119-134.

Dagan, G. (1979), The Generalization of Darcy's Law for Nonuniform flow, *Water Resources Research, 15*(1), 1-7.

Dagan, G. (1989), *Flow and Transport in Porous Formation*, Springer-Verlag.

Dear, J. (1972), *Dynamics of Fluids in Porous Media*, Dover Publication, New York.

DeVries, P. (1997), Riverine salmonid egg burial depths: review of published data and implications for scour studies, *Canadian Journal of Fisheries and Aquatic Sciences, 54*, 1685-1698.

Edwards, R. T. (1998), The Hyporheic Zone, in *River Ecology and Management: Lessons from the Pacific Coastal Ecoregion*, edited by R. J. Naiman and R. E. Bilby, Springer-Verlag, New York, 399-429.

Elliott, A., and N. H. Brooks (1997a), Transfer of nonsorbing solutes to a streambed with bed forms: Laboratory experiments, *Water Resources Research, 33*(1), 137-151.

Elliott, A., and N. H. Brooks (1997b), Transfer of nonsorbing solutes to a streambed with bed forms: Theory, *Water Resources Research, 33*(1), 123-136.

Fluent Inc. (2003), Fluent User's Guide, Distributor: Fluent US, Lebanon. NH.

Ghetti, A. (1980), *Idraulica*, Edizioni Libreria Cortine, Padova.

Gottesfeld, A. S., M. A. Hassan, J. F. Tunnicliffe, and R. W. Poirier (2004), Sediment dispersion in salmon spawning streams: The influence of floods and salmon redd construction, *J. Amer. Water Resour. Assoc., 40*, 1071-1086.

Hassanizadeh, M. S., and W. G. Gray (1979), General conservation equations for multi-phase systems: 1. Averaging procedure, *Advances in Water Resources, 2*, 131-144.

Hassanizadeh, M. S., and W. G. Gray (1987), High velocity flow in porous media, *Transport in porous media, 2*, 521-531.

Kim, B. K. A., A. P. Jackman, and F. J. Triska (1992), Modeling biotic uptake by periphyton and transient hyporheic storage of nitrate in a natural stream, *Water Resources Research, 28*(10), 2743-2752.

Kondolf, G. M., G. F. Cada, M. J. Sale, and T. Felando (1991), Distribution and Stability of Potential Salmonid Spawning Gravels in Steep Boulder-Bed Streams of the Eastern Sierra Nevada, *Transactions of the American Fisheries Society, 120*(2), 177-186.

Marion, A., M. Bellinello, I. Guymer, and A. I. Packman (2002), Effect of bed form geometry on the penetration of nonreactive solutes into a streambed, *Water Resources Research, 38*(10), 1209, doi:10.1029/2001WR000264.

McClain, M. E., R. E. Bilby, and F. J. Triska (1998), Nutrient Cycles and Responses to Disturbance, in *River Ecology and Management: Lessons from the Pacific Coastal Ecoregion*, edited by R. J. Naiman and R. E. Bilby, Springer-Verlag, New York.

Mendoza, C., and D. Zhou (1992), Effects porous bed on turbulent stream flow above bed, *Journal of Hydraulic Engineering*.

Montgomery, D. R., and J. M. Buffington (1997), Channel-reach morphology in mountain drainage basins, *Geological Society of American Bulletin, 109*, 596-611.

Montgomery, D. R., E. M. Beamer, G. R. Pess, and T. P. Quinn (1999), Channel type and salmonid spawning distribution and abundance, *Canadian Journal of Fisheries and Aquatic Sciences, 56*, 377-387.

Nagaoka, H., and S. Ohgaki (1990), Mass Transfer Mechanism in a Porous Riverbed, *Water Research, 24*(4), 417-425.

Packman, A. I., and K. E. Bencala, (1999), Modeling methods in study of surface-subsurface hydrological interactions, in *Stream and Ground Waters*, edited by J. B. Jones and P. J. Mulholland, Academic, San Diego, California, 45-80.

Packman, A. I., N. H. Brooks, and J. J. Morgan (2000), A physicochemical model for colloid exchange between a stream and a sand streambed with bed forms, *Water Resources Research, 36*(8), 2351-2361.

Shimizu, Y., T. Tsujimoto, and H. Nakagawa (1990), Experiments and macroscopic modeling of flow in highly permeable porous medium under free-surface flow, *Journal of Hydraulic Engineering, 8*(1), 69-78.

Triska, F. J., J. H. Duff, and R. J. Avanzino (1993a), Patterns of hydrological exchange and nutrient transformation in the hyporheic zone of a gravel bottom stream: examining terrestrial-aquatic linkages, *Freshwater Biology, 29*, 259-274.

Triska, F. J., J. H. Duff, and R. J. Avanzino (1993b), The role of water exchange between a stream channel and its Hyporheic zone in nitrogen cycling at the terrestrial-aquatic interface, *Hydrobiologia, 251*, 167-184.

Triska, F. J., V. C. Kennedy, R. J. Avanzino, G. W. Zellweger, and K. E. Bencala (1989), Retention and transport of nutrients in a third-order stream: Channel processes, *Ecology, 70*, 1894-1905.

Valett, M. H., S. G. Fisher, N. B. Grimm, and P. Camill (1994), Vertical hydrologic exchange and ecologic stability of a desert stream ecosystem, *Ecology, 75*, 548-560.

Vittal, N., K. G. Ranga Raju, and R. J. Garde (1977), Resistance of two-dimensional triangular roughness, *Journal Hydraulic Research, 15*(1), 19-36.

Wagner, B. J., and J. W. Harvey (1997), Experimental design for estimating parameters of rate-limited mass transfer: Analysis of stream tracer studies, *Water Resources Research, 33*(7), 1731-1741.

Winter, T. C., J. W. Harvey, O. L. Franke, and W. M. Alley (1998), *Ground water and surface water a single resource*, Circular, 1139, U.S. Geological Survey.

Wondzell, S. M., and F. J. Swanson (1996), Seasonal and storm dynamics of the Hyporheic zone of 4-th order mountain stream. 2: Nitrogen cycling, *North America Benthological Society, 15*, 20-34.

Chapter 2.

A THREE-DIMENSIONAL MODEL FOR HYPORHEIC EXCHANGE IN GRAVEL-BED RIVERS WITH POOL-RIFFLE MORPHOLOGY[1]

Hyporheic exchange has been extensively studied in sand-bed channels having two-dimensional dune-ripple morphologies, but few studies have examined hyporheic flow in pool-riffle channels, which are characterized by coarser sediment, steeper slopes, and three-dimensional bed forms that strongly influence surface flow. These channels are particularly important habitat for salmonids, many of which are currently at risk worldwide, and which incubate their offspring within the hyporheic zone. Here, we examine hyporheic exchange in gravel pool-riffle channels using a pumping transport model that accounts for spatial variations in total near-bed pressure resulting from flow over three-dimensional bedforms. We compared predicted hyporheic exchange with that observed in a series of laboratory experiments and found good agreement, indicating that the major mechanism for exchange is bedform-induced advection. Bedforms affect both the total near-bed pressure and the surface area available for hyporheic exchange at a

[1] Co-authored paper by Daniele Tonina and John M. Buffington, in review with *Water Resources Research*.

given discharge. We also tested the performance of the hydrostatic pressure as a proxy for the observed near-bed pressure, and found agreement with measured hyporheic exchange only for low bedform amplitudes and high flows (i.e., where topographic effects on channel hydraulics and hyporheic exchange are minimized).

2.1. Introduction

The presence of hydraulic head gradients over a porous medium generates flow paths inside the pores, the magnitude and direction of which are functions of the hydraulic conductivity of the medium and the hydraulic head [*Mendoza and Zhou*, 1992]. Generally, an obstruction in a moving fluid creates an upstream high-pressure zone and a downstream low-pressure zone, which cause flow under the object when it lays on porous media. In the same manner, bedforms, boulders, logs, or irregularities created by biotic processes like redds or beaver dams generate downwelling fluxes in which river water is forced into the stream bed and banks in regions of high pressure, and complimentary upwelling fluxes in which subsurface water is expelled into the river in regions of low pressure. This mechanism is known as pumping exchange [*Elliott and Brooks*, 1997a,b], and the subsurface flow area in which this exchange occurs is called the shallow hyporheic zone [*Edwards*, 1998].

The hyporheic zone is a band of permeable, saturated sediment surrounding a river, where surface water and groundwater mix. This includes river beds (shallow hyporheic zone), riverbanks, saturated sediments under dry bars (parafluvial zones), and riparian and floodplain zones (floodplain hyporheic flows) [*Edwards*, 1998]. The hyporheic zone is also an ecotone for benthic species and fish [*Stanford and Ward*, 1993; *Gibert et al.*, 1994] that is characterized by intense physical and chemical gradients due to the mixing of groundwater and surface water. Downwelling fluxes have multiple effects: they bring high concentrations of dissolved oxygen and nutrients into the sediment [*Coble*, 1961; *Findlay et al.*, 1993; *Triska et al.*, 1993a], while the sediment and benthic species living in the streambed filter the water, reducing the biological and chemical loads (BOD, COD, P, C, NO_x, etc.) [*Triska et al.*, 1993a]. Similarly, upwelling fluxes remove waste products of the hyporheic fauna from the sediment and bring filtered water to the river.

In the field, two methods are typically used to define the hyporheic zone: a combined geochemical and hydraulic method, and a biological method. *Triska et al.* [1989] have operatively defined the hyporheic zone from a physical perspective as the volume of sediment containing at least 10% surface water. The content can be determined by measuring solute concentrations or water quality components such as *pH*, or electrical conductivity. In contrast, the biological definition of the hyporheic zone is based on the presence of hyporheic fauna [*Gibert et al.*, 1994].

The exchange of surface and subsurface water through the hyporheic zone (referred to as hyporheic exchange) is an essential component of carbon and nitrogen cycling [*Triska et al.*, 1993b], benthic habitat [*Edwards*, 1998], and in-stream contaminant transport of solutes [*Bencala and Walters*, 1983]. Several models for solute transport in rivers take into account hyporheic exchange. *Elliott and Brooks* [1997a,b] proposed a pumping method based on bedform-induced pressure variations, as discussed above. In contrast, *Bencala and Walters* [1983] developed a first-order mass transfer model based on "transient storage" which uses two parameters to characterize the hyporheic exchange: the exchange coefficient, and the solute storage area within the hyporheic zone.

The extent of the hyporheic zone is a function of the local topography [*Harvey and Bencala*, 1993] and consequent spatial variation in the total near-bed pressure [*Vittal et al.*, 1977; *Savant et al.*, 1987] that drives subsurface flow. Previous studies of hyporheic exchange in rivers have primarily focused on fine-grained, sand-bed channels with two-dimensional dune and ripple bedforms [*Savant et al.*, 1987; *Elliott and Brooks*, 1997a,b; *Packman et al.*, 2000; *Marion et al.*, 2002]. Although, the effect of bed topography on intra-gravel flow is qualitatively understood [*Cooper*, 1965], few studies have been conducted for rivers with gravel-bed channel morphologies. This work addresses hyporheic exchange in gravel-bed rivers characterized by three-dimensional pool-riffle morphology [e.g., *Montgomery and Buffington*, 1997]. These channels are particularly important habitat for salmonid species, many of which are currently at risk worldwide [*Nehlsen et al.*, 1991; *Montgomery*, 2003]. Salmon and trout bury their eggs in streambed gravels for incubation within the hyporheic zone. After hatching, the alevins live in the hyporheic zone before emerging into the stream [*Levy and Slaney*, 1993].

Coarse-grained pool-riffle channels also differ from lower-gradient sand-bed rivers in that they exhibit a wide range of flow regimes that change seasonally. Hence, surface flow and the boundary conditions for driving hyporheic exchange tend to be more variable, which may cause temporal variations in the quality or quantity of hyporheic habitat.

In this study, we conduct a series of laboratory experiments to examine hyporheic exchange in pool-riffle channels spanning a broad range of discharge and bedform geometry. Observed exchange is compared with that predicted from a modified pumping transport model that accounts for near-bed pressure distributions resulting from flow over three-dimensional bedforms.

2.2. Theory: pumping exchange model

The pumping exchange model has been used and validated in flume experiments for fine particles with micro-bedforms having a two-dimensional dune-like morphology [*Savant et al.*, 1987; *Elliott and Brooks*, 1997a,b; *Packman et al.*, 2000; *Marion et al.*, 2002]. This method assumes a two-dimensional exchange process, a flat bed surface (because the bedform volume is small relative to the alluvial volume over which hyporheic flow occurs), and a downstream sinusoidal variation in total pressure due to the bedforms. However, these assumptions are not met for three-dimensional processes such as those that take place in pool-riffle channels.

The bed morphology and flow in pool-riffle channels are strongly three-dimensional [e.g., *Dietrich and Whiting*, 1989; *Carling*, 1992] and the total pressure distribution in these channels is no longer sinusoidal; rather, it varies in a complex manner in both the downstream and cross-channel directions. Consequently, it needs to be measured experimentally or predicted from computational fluid dynamics (*CFD*) software with appropriate closure. Moreover, pool-riffle bedforms have a large sediment volume and the flat-bed approximation used in two-dimensional models no longer holds.

Figure 2.1: Example of low-flow experimental conditions: exp6, 12.5 l·s^{-1} discharge, 0.0041 m·m^{-1} slope.

To address these issues, we propose a three-dimensional pumping model for driving hyporheic exchange, in which the bathymetry of the bedform is the physical upper boundary, and the boundary condition is the total near-bed pressure normal to the bed surface plus the elevation head. The components of the total pressure are the near-bed static and dynamic pressures normal to the bed surface. We apply the model to a series of laboratory experiments in which the near-bed pressure is measured with an array of micro-piezometers, and the hyporheic flow is predicted from these measurements coupled with *CFD* software (described in Section 2.3).

We treat the hyporheic flow as groundwater flow through a porous medium using Darcy's law. The Darcy equation is typically written in terms of laminar pore flow (i.e., small Reynolds numbers, *Re≈1*) [*Hassanizadeh and Gray*, 1987] and locally uniform velocities, but can be modified for variable flow regime, in which case inertial terms start to influence the flow field [*Dagan*, 1979]. The presence of sand in streambeds damps the turbulent effects of the surface flow, which remain confined to a thin near-surface region

that was observed to have a thickness of about one to two times the dimension of the median grain size, d_{50}, in our experiments (i.e., about the thickness of the armor layer). Hence, we assume low Reynolds number hyporheic flow and a simple Darcy equation

$$u_i = k\frac{\partial H}{\partial x_i} \tag{2.1}$$

Where u_i is the velocity along the i^{th} direction, k is the hydraulic conductivity of sediment, and H is the energy head defined as the total pressure (expressed in meters of water) plus the elevation head (bed surface height above the datum).

The proposed pumping exchange method is modified from *Elliott and Brooks*, [1997a] and describes bedform-induced advection of a solute into the hyporheic zone. It is based on the average downwelling flux over the bed, $\overline{q}$ and the flux-weighted average residence time distribution of the tracer into the bed, *RTD*. Additionally, to evaluate the solute mass exchange, the solute concentration in the stream, C, must be known.

The downwelling flux is calculated directly from the groundwater flow field at the bed surface

$$q(x,y) = \begin{cases} a\cdot\mathbf{u}\cdot\mathbf{n} & \text{if } \mathbf{u}\cdot\mathbf{n} > 0 \\ 0 & \text{if } \mathbf{u}\cdot\mathbf{n} \le 0 \end{cases} \tag{2.2}$$

where a is the area on which the uniform velocity vector is applied, $\mathbf{u}$ is the Darcy velocity at the boundary (positive entering the domain), and $\mathbf{n}$ is the unit vector orthogonal to the bed surface (positive pointing inward). The average flux is then calculated over the bedform-wetted bathymetry, W_p. The *RTD* is defined as

$$RTD(\tau) = \frac{1}{W_p\,\overline{q}}\int_{W_p} q(x,y)\; R_T(\tau,x,y)\; dx\,dy \tag{2.3}$$

where R_T is the cumulative probability that a tracer entering the bed at position (x, y) at time t_0 will remain in the bed later than τ, described by the relation

$$R_T(\tau,x,y) = \begin{cases} 1 & \tau \le T \\ 0 & \tau > T \end{cases} \tag{2.4}$$

where T is the residence time associated with the injection point (x, y), and τ is the elapsed time from the injection. Values of R_T were determined using the forward particle tracking method, in which a set of particles is released at the sediment surface. Hence, the

particle moves in short time intervals with the local velocity, and its pathline can be tracked and the relative residence time recorded.

The average depth of penetration, m_e, is assessed by convoluting the average downwelling flux by the equation

$$m_e(t) = \frac{1}{C(t)} \int_0^t \bar{q}\, RTD(\tau)\, C(t-\tau)\, d\tau \qquad \textbf{(2.5)}$$

For a recirculating flume experiment where the sediment is initially saturated with water and a tracer of initial concentration C_0 is homogeneous mixed into the surface flow, the mass balance between in-stream water and pore water is

$$\frac{C(t)}{C_0} = C^*(t) = 1 - \frac{W_p\, \vartheta}{V_w} m_e(t) \qquad \textbf{(2.6)}$$

where V_w is the total water volume present in the system, except for the pore water, and ϑ is the sediment porosity. C^* is the in-stream concentration normalized by the initial value, C_0.

Simultaneous solution of equations (2.5) and (2.6) gives the in-stream solute concentration $C(t)$. The model remains one dimensional in terms of assessing stream concentration, but it is three dimensional in assessing hyporheic flow dynamics.

Table 2.1: Hydraulic characteristics of the experiments

	Discharge	Wetted area of streambed	Surface of flowing water	Mean water depth	Mean width	Mean velocity	Water-surface slope
	[l·s^{-1}]	[m^2]	[m^2]	[m]	[m]	[m·s^{-1}]	[m·m^{-1}]
exp6	12.50	3.83	3.75	0.065	0.68	0.282	0.0041
exp8	21.00	4.13	4.03	0.075	0.73	0.384	0.0041
exp13	32.50	4.78	4.70	0.104	0.85	0.369	0.0018
exp15	12.50	4.05	4.01	0.056	0.73	0.308	0.0041
exp16	20.83	4.45	4.34	0.064	0.79	0.413	0.0041
exp17	32.50	4.94	4.90	0.087	0.89	0.421	0.0018
exp21	12.50	4.38	4.27	0.044	0.77	0.365	0.0041
exp22	21.10	4.89	4.80	0.053	0.87	0.460	0.0041
exp23	32.83	5.00	4.97	0.086	0.90	0.425	0.0018
exp28	12.93	4.98	4.97	0.039	0.90	0.367	0.0041
exp29	21.17	4.98	4.97	0.052	0.90	0.452	0.0041
exp30	32.58	4.98	4.97	0.082	0.90	0.442	0.0018

2.3. Methods

To analyze the solute transfer mechanism and model hyporheic exchange in gravel pool-riffle channels, a set of twelve experiments in a recirculating flume was conducted with uniform flow and constant discharge (Table 2.1). An immobile bed of gravel was molded into a uniform pool-riffle morphology, with four sets of bedform amplitudes examined, and three discharges for each set-up, simulating a range of natural channel conditions (Table 2.2). Total hyporheic exchange was measured using two tracers (NaCl and fluorescein). We tested our pumping model by comparing predicted and observed values of total hyporheic exchange, where predictions are based on a finite-element model of Darcy flow driven by measured values of total near-bed pressure. Finally, we examined the use of the hydrostatic pressure as a proxy for the observed near-bed pressure in predicting hyporheic exchange. The following sections describe the details of our approach.

Table 2.2: Pool-riffle characteristics per experiment

	Volume of sediment	Dry bar volume	Sediment mean depth	Bedform wavelength λ	Bedform amplitude Δ		Ratio Δ/λ
	[m3]	[m3]	[m]	[m]	[m]		[-]
exp6	1.486	0.044	0.287	5.52	0.12		0.022
exp8	1.486	0.028	0.290	5.52	0.12	BD1	0.022
exp13	1.486	0.002	0.295	5.52	0.12		0.022
exp15	1.471	0.018	0.289	5.52	0.09		0.016
exp16	1.471	0.009	0.291	5.52	0.09	BD75	0.016
exp17	1.471	0.000	0.293	5.52	0.09		0.016
exp21	1.469	0.007	0.291	5.52	0.06		0.011
exp22	1.469	0.001	0.292	5.52	0.06	BD05	0.011
exp23	1.469	0.000	0.292	5.52	0.06		0.011
exp28	1.464	0.000	0.291	5.52	0.036		0.007
exp29	1.464	0.000	0.291	5.52	0.036	BD03	0.007
exp30	1.464	0.000	0.291	5.52	0.036		0.007

2.3.1. Pool-riffle morphology and experimental set-up

The pool-riffle morphology used in the experiments was designed to represent a natural headwater stream, although simplified to a regular sequence of alternate bars and pools in a single straight channel. For low discharges, the flow in pool-riffle channels

meanders around the bars, plunging into the pools and accelerating over the riffles (Figure 2.1). At high flow, the bars become submerged, limiting the horizontal flow displacement. However, our experiments reveal that the effects of the bars on the flow persisted during high flow by maintaining a complex three-dimensional surface flow field. The wavelength and amplitude of pool-riffle topography depends on flow discharge, hydrograph history [*Tubino,* 1991], sediment size and grading [*Lanzoni and Tubino*, 1999], and presence of obstructions [*Buffington et al.*, 2002].

Figure 2.2: Pool-riffle bedform for ratio of bedform amplitude to wavelength (Δ/λ) of 0.0215, largest amplitude.

Our experiments examine a straight channel without obstructions, with alternate bars and pool-to-pool spacing of six channel widths. Self-formed pool-riffle channels typically have a mean pool wavelength (λ) of about five to seven bankfull widths [*Leopold et al.*, 1964; *Keller and Melhorn*, 1978], although values as low as three channel widths have been reported [*Carling and Orr*, 2000]. The residual pool depth [*Lisle and Hilton,* 1992], defined as the difference in elevation between the riffle crest and the

bottom of the pool, determines the pool-riffle amplitude, Δ. Some researchers define pool-riffle amplitude as the vertical difference between the deepest point in the pool and highest point on the bar; hence, their amplitude values are double the ones used in this work, since we consider symmetrical bedforms. In this study, we define bankfull depth as the water depth that completely submerges the highest bedform, and we examined four bedform amplitudes (0.12, 0.09, 0.06, 0.036 m), corresponding with residual pool depths of 1, 0.75, 0.5 and 0.3 times the bankfull depth (referred to as BD1, BD75, BD05 and BD03, respectively). With a constant bedform wavelength (5.52 m), the ratio Δ/λ yields values of 0.022, 0.016, 0.011, and 0.007 (Table 2.2), which cover typical ranges for self-formed pool-riffle channels [*Buffington and Montgomery*, 1999]. The basic shape of the bed topography was predicted from the weakly nonlinear theory of *Colombini et al.* [1987] and *Tubino* [1991], adjusted for grain heterogeneity by *Lanzoni and Tubino* [1999]. The predicted topography was then modified for the desired bedform amplitude of each experiment.

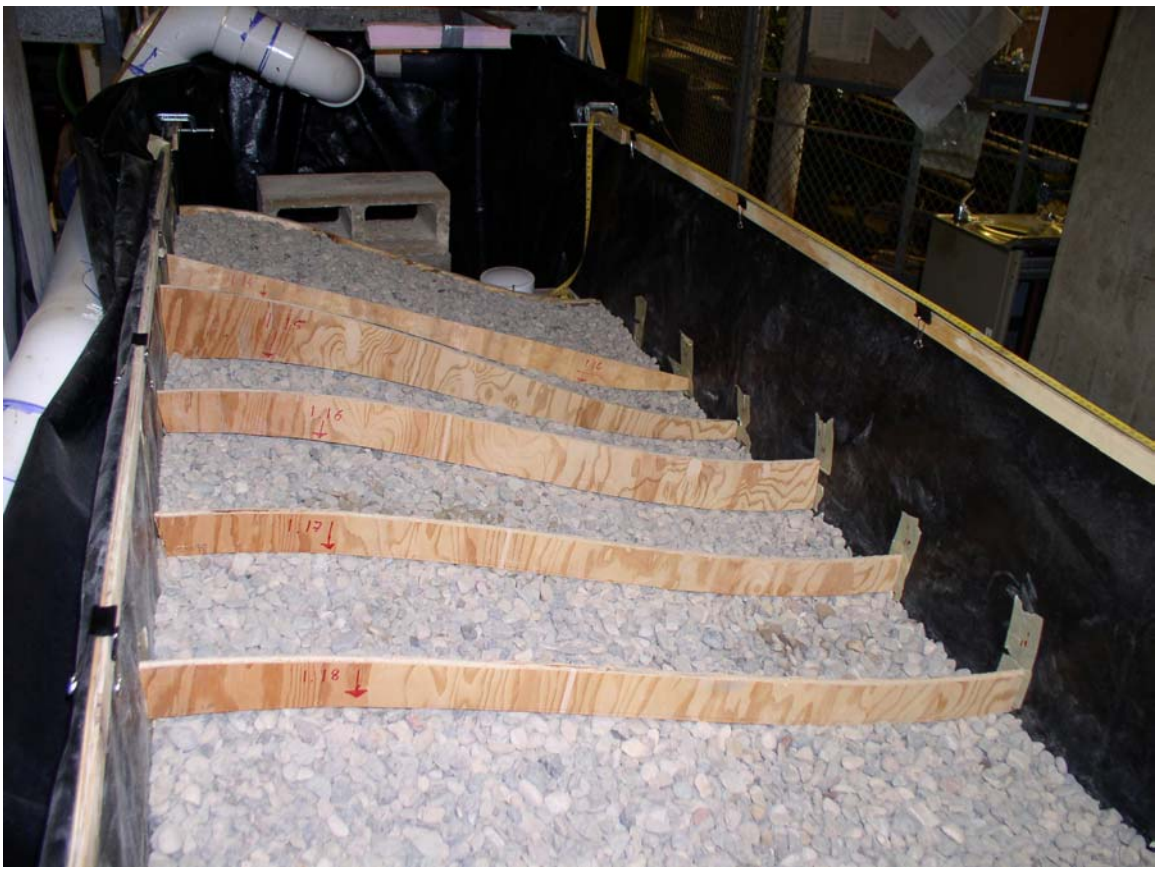

Figure 2.3: Process of pool-riffle construction using wooden molders.

The experiments were carried out at the Saint Anthony Falls Laboratory in their tilting flume, which is 14.6 m long, 0.9 m wide and 0.6 m deep. The experimental bed was 13.92 m long, over which an immobile pool-riffle topography was shaped by hand, comprising a 2.5λ long section (Figure 2.2). A series of wooden ribs was used to mold the desired cross-sectional shape of the channel for each experiment (Figure 2.3). Figure 2.2 shows the final bed shape for the largest amplitude (BD1).

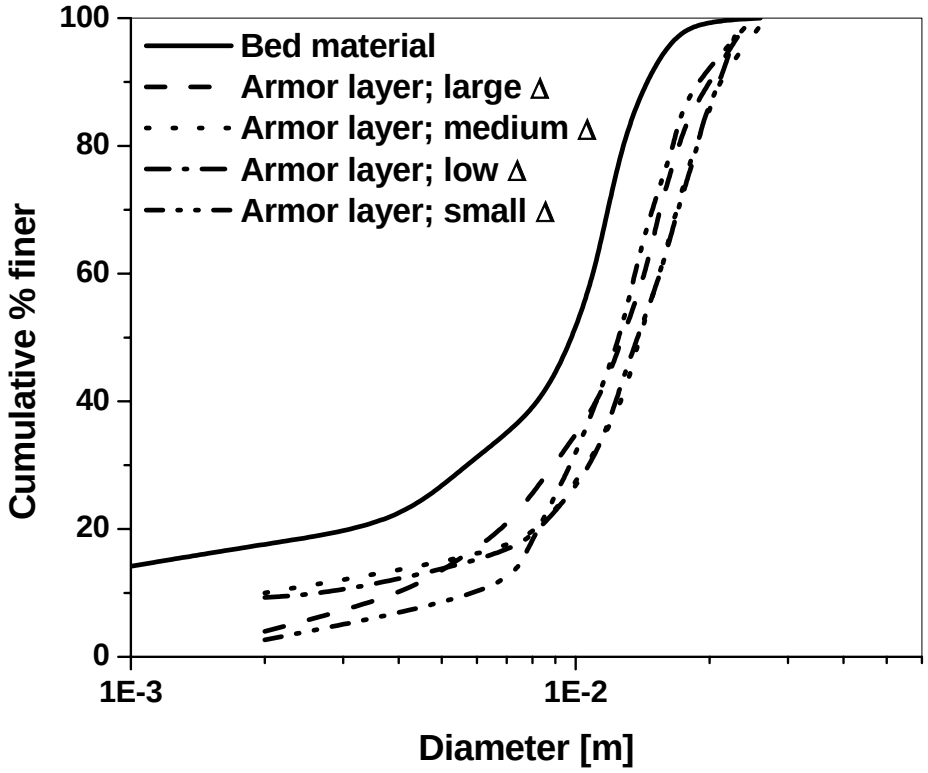

Figure 2.4: Sediment grading curve used in the experiments and armor layer developed over the riffle area for each bedform amplitude (Δ, Table 2).

The substrate was created using a mixture of one part Class Six Gravel and one part Class Seven Gravel, to which 20% Safety Grit Sand was added. The resulting sediment grading curve is shown in Figure 2.4, with a median grain size, d_{50}, of 1 cm. The amount of fine particles (sediment smaller than 6.4 mm) used in these experiments was chosen to match the threshold for successful survival to emergence of salmonid fry (90% survival when fines comprise ≤ 20% of the sediment distribution [*Bjornn and Reiser*, 1991]; the number of survivors drops drastically for higher percentages of fine particles). To avoid segregation of the fine and coarse materials during the molding of the bed, the two gravels were first mixed and wetted with water, and then the Safety Grit

Sand was added. After mixing was completed, the material was placed in the flume and manually consolidated. To change the bedform amplitude, the riffle crest was held at a constant height of thirty centimeters, while the bar top and pool concavity were adjusted to obtain the desired bedform topography. Sediment depths were shallowest below the pool, ranging from 18 to 26 cm for the largest and smallest bedform amplitudes, respectively.

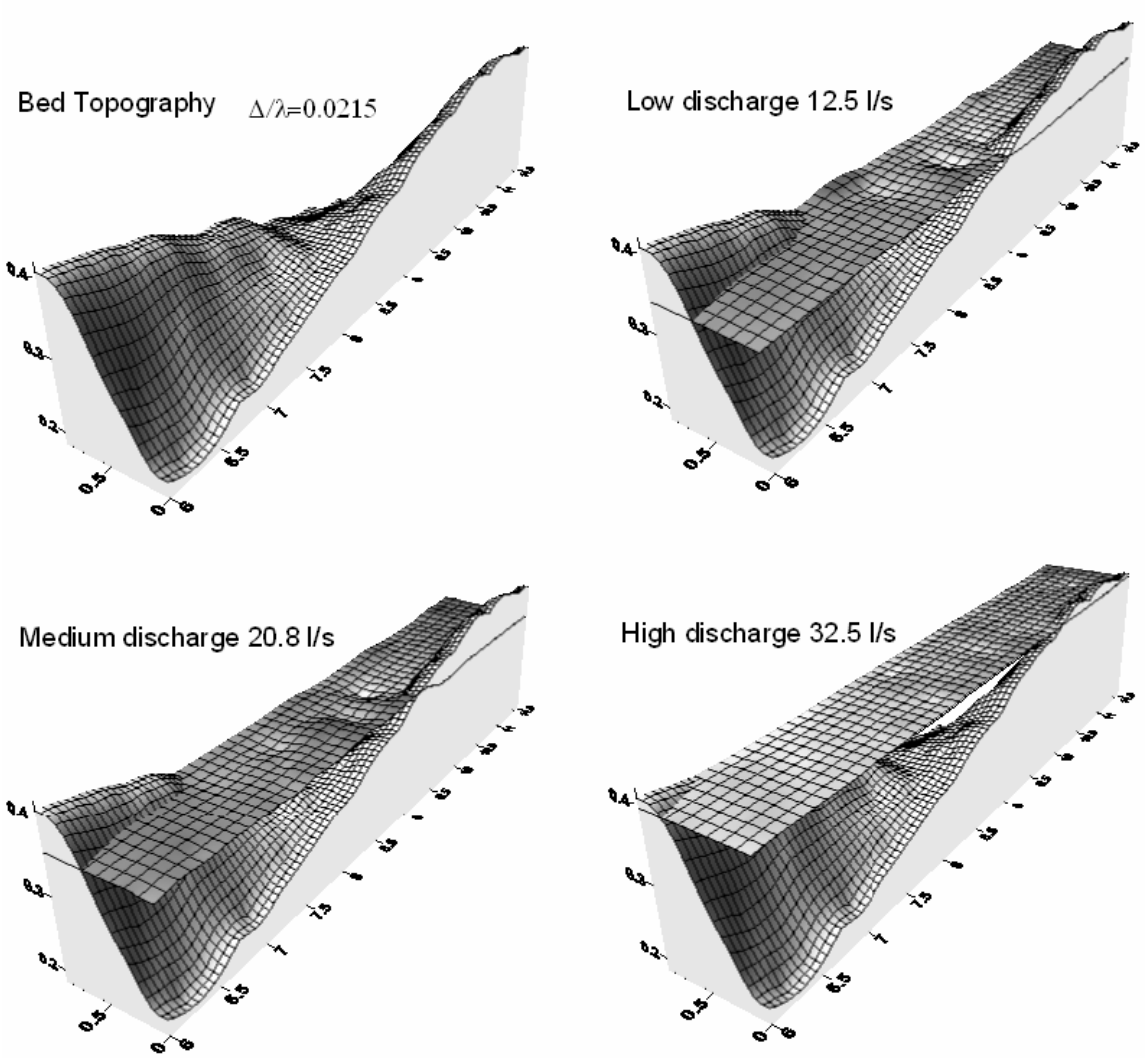

Figure 2.5: Pool-riffle topography (BD1, largest bedform amplitude) and degree of submergence for three different discharges.

2.3.2. Discharge and slope

We examined three discharges for each bedform amplitude (Tables 2.1 and 2.2). The first two discharges were 12.5 and 21 $l \cdot s^{-1}$, simulating low discharges where the flow meandered around the bars. Low discharges of this sort are important because they are the most common flow in mountain rivers. The third discharge submerged the entire bed topography to a flow height close to the bar top, representing a high-flow event with a discharge of 32.5 $l \cdot s^{-1}$ (Figure 2.5). The flume was adjusted to two slopes: a steeper slope of 0.0041 $m \cdot m^{-1}$ used for the low discharges, and a lower slope of 0.0018 $m \cdot m^{-1}$ used for the largest flow. The lower slope was chosen in order to submerge the bed at high flow. Water was recirculated during the experiments, and the flume was lined with a thin plastic sheeting to prevent water leakage. There was no sediment motion during any experiment, except for some winnowing of fine sediment from the bed surface (Section 2.3.3.3).

2.3.3. Measurements

Because we imposed a uniform topography and homogeneous sediment, we assumed that the solute exchange took place in the same way over each pool-riffle unit. Therefore, we focused on studying one pool-to-pool section in detail, and then extend the results over the entire experimental domain (Figure 2.6). The study reach was one morphological unit long (5.52 m), located between cross sections 14b and 14c (Figure 2.6).

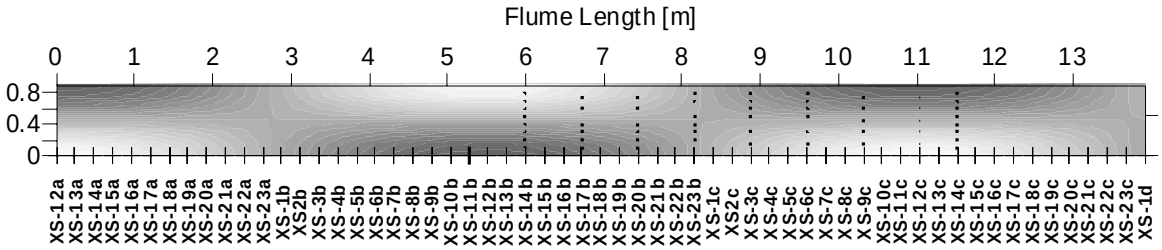

Figure 2.6: Shaded relief plan-view of pool-riffle bed topography; darker areas correspond with pools and white areas with bar tops. The study reach is between XS 14b-c, and the dots indicate locations of surface micro-piezometers.

2.3.3.1. Pressure

The pressure distribution at the bed surface was measured with micro-piezometers composed of super-thin (ether) tubes (1/16” inside diameter and 1/8” outside diameter) (Figure 2.7). Nests of subsurface piezometers were also placed at the end points of the study reach (cross sections 14b and 14c). The surface piezometers had a longitudinal spacing of 72 cm and were placed in cross-sectional sets at 10 cm intervals across the channel. The subsurface piezometers had a 10 cm lateral spacing and a 6 cm vertical spacing.

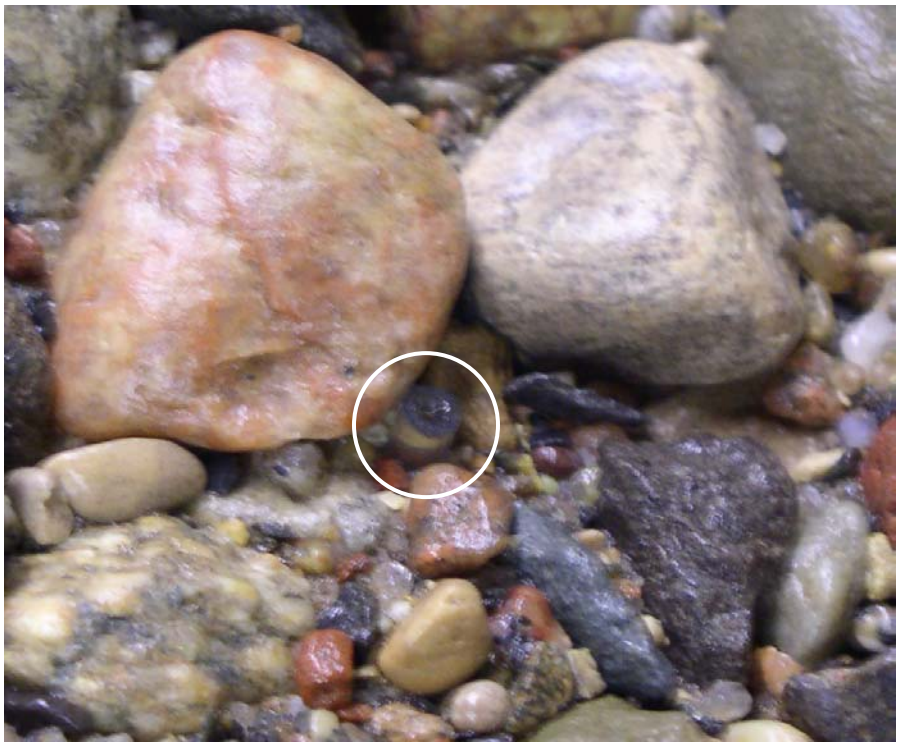

Figure 2.7: Photograph of a micro-piezometer for measuring pressure at the sediment-water interface.

The surface piezometers were placed flush with the sediment surface to minimize disturbance of the flow and were installed during the molding of the bed topography. Due to the small diameter of the tube, a capillary rise was measured and subtracted from the recorded values. The water height in the tubes was gauged using calipers, with an estimated maximum measurement error of about 1 mm.

Measuring spatial variations in the near-bed pressure is laborious in channels with complex topography, particularly in field studies [*Baxter and Hauer*, 2000]. However,

the hydrostatic pressure may approximate the actual near-bed pressure under special circumstances, and is considerably easier to measure. We expect that it will be a useful proxy when the dynamic pressure and associated turbulent losses are minimized, such as for gradually-varying flow (typical of self-formed pool-riffle channels, where gradually-varying topography minimizes flow separation in the lee of bedforms). Alternatively, the hydrostatic pressure may approximate the near-bed pressure when flow depths are large relative to bedform amplitude, causing the near-bed dynamic pressure to be much less than the static pressure. We examined this issue by comparing the hyporheic flux predicted from the observed near-bed pressure versus that of the hydrostatic pressure.

After construction of the bedform, its topography was measured using a manual point gauge mounted on a trolley fixed to the flume. The topography and water elevation for each discharge were measured to the nearest half-millimeter on a grid with a transverse spacing of 10 cm and a longitudinal spacing of 24 cm.

2.3.3.2. Passive tracer

Sodium chloride (NaCl) and fluorescein were used as tracers to assess solute exchange between in-stream water and pore water. The advantages of NaCl are its low cost and its resistance to decay. The disadvantages include inability to measure low salt concentrations by most conductivity meters, the high temperature coefficient (2% change per ºC), and the small range of linear correlation between concentration and conductivity.

In contrast, fluorescein has a smaller temperature coefficient (-0.36% per ºC) and is detected at very low concentrations (10 parts per trillion), but direct sunlight rapidly destroys it. Because the experiments were conducted in a laboratory flume with very low sunlight and no direct exposure, the latter effect is negligible. The fluorescein was prepared with a concentration of 0.05 $g \cdot l^{-1}$ in a one liter of bottle of tap water covered by a paper wrapper and stored in a closed drawer. One bottle was poured into a bucket containing 1.8 kg of NaCl diluted into 10 l of tap water. The two tracers do not react, and the water was stirred until the salt was completely dissolved. Electrical conductivity of the water was measured using a conductivity meter (Horiba ES-12). At the beginning of each experiment, values were manually recorded every five seconds. When the values remained constant for at least three consecutive points, the time lag was doubled.

Therefore, the time intervals were ten, twenty, forty seconds, then one, two, five, ten, twenty and thirty minutes.

We used a flow-through cell 10-AU Fluorometer (Turner Designs, Inc.) to measure the fluorescein concentration. The fluorometer was calibrated between the fluorescence of the tap water and the fluorescein concentration present in the flume at the initial condition, and the temperature correction was set in our concentration range. Concentration values were averaged every eight seconds and logged every ten seconds.

The tracers were poured into the downstream end of the flume in the highly turbulent section before the water dropped into the sump and entered the pump inlet. This location was chosen to ensure full mixing of the solutes with the water before they entered the flume.

2.3.3.3. Surface grain size and armor layer

After each set of experiments (and before changing the bed morphology), a surface pebble count [*Wolman*, 1954] was made to assess the grading curve of the surface material. The study reach was divided into three zones: riffle, pool, and bar. From each zone 150 particles were randomly selected, by pointing at the bed with a pencil without looking at the bed surface. We measured the intermediate diameter (b-axis) with a caliper and then we assessed the thickness of the armor layer by digging several holes and measuring the depth of armoring. A weak armor layer developed through surface winnowing of fine grains (Figure 2.4), but the rest of the bed remained immobile during the experiments.

2.3.3.4. Hydraulic conductivity of the sediment

Hydraulic conductivity is not only a function of the material composition, but also of the packing and orientation of the particles. In placing the sediment, care was taken to create a fairly homogeneous and isotropic matrix. This was done to provide experimental control, however we recognize that natural channels can be substantially more complex, having heterogeneous sediment mixtures that are commonly anisotropic and possibly influenced by organic matter. These natural complexities can significantly alter subsurface flow properties. At the end of the experiments, we dug transects into the

sediments to verify that there was no settling of fine particles, or substantial heterogeneities. Due to the large requisite volume of material needed to characterize the conductivity of such coarse sediment, and to avoid potential bias caused by disturbing the sediment, we used the entire flume as a permeameter. To measure hydraulic conductivity, we flattened the bed, tilted the flume slope to 0.18%, and opened the valve until a constant discharge was established without creating a free surface flowing over the sediment. The hydraulic conductivity was then determined as

$$K = \frac{Q}{Ai} \qquad \textbf{(2.7)}$$

where Q is the measured discharge, A is the cross-sectional area of saturated sediment, and i is the flume slope (representing the energy gradient). The hydraulic conductivity was found to be 5 $cm \cdot s^{-1}$, as expected for this type of material [*Freeze and Cherry*, 1979].

2.4. Numerical model

The hyporheic flow was modeled using FLUENT 6.0 (FLUENT Inc.), a finite element software package. The study reach was meshed with a grid of three-centimeter sided hexahedral elements. This dimension is larger than the size of sediment pores and at the same time, is small compared to the domain size, allowing appropriate application of Darcy's law [*Hassanizadeh and Gray*, 1979]. We also evaluated the sensitivity of the results to mesh size. Results varied by less than 3% when mesh dimensions were increased or decreased by 30%, which is consistent with FLUENT's definition of mesh independence.

To solve the flow field we need six boundary conditions plus a seventh for dry sections of bars that are not fully submerged. Three boundary conditions were the two flume sidewalls and bottom that were modeled as impervious layers. The boundaries at the bed surface and the vertical ends of the sediment volume were set in FLUENT as pressure inlet boundaries. Exposed sections of bars were modeled as a wall boundary. Once the flow field was generated using Darcy's law, the bed surface was divided into 9 cm^2 sub-areas, and from their centers of gravity a particle was numerically injected, and the particle tracking method was applied to evaluate flow paths and residence times.

Hence, for each sub-area, the exchange flux and residence time were assessed and used to evaluate equations (2.5) and (2.6).

2.5. Experiments

We used tap water instead of Mississippi River water in the experiments since the fluorescein was found to react with some solutes present in the river water, causing the tracer to form a yellow foam in the sump. A second motivation was the high content of organic matter present in the river water. Deposition of organic matter and its infiltration into the sediment could locally alter the hydraulic conductivity, making the porous medium no longer homogeneous and isotropic.

We ensured uniform flow by checking that the water elevations were nearly constant at selected points having one-wavelength spacing. Constant elevations ensure that backwater or acceleration effects at the end of the flume were not present and that the flume was simulating a section of an infinite sequence of pool-riffle units. Then, we siphoned the mini-piezometer tubes with a syringe to remove air bubbles from each line.

The recirculation time of the system was calculated, and the tracers were added at a constant discharge over the time required for a single recirculation. This was done to ensure that no strong longitudinal gradients were formed. We timed the entire experiment with a stopwatch, starting with the moment the tracer was added. At the end of each run, the sediment was cleaned by replacing all of the water in the system with clean water and letting the pump run, rinsing the sediment until the background conductivity values were reached. The cleaning process lasted at least four hours after the end of each experiment.

2.6. Results and discussion

2.6.1. Comparison of salt versus fluorescein tracers

We found that while the fluorescein concentration systematically decreases during each experiment, the salt concentration initially decreases, but then begins to rise again (Figure 2.8). This is due to two phenomena that affect the salt concentration reading: the simple, and probably inadequate, algorithm for temperature correction used by the conductivity meter, and the fact that the meter cannot resolve low salt concentrations,

such as those reached at the end of the experiment. The initial concentrations of NaCl were between 600 and 400 $mg \cdot l^{-1}$, depending on the flowing water volume above the background concentration. The fluorescein and salt tracer concentration curves started diverging after a 15% drop in concentration relative to initial values. NaCl has been widely used for measuring hyporheic exchange [*Marion et al.*, 2002], and it performs well as long as the in-stream concentration remains high and there is not an intense exchange of pore water. However, rapid exchange occurs in our experiments due to the coarse, permeable sediment examined. Consequently, sensitivity becomes an issue in describing the tail of the concentration curve. Adding high concentrations of salt to increase the measurement range is not recommended since salt can create density currents that force gravitationally-induced hyporheic flow.

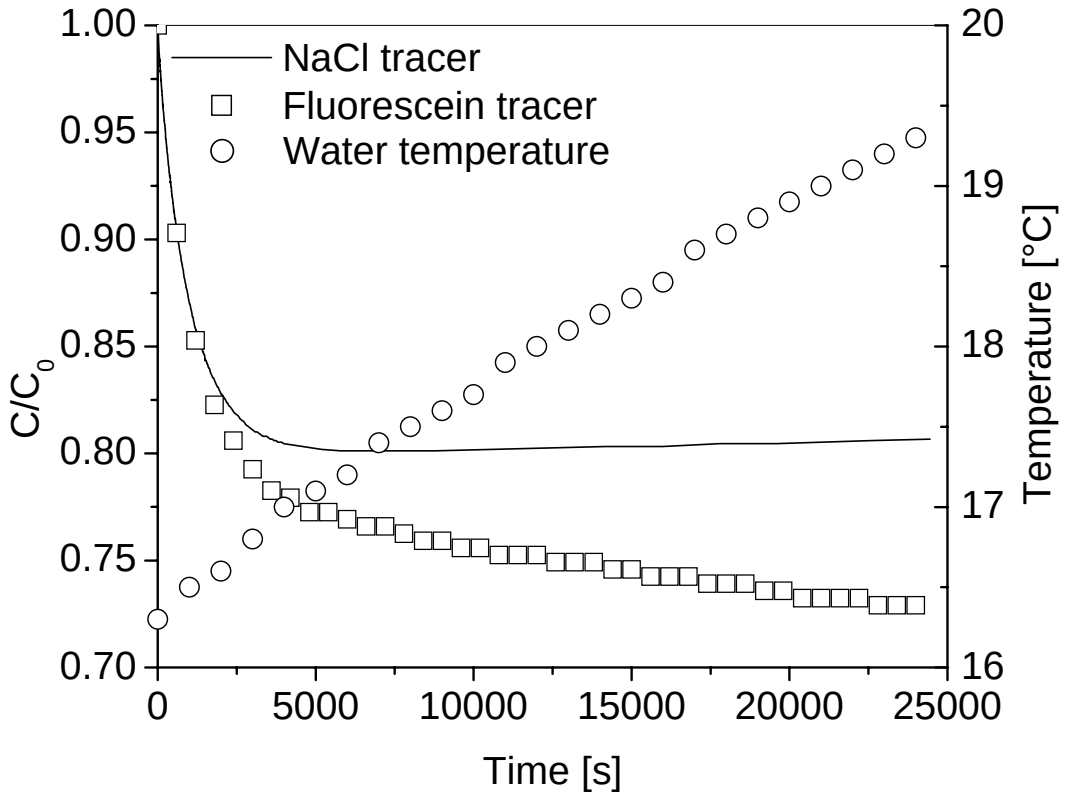

Figure 2.8: Comparison between salt and fluorescein tracers from exp22 (low-amplitude bedform, medium discharge).

2.6.2. Pressure distribution

Figure 2.9 shows an example of longitudinal changes in both the near-bed and hydrostatic pressures over the pool-riffle unit. The tails of the pools (XS 12-17) and the

stoss side of riffles (XS 17-23) tend to have higher near-bed pressure than the lee side of riffles (XS 1-6) and the heads of pools (XS 6-12). Pressure variations are also present laterally along the channel cross section, creating a three-dimensional pressure distribution.

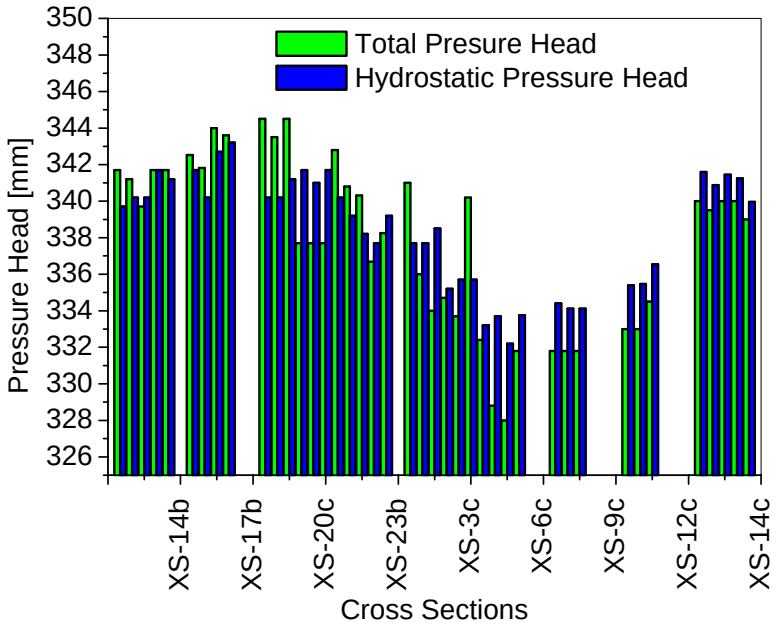

Figure 2.9: Comparison of near-bed total pressure versus hydrostatic pressure for exp6 (large-amplitude bedform, low discharge).

In general, the hydrostatic and near-bed pressure profiles are similar (Figure 2.9), although local discrepancies are observed, particularly for low discharges and high-amplitude bedforms. For those conditions, the area around the riffle crest had much higher Froude numbers than the pool, creating a zone of high instability (hydraulic jumps or surface waves). This area was characterized by vortices and eddies with strong dynamic head at the boundary, generating a pressure distribution different from that described by the local water elevation. Differences between hydrostatic and near-bed pressures may also be due to small surface irregularities (e.g., micro-topography of particle clusters) that create dynamic pressure variations that are detected by the near-bed piezometers, but are too small to substantially affect water-surface elevations and consequent hydrostatic pressures. Moreover, observed differences may be due to the unsteady, pulsating movement of the water surface, which can cause measurement error of the surface elevation. Nevertheless, regions of higher near-bed pressures were also characterized by higher static pressure.

2.6.3. Hyporheic exchange

2.6.3.1. Concentration curves

Figure 2.10 shows in-stream measurements of fluorescein concentration for each experiment normalized by the initial concentration, C_0, and with the data grouped by bedform amplitude. Since the recirculating system was a closed circuit without water leakage or inflow, the observed decay of tracer concentration represents solute mixing with fresh water present in the sediment interstices, confirming that solute mass was transferred from the surface water into the sediment by hyporheic exchange. Figure 2.10 also shows that hyporheic exchange happened in two stages: a rapid exchange that characterizes the initial part of the experiments (steep part of the curve), and a second stage of slow mixing (tail of the curve). Most of the mixing occurred in this first stage, with a 15%-20% decrease in in-stream concentration. This mixing was rapid (occurring in the first 30-60 minutes), and was predominated by hyporheic exchange across the riffles and bars, where short and fast pathlines are located (section 2.6.3.2). The second stage of exchange had a linear and roughly constant rate of decay that persisted for the remainder of each experiment.

We focus first on the results for the low and medium discharges (12.5-21 $l \cdot s^{-1}$, Figure 2.10), where the flume slope was held constant across these experiments. We find that increasing the discharge has a negligible affect on hyporheic exchange for the larger-amplitude bedforms (BD1 and BD75), but causes a decrease in hyporheic exchange (larger C/C_0 values with greater discharge) for the smaller-amplitude bedforms (BD05 and BD03).

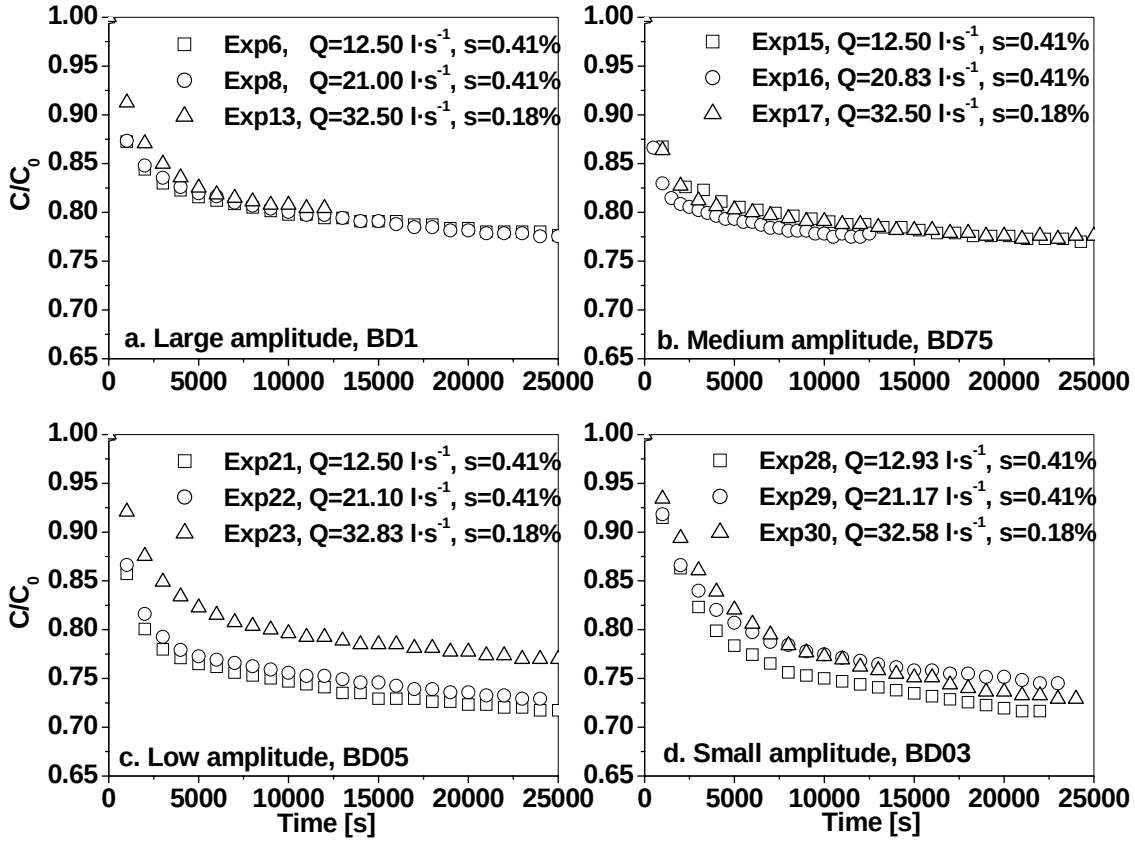

Figure 2.10: Hyporheic exchange of fluorescein for increasing discharge grouped by bedform amplitude (a-d).

This result for pool-riffle channels contrasts with those observed for dune-ripple morphologies [*Elliott and Brooks*, 1997b; *Packman and Bencala*, 1999; *Marion et al.*, 2002] and is likely due to differences in relative bedform size and resultant hydraulics between these two channel types. In dune-ripple channels, the bedforms are entirely submerged and are small compared to the water depth, with a water surface profile that is minimally influenced by local bedform topography and roughness. For such channels, the pressure profile strongly depends on the dynamic pressure, which is a function of mean flow velocity raised to the second power [*Vittal et al.*, 1977], and which increases with greater discharge. Hence, hyporheic flow tends to increase with discharge in dune-ripple channels, contrary to what we observe for our pool-riffle experiments (Figure 2.10). Moreover, because the relative submergence is high in dune-ripple channels, the water surface profile is relatively smooth, minimizing spatial variations in water-surface topography and its influence on flow depth and total pressure.

This differs from pool-riffle channels, in which the total pressure is a function of the effect of bedforms on both the dynamic pressure and the water surface profile (and thus flow depth and the static pressure). The relatively large size and three-dimensional structure of bedforms in pool-riffle channels strongly influence the water-surface topography and consequent pressure distribution. For low discharges or large bedform amplitudes, the water surface meanders around the gravel bars and exhibits water-surface topography that varies both laterally and longitudinally, enhancing the spatial divergence of pressure and the magnitude of hyporheic exchange. On the other hand, for larger discharges or bedform amplitudes that are small relative to flow depth, the water surface shows less variation and less spatial divergence of pressure, particularly across the riffle, where a large pressure drop is present. Consequently, the residence time distribution shortens and the hyporheic flow remains shallow, reducing the amount of pore water mixing (e.g., Figure 2.10d, Experiment 29 vs. 28).

Although we observe reduced hyporheic exchange with increasing discharge for the smaller-amplitude bedforms (Figures 2.10c and 2.10d), changes in discharge for the larger-amplitude bedforms resulted in negligible variation of solute exchange (Figures 2.10a and 2.10b). We hypothesize that this result is due to changes in bedform exposure with discharge, altering the surface area available for hyporheic exchange. As we increased the discharge in our experiments, we observed substantial increases in the exchange area. For example, exchange area increased by 8 and 25%, respectively, across Experiments 6, 8 and 13 (Table 2.2). Consequently, for large bedform amplitudes the reduction in pressure difference over the riffle due to greater discharge and smoother water-surface profiles is counterbalanced by an increase in surface area available for hyporheic exchange, maintaining a nearly constant exchange rate (Figure 2.10a). Bedform exposure and the consequent surface area for hyporheic exchange may be a particularly important control on both the availability and quality of aquatic habitat in pool-riffle channels. Larger bedform size and relatively lower flow depths cause pool-riffle bedforms to be more frequently exposed than lower-gradient channels with dune-ripple morphology. Consequently, the spatial extent and local magnitude of hyporheic exchange in pool-riffle channels will vary seasonally with discharge, creating a highly

diverse habitat that may cause benthic species to adapt to seasonal variations in the character and extent of hyporheic habitat.

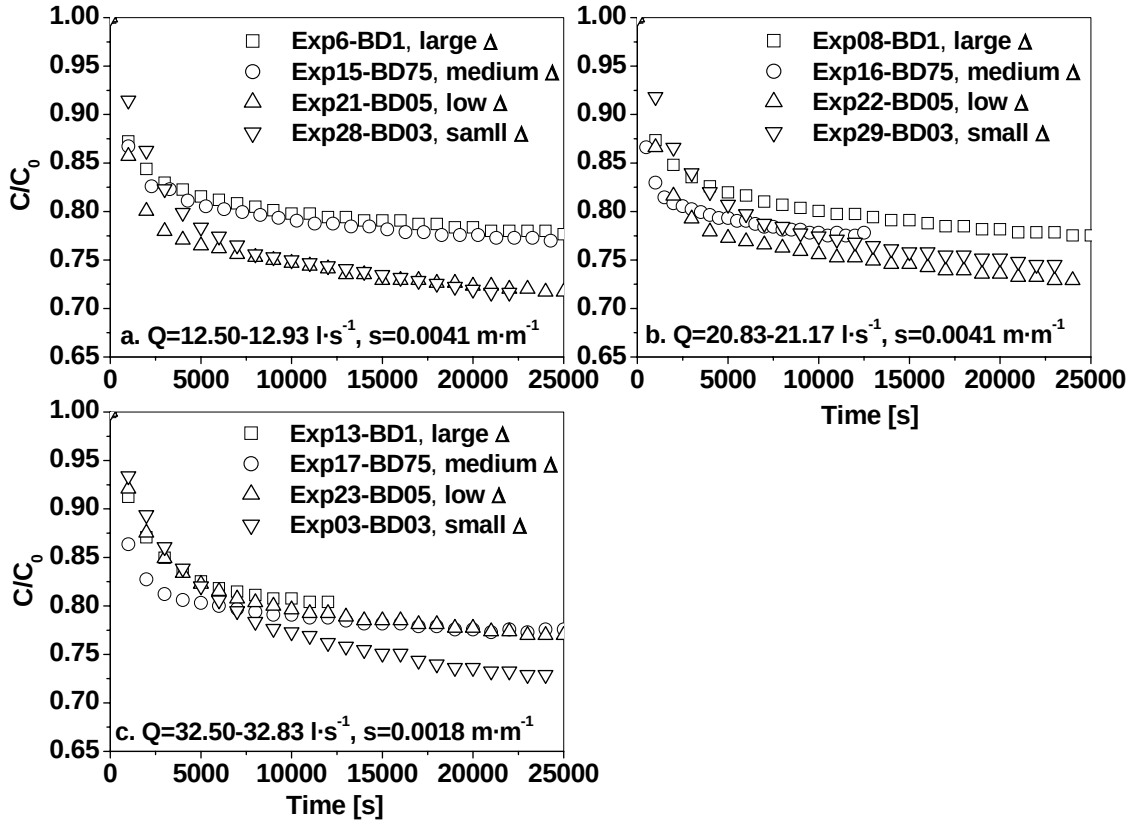

Figure 2.11: Fluorescein exchange for large- to small-amplitude bedforms grouped by constant values of discharge and slope (a-c).

In Figure 2.11, we present the results grouped by discharge and slope, showing the effect of bedform amplitude on hyporheic exchange. Contrary to expectations, for the two lowest discharges we find a systematic increase in hyporheic exchange (lower C/C_0 values) with decreasing bedform amplitude up until bedform BD05, after which there is a decline in hyporheic exchange for the lowest amplitude bedform, BD03 (Figures 2.11a and 2.11b).

We also find that hyporheic exchange is stronger over time for conditions of high discharge and low bedform amplitude (Figure 2.11c, Experiment 3). The magnitude and rate of solute exchange for Experiment 3 is initially low, but the exchange persists longer, and after 2.8 hours the exchange curve crosses those of the other experiments, reaching an overall larger total exchange (Figure 2.11c). In this case, the low-amplitude bedform is submerged by a high discharge, causing both the water-surface and the near-bed pressure

profiles to be smoother than those of the higher-amplitude bedforms, generating less intense downwelling that persists longer.

The above results indicate that bedform amplitude is not the only control on hyporheic exchange. In particular, pool-riffle bedforms have a strong impact on the flow regime; their amplitude affects the surface area available for exchange, and their drag force together with the wetted perimeter control the water-surface profile, depth, and near-bed pressure, all of which are essential components in the hyporheic exchange process. For the two low discharges, bedform BD05 had the better combination of these factors despite its low amplitude, and it consistently generated high total solute exchange (Figures 2.11a and 2.11b). Furthermore, it also had the fastest initial rate of decay at low discharge, but the medium-amplitude bedform (BD75) had the fastest initial exchange for larger discharges (cf. Figures 2.11a and 2.11c). Bedform BD1 had the largest amplitude, but neither the fastest initial exchange nor the largest total exchange for the discharges examined here. This may be due to the smaller surface area available for hyporheic exchange in those experiments, as discussed above.

Together, these observations show that hyporheic exchange in pool-riffle channels depends on a complex interaction of discharge and bedform amplitude. Moreover, the hyporheic exchange observed in our pool-riffle channels was stronger than that previously reported for sand-bed experiments. This is due to the high permeability of our coarse-grained sediment and the strong head gradients created by pool-riffle topography and low relative submergence, suggesting that the river and its underlying aquifer are closely coupled by active hyporheic flow in coarse-grained mountain rivers.

2.6.3.2. Flow paths

We can follow the hyporheic exchange of the solute into the sediment using pathlines to trace the trajectories of particles through the subsurface. Figure 2.12 shows predicted pathlines for Experiment 15 (medium-amplitude bedform, low discharge). Predictions indicate that an intense flux crossed the riffle crest, and that a second one was located at the head of the pool. The figure also shows that hyporheic flow occurs in both downstream and upstream directions, depending on local head gradients. For instance, some pathlines from the middle of the riffle had an upstream direction and went toward

the upstream pool. The pathlines also show that the depth of hyporheic exchange is spatially variable, as is the solute concentration (indicated by the distance between pathlines). High concentrations are localized around the riffle crest were pathlines converge, while lower concentrations (widely spaced pathlines) occur around the pool. Furthermore, a surface enveloping the pathlines could be used to hydraulically define the hyporheic volume, recognizing that the solute concentration and strength of hyporheic exchange vary within this volume.

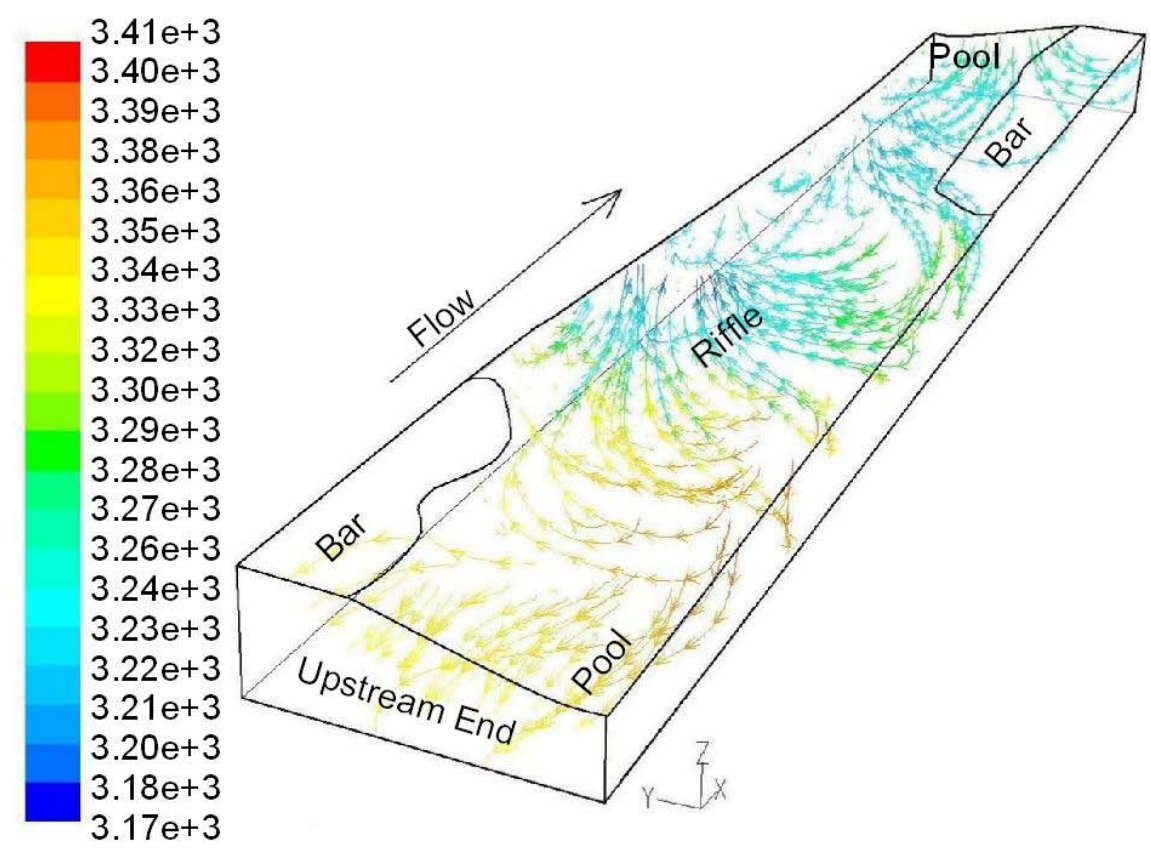

Figure 2.12: Predicted hyporheic pathlines for exp15 (medium-amplitude bedform, low discharge), colored by total pressure (Pascal).

2.6.3.3. Comparison with exchange models

In Figure 2.13, we compare the measured hyporheic exchange to that predicted from two models: *Elliott and Brooks*' [1997a] model for two-dimensional dune-like bedforms, and the three-dimensional pool-riffle model presented in section 2.2. We also compare results for the three-dimensional model driven by the near-bed pressure distribution versus that of the hydrostatic pressure.

We modified *Elliott and Brooks*' [1997a] model for a finite depth of alluvium, d_b, corresponding to the average sediment thickness in the flume defined as the saturated volume of sediment divided by the bed surface area. Additionally, we assumed two-dimensional bedforms having amplitude and wavelength values equivalent to our pool-riffle bedforms (Table 2.2). We find that *Elliott and Brooks*' [1997a] model performs well under some conditions, but significant deviations are noted under other conditions (e.g., Experiments 6 and 22, Figure 2.13). It underestimates the initial exchange, and for long runs it overestimates the downwelling fluxes, giving the erroneous impression that the *RTD* has a long and persistent tail. Nevertheless, it works better than we expected given that it was originally developed for two-dimensional dune-like bedforms. However, results are sensitive to how d_b is defined. For example, the model does not perform as well if d_b is defined as the average value between the sediment depths at the pool bottom and riffle crest.

The three-dimensional pumping exchange model driven by the near-bed pressure predicts the overall hyporheic exchange reasonably well, (Figure 2.13). When the hydrostatic pressure is used as a surrogate for the near-bed pressure, the model does not perform well for high-amplitude bedforms and low discharges, underestimating the exchange (Figure 2.13, panels Exp6, Exp8, Exp15, and Exp16). However, we find that the performance of the hydrostatic model improved by increasing the discharge and by reducing the bedform amplitude (Figure 2.13, moving from left to right panels of a given row, or top to bottom ones of a given column). For conditions of low flow and high bedform amplitude, substantial dynamic pressure variations exist, which are not accounted for by the hydrostatic pressure, making it a poor proxy for the near-bed pressure. Furthermore, in these cases, the water surface exhibited unsteady surface waves above the high velocity core [*Dietrich and Whiting*, 1989], which made the water-surface profile measurements difficult to make and more prone to error (Figure 2.1). However, as flow depth increases relative to bedform amplitude, the static pressure head dominates and can be used as a surrogate for the near-bed pressure. These results indicate that the hydrostatic pressure is a useful proxy for the near-bed pressure only for low bedform amplitudes or high flows (i.e., where topographic effects on hydraulics and hyporheic exchange are minimized).

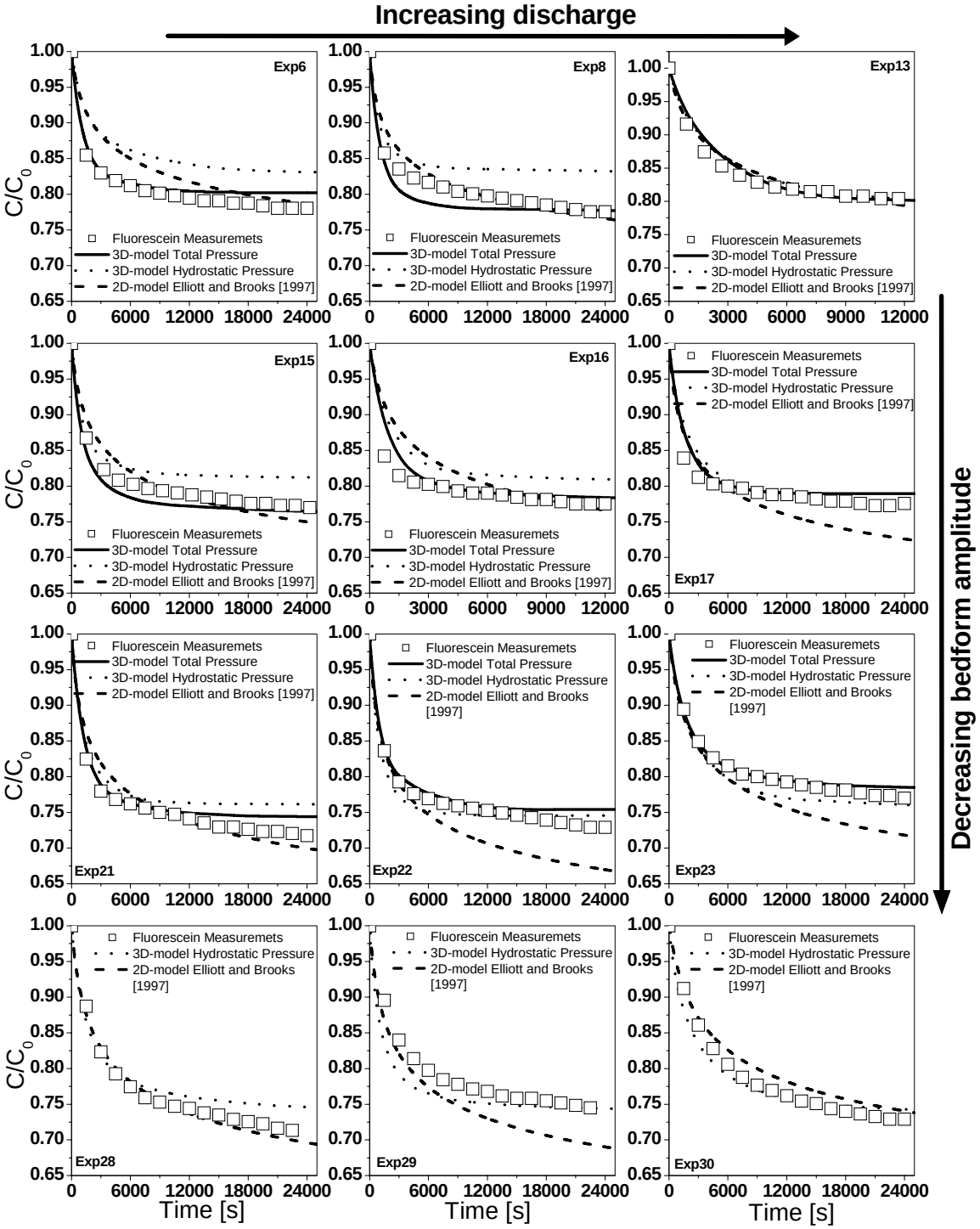

Figure 2.13: Observed versus predicted hyporheic exchange for each experiment. Discharge increases across the panels from left to right, and bedform amplitude decreases across the panels from top to bottom (Tables 2.1 and 2.2). Values of total near-bed head were not measurable in the last set of experiments (exp28, exp29 and exp30).

2.7. Conclusion

We propose a three-dimensional groundwater model to predict the hyporheic flow in gravel pool-riffle channels, in which bed topography variations are captured and the observed pressure profile at the bed surface drives hyporheic flow. Comparison between modeled and measured exchange shows agreement, suggesting that hyporheic exchange in these channels is predominantly driven by bedform-induced advection. Bedforms affect both the near-bed pressure and the surface area available for hyporheic exchange at a given flow. A primary finding of our study is that bedform amplitude in pool-riffle channels is not the only key factor for driving hyporheic exchange; rather, there is a complex interaction between discharge and bedform topography that drives flow regime (wetted perimeter, water-surface profile, depth, near-bed velocity and pressure) and the consequent magnitude and pattern of hyporheic exchange.

We find that *Elliott and Brooks*' [1997a] two-dimensional model for sand-bed rivers with dune-like bedforms does not perform well in gravel-bed rivers with pool-riffle morphology and highly three-dimensional flow characteristics. For dune-ripple morphologies, the relative submergence of the bedform (flow depth relative to bedform amplitude) is high and the water surface is not strongly affected by the bedforms. Changes in pressure are predominantly due to the dynamic pressure and *Elliott and Brooks*' [1997a] model is based on this component of the total pressure. On the other hand, in pool-riffle channels, the water surface responds to bedform shape and amplitude, and the near-bed pressure profile is mainly influenced by the change in water elevation, which affects both the static and dynamic pressures. Moreover, at low flow, unstable standing waves occur downstream of the riffle crest in pool-riffle channels due to flow detachment in the lee of the riffle. These complexities are not recognized in *Elliott and Brooks*' [1997a] model, causing it to perform poorly in such cases.

We also find that the hydrostatic pressure can be substituted for the total near-bed pressure in our three-dimensional model under conditions of high discharge and/or low-amplitude bedforms. However, it does not work well for low flows, where strong surface waves form, below which the near-bed pressure is no longer hydrostatic. Nevertheless, the hydrostatic pressure may provide a useful first-order solution of hyporheic exchange

in field studies of pool-riffle channels where near-bed pressure measurements are difficult to make [e.g., *Baxter and Hauer*, 2000]. Moreover, the hydrostatic model is superior to *Elliott and Brooks*' [1997a] model in predicting locations of upwelling and downwelling and describing the spatial pattern of hyporheic flow.

We also note that all of the models examined here consider only the advective part of the dispersion process; no diffusion mechanism is incorporated. Over short periods, the hyporheic exchange is fully advective, but over longer periods diffusion starts to smooth the concentration gradients within the sediment and to affect the concentration distribution. Prediction errors in the tails of the concentration curves may be due, in part, to exclusion of diffusional exchange in these models. Diffusional processes should be added to the models in cases where low concentrations and/or long periods of observation are of interest.

We find that pool-riffle channels not only have complex surface hydraulics with spatially varying flow depths and velocities that change with discharge, but they also have corresponding spatial and temporal complexity of hyporheic flow, creating a highly diverse environment that may cause benthic species to adapt to seasonal variations in flow. Because of these physical heterogeneities, it is important to have a holistic perspective that links in-stream and hyporheic flows in studies of solute transport and aquatic habitat in pool-riffle channels.

Acknowledgements. This work was supported in part by the STC Program of the National Science Foundation under Agreement Number EAR-0120914, by the USDA Forest Service Yankee Fork Ranger District (00-PA-11041303-071), by the US Department of Education Fund for the Improvement of Postsecondary Education (P116Z010107), and by the USDA Forest Service Rocky Mountain Research Station (03-JV-11222014-060). We also thank the Saint Anthony Falls Laboratory staff, especially the assistance of Sara R. Johnson.

References

Baxter, C. V., and R. F. Hauer (2000), Geomorphology, hyporheic exchange, and selection of spawning habitat by bull trout (*Salvelinus confluentus*), *Can. J. Fish. Aquat. Sci., 57*, 1470-1481.

Bencala, K. E., and R. A. Walters (1983), Simulation of solute transport in a mountain pool-and-riffle stream: a transient storage model, *Water Resources Research, 19*(3), 718-724.

Bjornn, T. C., and D. W. Reiser (1991), Habitat requirements of salmonids in streams, in *Influences of forest and rangeland management on salmonid fishes and their habitat*, edited by W. R. Meehan, pp. 83-138, American Fisheries Society Special Publication 19, Bethesda, Md.

Buffington, J. M., T. E. Lisle, R. D. Woodsmith, and S. Hilton (2002), Controls on the size and occurrence of pools in coarse-grained forest rivers, *River Research and applications, 18*, 507-531.

Buffington, M. J., and D. R. Montgomery (1999), Effects of hydraulic roughness on surface textures of gravel-bed rivers, *Water Resources Research, 35*(11), 3507-3521.

Carling, P. (1992), In-stream hydraulics and sediment transport, in *The Rivers Handbook*, vol. 1, edited by P. Carlow and G. E. Petts, pp. 101-125, Blackwell Scientific Publications, Oxford.

Carling, P., and H. G. Orr (2000), Morphology of riffle-pool sequences in the River Severn, England, *Earth Surface Processes and Landforms, 25*, 369-384.

Coble, D. W. (1961), Influence of water exchange and dissolved oxygen in redds on survival of steelhead trout embryos, *Transaction of the American Fisheries Society, 90*, 469-474.

Colombini, M., G. Seminara, and M. Tubino (1987), Finite-amplitude alternate bars, *Journal Fluid Mechanics, 181*, 213-232.

Cooper, A. C. (1965), The effect of transported stream sediments on the survival of sockeye and pink salmon eggs and alevin, in *Bulletin 18*, International Pacific Salmon Fisheries Commission, New Westminster, B.C., Canada.

Dagan, G. (1979), The generalization of Darcy's Law for nonuniform flow, *Water Resources Research, 15*(1), 1-7.

Dietrich, W. D., and P. J. Whiting (1989), Boundary shear stress and sediment transport in river meanders of sand and gravel, in *River Meandering, Water Resources Monograph.*, vol. 12, edited by S. Ikeda and G. Parker, pp. 1-50, AGU, Washington D.C.

Edwards, R. T. (1998), The Hyporheic Zone, in *River Ecology and Management: Lessons from the Pacific Coastal Ecoregion*, edited by R. J. Naiman and R. E. Bilby, pp. 399-429, Springer-Verlag, New York.

Elliott, A., and N. H. Brooks (1997a), Transfer of nonsorbing solutes to a streambed with bed forms: Theory, *Water Resources Research, 33*(1), 123-136.

Elliott, A., and N. H. Brooks (1997b), Transfer of nonsorbing solutes to a streambed with bed forms: Laboratory experiments, *Water Resources Research, 33*(1), 137-151.

Findlay, S., W. Strayer, C. Goumbala, and K. Gould (1993), Metabolism of streamwater dissolved organic carbon in the shallow hyporheic zone, *Limnology and Oceanography, 38*, 1493-1499.

Freeze, R. A., and J. A. Cherry (1979), *Groundwater*, Prentice Hall, Englewood Cliffs, New Jersey, USA.

Gibert, J., J. A. Stanford, M. J. Dole-Oliver, and J. V. Ward (1994), Basic attributes of groundwater ecosystems and prospects for research, in *Groundwater ecology*, edited by J. Gilbert, D. L. Danielpol, and J. A. Standford, 8-40, Academic Press, San Diego.

Harvey, J. W., and K. E. Bencala (1993), The effect of streambed topography on surface-subsurface water exchange in mountain catchments, *Water Resources Research, 29*, 89-98.

Hassanizadeh, M. S., and W. G. Gray (1979), General conservation equations for multi-phase systems: 1. Averaging procedure, *Advances in Water Resources, 2*, 131-144.

Hassanizadeh, M. S., and W. G. Gray (1987), High velocity flow in porous media, *Transport in porous media, 2*, 521-531.

Keller, E. A., and W. N. Melhorn (1978), Rhythmic spacing and origin of pools and riffles, *Geological Society of American Bulletin, 89*, 723-730.

Lanzoni, S., and M. Tubino (1999), Grain sorting and bar instability, *Journal Fluid Mechanics, 393*, 149-174.

Leopold, L. B., M. G. Wolman, and J. P. Miller (1964), *Fluvial Processes in Geomorphology*, Freeman, W.H., San Francisco.

Levy, D. A., and T. L. Slaney (1993), A review of habitat capability for salmon spawning and rearing, B.C. Resources Inventory Committee (RIC) c/o Habitat Management Division Dept. of Fisheries and Oceans, Vancouver B.C.

Lisle, T. E., and S. Hilton (1992), The volume of fine sediment in pools: an index of sediment supply in gravel-bed streams, *Water Resources Bulletin, 28*(2), 371-382.

Marion, A., M. Bellinello, I. Guymer, and A. I. Packman (2002), Effect of bed form geometry on the penetration of nonreactive solutes into a streambed, *Water Resources Research, 38*(10), 1209, doi:10.1029/2001WR000264.

Mendoza, C., and D. Zhou (1992), Effects porous bed on turbulent stream flow above bed, *Journal of Hydraulic Engineering.*

Montgomery, D. R. (2003), *King of Fish: The Thousand-Year Run of Salmon*, Westview Press, Boulder, CO, 290 p.

Montgomery, D. R., and J. M. Buffington (1997), Channel-reach morphology in mountain drainage basins, *Geological Society of American Bulletin, 109*, 596-611.

Nehlsen, W., J. E. Williams, and J. A. Lichatowich (1991), Pacific salmon at the crossroads: stocks at risk from California, Oregon, Idaho, and Washington, *Fisheries, 16*(2), 4-21.

Packman, A. I., and K. E. Bencala (1999), Modeling methods in study of surface-subsurface hydrological interactions, in *Stream and Ground Waters*, edited by J. B. Jones and P. J. Mulholland, pp. 45-80, Academic, San Diego, California.

Packman, A. I., N. H. Brooks, and J. J. Morgan (2000), A physicochemical model for colloid exchange between a stream and a sand streambed with bed forms, *Water Resources Research, 36*(8), 2351-2361.

Savant, A. S., D. D. Reible, and L. J. Thibodeaux (1987), Convective transport within stable river sediments, *Water Resources Research, 23*(9), 1763-1768.

Stanford, J. A., and J. V. Ward (1993), An ecosystem perspective of alluvial rivers: connectivity and the hyporheic corridor, *Journal of the North American Benthological Society, 12*, 48-60.

Triska, F. J., J. H. Duff, and R. J. Avanzino (1993a), Patterns of hydrological exchange and nutrient transformation in the hyporheic zone of a gravel bottom stream: examining terrestrial-aquatic linkages, *Freshwater Biology, 29*, 259-274.

Triska, F. J., J. H. Duff, and R. J. Avanzino (1993b), The role of water exchange between a stream channel and its hyporheic zone in nitrogen cycling at the terrestrial-aquatic interface, *Hydrobiologia, 251*, 167-184.

Triska, F. J., V. C. Kennedy, R. J. Avanzino, G. W. Zellweger, and K. E. Bencala (1989), Retention and transport of nutrients in a third-order stream: channel processes, *Ecology, 70*, 1894-1905.

Tubino, M. (1991), Growth of alternate bars in unsteady flow, *Water Resources Research, 27*(1), 37-52.

Vittal, N., K. G. Ranga Raju, and R. J. Garde (1977), Resistance of two-dimensional triangular roughness, *Journal Hydraulic Research, 15*(1), 19-36.

Wolman, M. G. (1954), Method of sampling coarse river bed material, *Eos (Transactions, American Geophysical Union), 35*, 951-956.

Chapter 3.

EFFECTS OF PHYSICAL CHARACTERISTICS ON HYPORHEIC FLOW IN POOL-RIFFLE CHANNELS[2]

Gravel-bed rivers are highly complex, diverse ecosystems where micro-invertebrates dwell and salmonid species spawn and rear in the first stage of their life. Hyporheic flow keeps this environment aerobic and enhances the solute exchange between the river and the riverbed. In this work, we investigate the effects of bed topography, groundwater flow velocity, depth of alluvium, hydraulic conductivity and flow regime on hyporheic flow in pool-riffle reaches, and we propose two empirical formulae to predict the storage area and storage exchange coefficients used in the Transient Storage Model. Hyporheic exchange is predicted with a three-dimensional pumping model, and hyporheic flow is modeled as a Darcy flow. We find that bedform amplitude, flow regime, and permeability of the medium are important factors of the hyporheic exchange. Depth of alluvium has a significant effect on hyporheic flow when

[2] Co-authored paper by Daniele Tonina and John M. Buffington, to be submitted to *Water Resources Research*.

its depth is less than half of the bedform wavelength. Moreover, groundwater flows higher than 10^{-4} $m \cdot s^{-1}$ reduce the hyporheic volume and residence time distribution.

3.1. Introduction

Most rivers are surrounded by saturated sediment with high permeability, which forms the hyporheic zone. The extent of this zone has been defined in many ways, but essentially, it is identified by the percent of river water present in the sediment [*Triska et al.,* 1989]. Laterally, this volume can extend from between a few meters to several hundred meters away from the river into the flood plain. Moreover, paleochannels can create preferential flow paths through alluvial valleys, rapidly conveying hyporheic flow away from the stream, and potentially increasing the lateral and longitudinal paths of the flow before it rejoins the downstream channel [*Harvey and Bencala,* 1993; *Kasahara and Wondzell,* 2003]. Less information is available about the vertical extent of hyporheic flow, a factor that will be addressed here.

Hyporheic flow possesses unique chemical and biological properties stemming from the mixing between groundwater and river water. Groundwater is usually low in oxygen and rich in reduced elements, with relatively constant temperature that is not strongly influenced by daily and seasonal variations. In contrast, river water is well oxygenated, rich in oxidized elements, and greatly affected by surrounding conditions. Furthermore, in-stream water properties are more variable due to rapid response to external input.

This mixing creates a stratified biological environment [*Grimm and Fisher,* 1984], whose gradient depends on the extent and amount of exchange between surface and subsurface waters. Benthic, hyporheic, and groundwater species temporarily or permanently dwell in the hyporheic zone [*Reeves et al.,* 1998]. Salmonids use well-oxygenated, near-surface hyporheic zones in gravel-bed rivers as spawning areas to lay their eggs for incubation. After hatching, the alevins rear in the gravel before emerging [*Levine and Salvucci,* 1999].

Hyporheic exchange also advects suspended and dissolved matter carried by the river into the surrounding sediment [*Elliott and Brooks,* 1997b, a; *Packman et al.,* 2000]. Previous laboratory studies with dune-like sand-bed morphology show that this advective

process is much stronger than molecular diffusion, and that variations in bed topography create pressure head differences on the riverbed that trigger hyporheic flow [*Savant et al.*, 1987; *Elliott and Brooks*, 1997b, a; *Packman et al.*, 2000; *Marion et al.*, 2002]. Areas of the riverbed with near-bed high pressure are characterized by downwelling fluxes in which water enters the sediment, and areas with near-bed low pressure contain upwelling fluxes in which water enters the river [*Vittal et al.*, 1977; *Savant et al.*, 1987]. Dunes are typically characterized by a high-pressure zone on their stoss side and a low-pressure area on their lee side caused by flow separation at the dune crest [*Vittal et al.*, 1977]; this pressure differential drives hyporheic flow. A different type of mixing mechanism takes place when bedload transport is active in these rivers. Bed erosion releases subsurface pore water, and sediment entrains river water during the deposition stage. This mechanism is known as turnover [*Elliott and Brooks*, 1997b, a]. Hyporheic flow develops over scales ranging from channel-unit morphology (tenths to tens of meters, at the scale of individual pools and riffles) to reach scale (tens to hundreds of meters) [*Edwards*, 1998]. At large scales, changes in river slope, confinement, and the presence of knickpoints generate convective flows into and out of the sediment [*Harvey and Bencala*, 1993; *Baxter and Hauer*, 2000].

In mountain gravel-bed rivers, substantial bedload transport is relatively infrequent, occurring mainly during near-bankfull flows that are typically short in duration. Additionally, large bedforms and coarser sediment characterize these rivers, thus the turnover process is negligible at low flows. Mountain gravel-bed rivers commonly have a pool-riffle morphology, with riffles creating oblique, transverse obstructions that alternate downstream with pools, thereby influencing channel hydraulics and near-bed pressure gradients that drive hyporheic flow [*Tonina and Buffington*, submitted (Chapter 2)]. Few studies have examined hyporheic exchange in gravel pool-riffle channel. *Storey et al.* [2003] analyzed the effect of hydraulic conductivity and aquifer gradient, but pool-riffle pairs were treated as two-dimensional features. In our work, bedforms are fully three-dimensional, with the wetted surface area of the riverbed dependent on flow regime, a characteristic that is lost in two-dimensional analysis. Additionally, mountain rivers show a wide range of pool-riffle dimensions, flow regimes, depths of alluvium, hydraulic conductivities of sediment, and groundwater flow velocities

(where groundwater refers to the deeper aquifer flow bounding the topographically-induced hyporheic flow). Here, we use a three-dimensional pumping exchange model [*Tonina and Buffington*, submitted (Chapter 2)] to examine the effects of these factors on the magnitude, extent, and residence time of the hyporheic flow. Channel characteristics and stream hydraulics are based on a set of earlier flume experiments [*Tonina and Buffington*, submitted (Chapter 2)]. We also apply the results of our current analysis to the Transient Storage Model [*Bencala and Walters,* 1983], which is commonly used to predict riverine solute transport. Specifically, we formulate physically-based predictions of the exchange coefficient and the storage zone parameters of that model; values that normally require field calibration.

3.2. Methods

We used near-bed pressure distributions measured in a set of flume experiments with pool-riffle morphology to define the boundary conditions for the hyporheic flow model [*Tonina and Buffington*, submitted (Chapter 2)]. The model is a three-dimensional groundwater simulation based on Darcy's law. During the flume experiments, the bedforms were stationary and there was no appreciable sediment transport, except for the development of an armor layer by winnowing of fine particles from the surface, which ended before our measurements of hyporheic exchange.

3.2.1. Flume experiments

We molded a set of pool-riffle morphologies with a constant bedform wavelength, λ, of 5.52 m and four amplitudes of 12, 9, 6 and 3.6 cm (identified as BD1, BD75, BD05, BD03) in the tilting-bed flume at Saint Anthony Falls Laboratory [*Tonina and Buffington*, submitted (Chapter 2)]. The bedform wavelength corresponds to six flume widths, which is within the typical range of values reported for self-formed pool-riffle channels [e.g., *Leopold et al.*, 1964]. Moreover, values of the ratio between bedform amplitude and wavelength used in our experiments (0.007-0.022, riffle crest; 0.014-0.044, bar top) are typical for this type of channel [*Buffington and Montgomery,* 1999]. We define bedform amplitude as the residual pool depth (difference in elevation between the riffle crest and the bottom of the pool [*Lisle and Hilton,* 1992]).

To analyze the effect of flow regime, we ran three discharges, 12.5, 21, and 32.5 $l \cdot s^{-1}$, over each bedform and used two bed slopes, 0.0041 $m \cdot m^{-1}$ for the two lowest discharges, and 0.0018 $m \cdot m^{-1}$ for the highest discharge, which ensured that the bars were submerged. Our experiments are mostly for low flow, when bedforms are not entirely submerged yet, and when discharge strongly affects water surface elevation and flow depth, which is the most common scenario in mountain rivers, where gravel bars are inundated only during rare large flood events.

During each experiment, we recorded the water surface elevation and the pressure distribution at the sediment interface by placing mini-piezometers over one pool-to-pool unit. A point gauge mounted on the flume was used to measure the bathymetry of the bedforms. The average sediment depth, defined as the fully saturated sediment volume divided by the riverbed surface, was approximately 0.29 m (Table 3.1). The hydraulic conductivity of the sediment was measured by using the flume as a permeameter where a constant head was maintained in the head tank, and was found to be 5 $cm \cdot s^{-1}$. Further information about the experiments can be found in the work of *Tonina and Buffington* [submitted (Chapter 2)].

Table 3.1: Experimental conditions

	Mean sediment depth [m]	**Bedform amplitude [m]**		**Mean water depth [m]**	**Mean wetted width [m]**	**Mean velocity [$m \cdot s^{-1}$]**	**Slope [$m \cdot m^{-1}$]**	**Discharge [$l \cdot s^{-1}$]**
Exp6	0.287	0.24		0.065	0.68	0.282	0.0041	12.5
Exp8	0.290	0.24	BD1	0.075	0.73	0.384	0.0041	21
exp13	0.295	0.24		0.104	0.85	0.369	0.0018	32.5
exp15	0.289	0.18		0.056	0.73	0.308	0.0041	12.5
exp16	0.291	0.18	BD75	0.064	0.79	0.413	0.0041	20.83
exp17	0.293	0.18		0.087	0.89	0.421	0.0018	32.5
exp21	0.291	0.12		0.044	0.77	0.365	0.0041	12.5
exp22	0.292	0.12	BD05	0.053	0.87	0.46	0.0041	21.1
exp23	0.292	0.12		0.086	0.9	0.425	0.0018	32.83
exp28	0.291	0.072		0.039	0.9	0.367	0.0041	12.93
exp29	0.291	0.072	BD03	0.052	0.9	0.452	0.0041	21.17
exp30	0.291	0.072		0.082	0.9	0.442	0.0018	32.58

3.3. Groundwater simulations

A finite element model, FLUENT (Fluent Inc.), was used to model the hyporheic flow with Darcy's law, which describes flow through porous media when the flow has low Reynolds numbers and convective accelerations are negligible [*Dagan,* 1979]. In this case, the flow field can be evaluated by solving the following set of equations in a three-dimensional domain:

$$\nabla p_x = \sum_{j=1}^{3} \frac{\mu}{\alpha_{x\,j}} v_j$$
$$\nabla p_y = \sum_{j=1}^{3} \frac{\mu}{\alpha_{y\,j}} v_j \qquad \textbf{(3.1)}$$
$$\nabla p_z = \sum_{j=1}^{3} \frac{\mu}{\alpha_{z\,j}} v_j$$

where μ is the dynamic fluid viscosity, α_{ij} is the permeability tensor of the porous formation, and v_i are the velocity components in the three principal directions. Darcy's law is applicable over a volume that is larger than the microscopic characteristic length of the medium, represented by the pore diameter [*Hassanizadeh and Gray*, 1979]. Therefore, we chose a mesh size for our numerical simulations that was small enough to obtain a good resolution of the flow field, but large enough to satisfy Darcy's averaging of the microscopic quantities of the porous medium.

The numerical domain is defined by seven boundaries. The flume walls and bottom, and the dry part of the bars are represented as impervious layers. Additionally, the upstream and downstream ends of the flume are set as periodic boundaries. The final boundary is the sediment-river interface, with boundary conditions determined from the near-bed pressure profile measured from the mini-piezometers, except for the experiments with the small amplitude bedform, BD03, when hydrostatic pressures were used.

To analyze the effect of alluvium depth and the vertical position of an impervious layer, the numerical domain was created with three alluvial depths of 1λ, 0.5λ, and 0.05λ, where λ is the bedform wavelength. Moreover because hydraulic conductivity can change vertically [*Rus et al.,* 2001], we investigated the effects of an exponential decrease of *k*

between 0.05 $m \cdot s^{-1}$ (highly permeable) and 10^{-6} $m \cdot s^{-1}$ (low permeability) below a homogeneous (highly permeable) near-surface layer that is 20 cm deep and encompasses the bedform volume.

The groundwater velocity was changed by imposing the Pressure Gradient option ($Pa \cdot m^{-1}$) in FLUENT, and the particle tracking method estimated the residence time of the solute. In FLUENT, we used the pathline option for particle tracking of weightless particles that are advectively transported by the flow. At the riverbed, we released a set of particles, and the transit time through the sediment was recorded. Moreover, we used the surface which envelopes the particle trajectories (pathlines) together with the wetted riverbed surface to define the hyporheic volume. Particle trajectories that are lost to the deep aquifer and that do not re-emerge at the riverbed within our numerical domain are excluded from the hyporheic volume. The amount excluded is typically small (less than 1% of the total flux entering the riverbed surface).

3.4. Residence time distribution

The residence time distribution is defined as the cumulative probability that a tracer entering the bed at position (x, y) at time t_0 remains in the bed longer than time τ, and it is described by the relation:

$$R_T(x, y, \tau) = \begin{cases} 1 & \tau \le T \\ 0 & \tau > T \end{cases} \qquad \textbf{(3.2)}$$

where T is the residence time. Since the downwelling flux is a function of position (x, y), we defined the weighted residence time distribution, *RTD*, by weighting R_T by the local downwelling flux q over a representative area. In our simulations, the flow conditions replicate themselves over each pool-riffle sequence, thus the representative surface area is that of the wetted pool-to-pool bathymetry, W_p. The *RTD* is calculated using the following equation:

$$RTD(\tau) = \frac{1}{W_p \, \bar{q}} \int_{W_p} q(x, y) \; R_T(\tau, x, y) \; dx \, dy \qquad \textbf{(3.3)}$$

where $\bar{q}$ is the average downwelling flux over W_p, and q is the local downwelling flux. Our model is based on the two-dimensional framework developed by *Elliott and Brooks* [1997a, b].

3.5. Results and discussion

3.5.1. Effects of alluvial depth, flow regime and bedform amplitude on hyporheic dynamics

3.5.1.1. Mean hyporheic depth

To estimate the vertical range of the hyporheic flow, we define the mean hyporheic depth as the total hyporheic volume divided by the wetted bathymetry of the riverbed. Figure 3.1 shows mean hyporheic depth as a function of depth of alluvium and experiment set up (bedform amplitude and discharge combination) for constant hydraulic conductivity (k=0.05 m·s^{-1}). Inspection of the figure shows that bedform amplitude affects the mean hyporheic depth for deep alluvium (0.5-1 λ). The bedforms with the two largest amplitudes (large and medium amplitude) have the deepest hyporheic flow, which occurs at low flow when the near-bed pressure differential is larger [*Tonina and Buffington*, submitted (Chapter 2)]. However, when the impervious layer is shallow, the alluvial depth above it confines and determines the vertical extent of the hyporheic flow. For example, mean hyporheic depth takes a uniform value regardless of bedform amplitude for shallow alluvium (Figure 3.1, 0.05λ). Therefore, deep alluvium allows the hyporheic volume to develop vertically without constrains, while shallow alluvium restricts the hyporheic volume to a near-surface area.

The effect of bedform amplitude also depends on discharge, flow regime, and degree of bedform submergence [*Tonina and Buffington*, submitted (Chapter 2)]. When bedforms are partially submerged (large, medium and low amplitude bedforms), an increase of discharge causes a reduction in hyporheic depth, all other factors being constant. The reason for this behavior lies in the reduction of pressure differences along the streambed as the bedforms become submerged at higher discharges, reducing their influence on the water-surface profile.

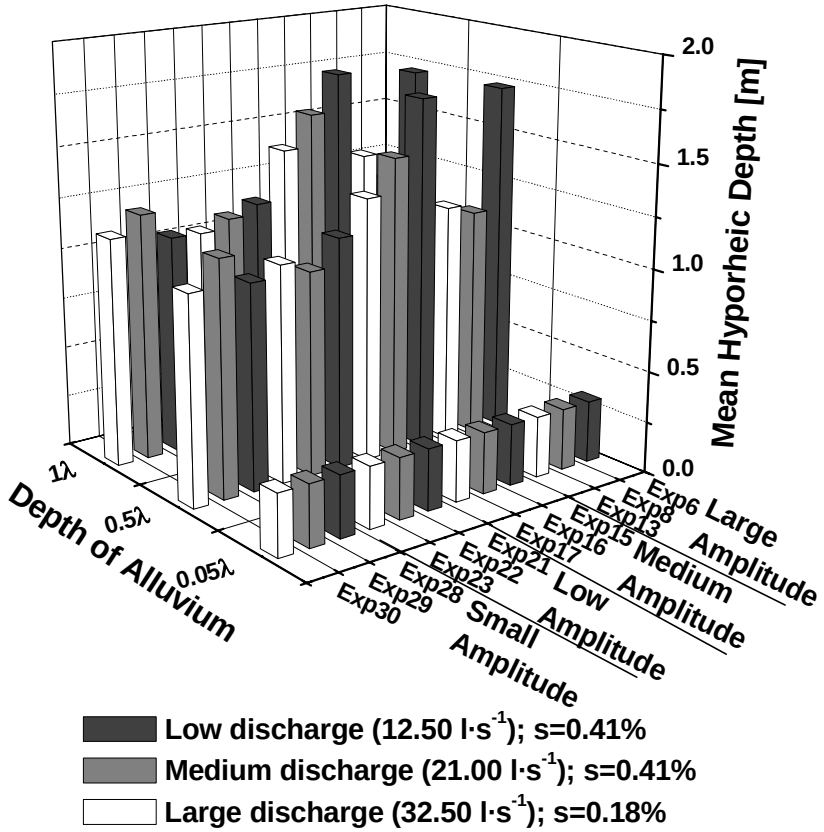

Figure 3.1: Mean hyporheic depth as a function of flow regime, bedform amplitude and depth of alluvium.

Additionally higher flows inundate more of the bedform, altering the upwelling and downwelling areas, the extent and location of which depend on the near-bed pressure profile. Because the experiment with the largest discharge had a lower gradient (slope of 0.18%), it shows a smaller mean hyporheic depth. This suggests that bed slope, i.e. energy slope, influences the hyporheic depth by controlling the river hydraulics. For given values of channel resistance and discharge, lower slopes generate slower currents with deeper flows, which are less affected by pool-riffle amplitude, resulting in less bedform-induced exchange.

The effects of flow regime and bedform amplitude on hyporheic depth become negligible when the impervious layer interacts with the hyporheic flow, in which case the depth of alluvium limits the mean hyporheic depth (Figure 3.1).

3.5.1.2. Residence time

Figure 3.2 shows box plots of the residence time distribution and its mean value for deep (1 λ) versus shallow (0.05 λ) alluvium. The weighted residence time distribution, *RTD*, does not change significantly between 1λ and 0.5λ, when the impervious layer is deeper than the hyporheic flow and, therefore, is not reported in the figures.

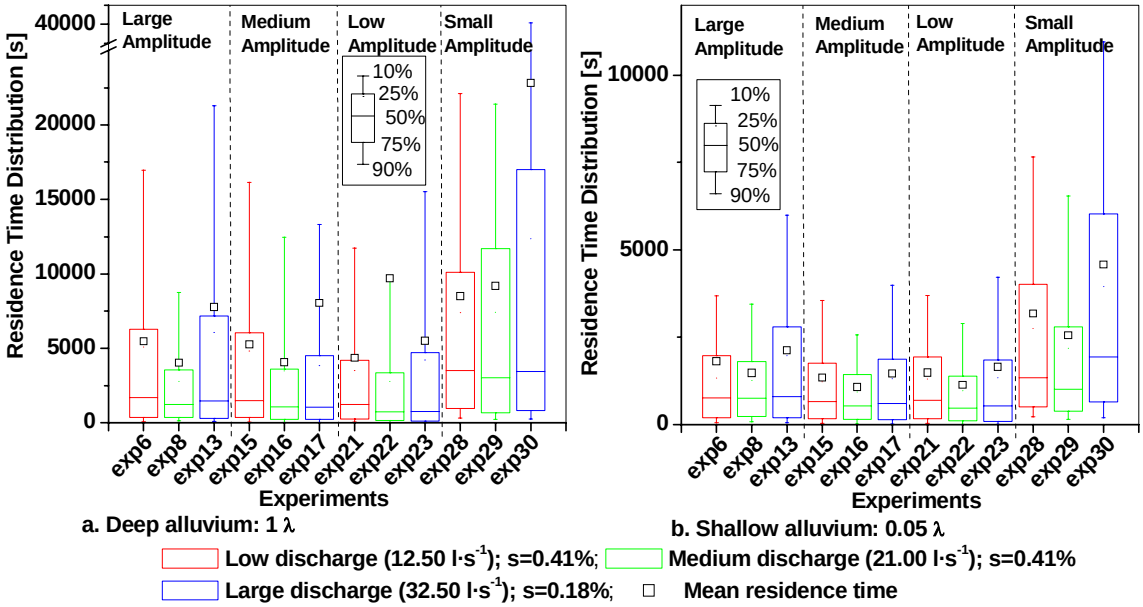

Figure 3.2: Residence time distribution (whiskers and box labels from top to bottom are 10%, 25%, 50%, 75% and 90%) and mean residence time (square) as functions of flow regime, bedform amplitude and alluvial depth for a) deep alluvium and b) shallow alluvium. Please note the difference in scale between (a) and (b).

Figure 3.2a shows that an increase in discharge (low and medium discharge experiments) causes a reduction in *RTD* for the three largest bedforms, keeping all other factors constant. Moreover, *RTD* decreases with lower bedform amplitudes up to low-amplitude bedform. The small-amplitude bedform shows a wider residence time distribution, which increases with discharge for deep alluvium (exp 28-30, Figure 3.2a). The simulations with low slopes and large discharge create longer residence times due to slow intra-gravel velocities (Figure 3.2, exp 13, 17, 23, 30). When the depth of alluvium is shallow, there is a strong reduction in the residence time distribution (cf. Figure 3.2a to Figure 3.2b), and in-stream water resides in the sediment for less time with larger discharge.

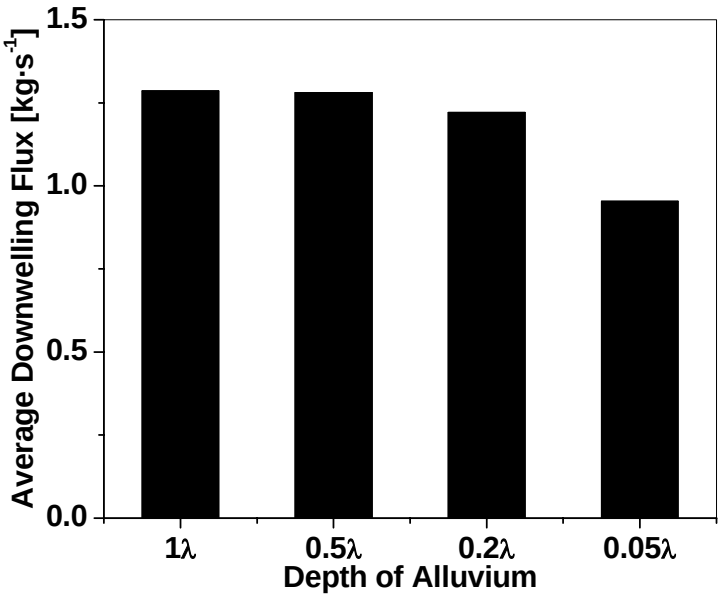

Figure 3.3: Average downwelling flow as a function of alluvial depth for experiment 6, large bedform amplitude and low discharge.

3.5.1.3. Average downwelling flow

Shallow alluvium causes less downwelling flux than deeper alluvium (Figure 3.3) since a larger volume of sediment is available for developing hyporheic flow. The change is negligible between 1λ and 0.5λ, when the impervious layer is deeper than the hyporheic flow (Table 3.2).

Table 3.2: Percentage change in downwelling flux and mean hyporheic depth as a function of alluvium thickness.

		Downwelling flux, 1λ to 0.5λ	Downwelling flux, 0.5λ to 0.05 λ
	exp6	0%	-25.66%
BD1	**exp8**	0%	-20.62%
	exp13	0%	-17.61%
	exp15	0%	-26.04%
BD075	**exp16**	0%	-23.80%
	exp17	0%	-18.31%
	exp21	0%	-19.77%
BD05	**exp22**	0%	-15.55%
	exp23	0%	-11.93%
	exp28	0%	-29.05%
BD03	**exp29**	0%	-27.92%
	exp30	0%	-17.91%

However, there is a 12-29% decrease in average downwelling flux when the depth of alluvium is reduced from 0.5λ to 0.05λ (Figure 3, Table 2). River discharge has a smaller effect on the downwelling flow (Table 3.2, cf. percent change between experiments).

The amount of water that enters the hyporheic volume and remains in the sediment for a given time is a function of the residence time distribution and of the downwelling flux. This is particularly important for chemical reactions and biological transformations that occur within the sediment; for example, nitrification and denitrification processes need a certain amount of time to develop.

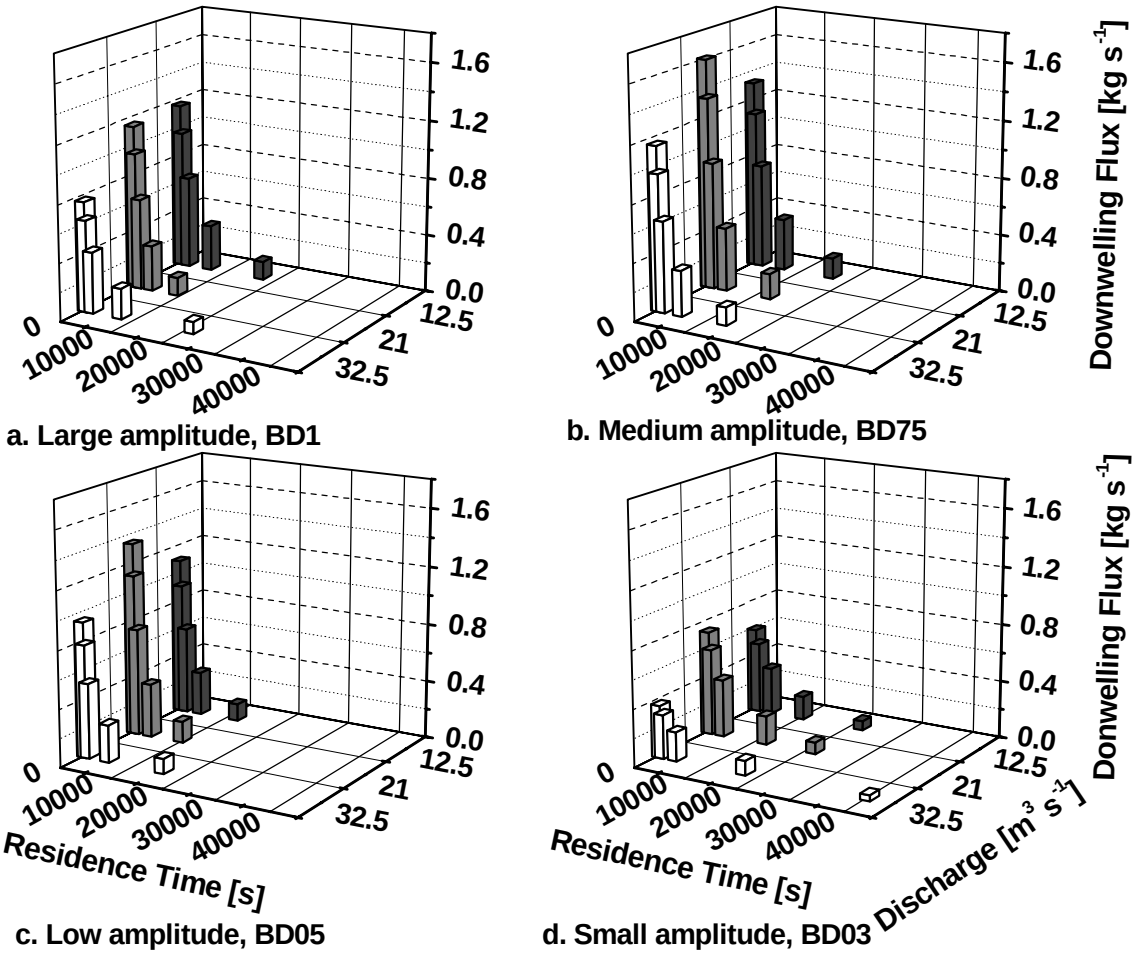

Figure 3.4: Downwelling flux at 90, 75, 50, 25, and 10% of the residence time distribution for 1λ deep homogeneous alluvium. White, gray and dark gray shade defines large, medium, and small discharges, respectively.

Depth of alluvium has a strong impact on the time an amount of in-stream water resides in the sediment. Figures 3.4 and 3.5 show the downwelling fluxes at 90, 75, 50, 25, and 10% of the residence time distribution as a function of discharge for the four bedform amplitudes and for deep (Figure 3.4) versus shallow (Figure 3.5) alluvium.

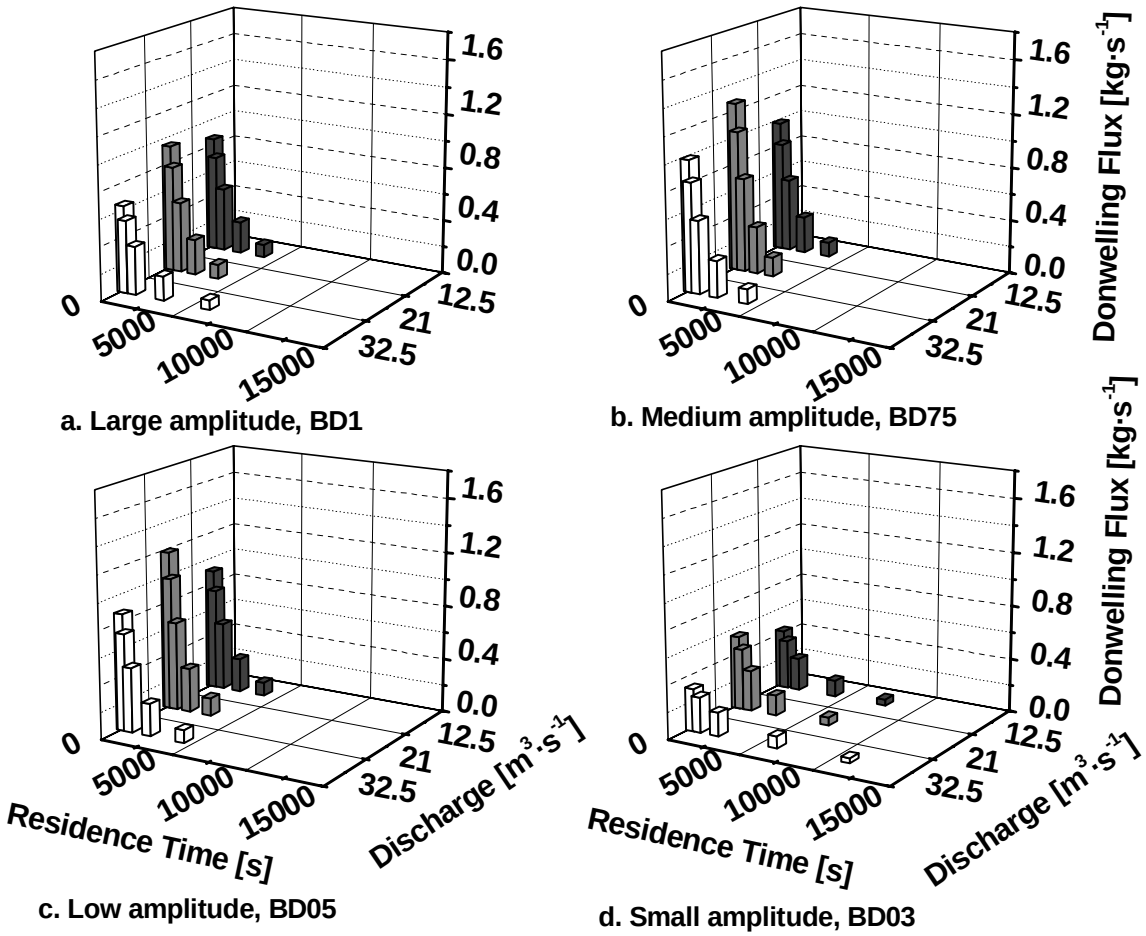

Figure 3.5: Downwelling flux at 90, 75, 50, 25, and 10% of the residence time distribution for 0.05λ deep homogeneous alluvium. White, gray and dark gray shade defines large, medium, and small discharges, respectively.

The graphs represent the flow of in-stream water that persists in the sediment after a given time. For instance, in exp17 with shallow alluvium (Figure 3.5b, discharge of 32.5 $m^3 \cdot s^{-1}$), only 10% of the average downwelling flux (0.11 $kg \cdot s^{-1}$) is still flowing into the sediment after 66 minutes (3960 seconds); instead, for the same case with deep alluvium (Figure 3.4), it takes 3.7 hours (13,320 seconds) to decay to a similar value of 0.12 $kg \cdot s^{-1}$. In general, bio-chemical reactions need time to take place, and they can occur

only for the portion of the infiltrating water that stays in the sediment longer than the reaction time. Consequently, our predicted differences in residence time suggest that longer reaches may be required for equivalent mixing in shallow alluvium, such that surface water is pumped through the riverbed several times to have the same contact time as that of a shorter reach of deep alluvium. Additionally, inspection of Figures 3.4 and 3.5 shows that increased discharge causes an increase in downwelling flux for lower bedform amplitudes (Figures 3.4b-d and 3.5b-d, discharges 12.5-21 $l \cdot s^{-1}$) due to greater bedform submergence, which widens the bed surface area for hyporheic exchange and shortens the flow paths.

3.5.2. Effects of mean aquifer velocity, flow regime and bedform amplitude on hyporheic dynamics

3.5.2.1. Mean hyporheic depth

Mean groundwater flow velocity significantly influences the hyporheic volume, causing a reduction in hyporheic depth with increasing aquifer velocity (Figure 3.6). The largest reduction in mean hyporheic depth, approximately 80%, occurs for velocities between $9 \cdot 10^{-5}$ and $2.05 \cdot 10^{-4}$ $m \cdot s^{-1}$. In contrast, there is only about a 20% decrease in mean hyporheic depth for a decline in aquifer velocity from $5 \cdot 10^{-4}$ to $1.5 \cdot 10^{-3}$ $m \cdot s^{-1}$. For low groundwater velocities, both bedform topography and flow regime affect the shape and the extent of the hyporheic flow [*Tonina and Buffington*, submitted (Chapter 2)]. When the groundwater velocity is higher than $5 \cdot 10^{-4}$ $m \cdot s^{-1}$, the impact of bedform amplitude and flow regime is reduced considerably compared to lower groundwater velocities (Figure 3.6). This happens because high groundwater velocities compress the hyporheic zone and confine it to a shallow near-surface region with most of the exchange taking place in the riffle and bar.

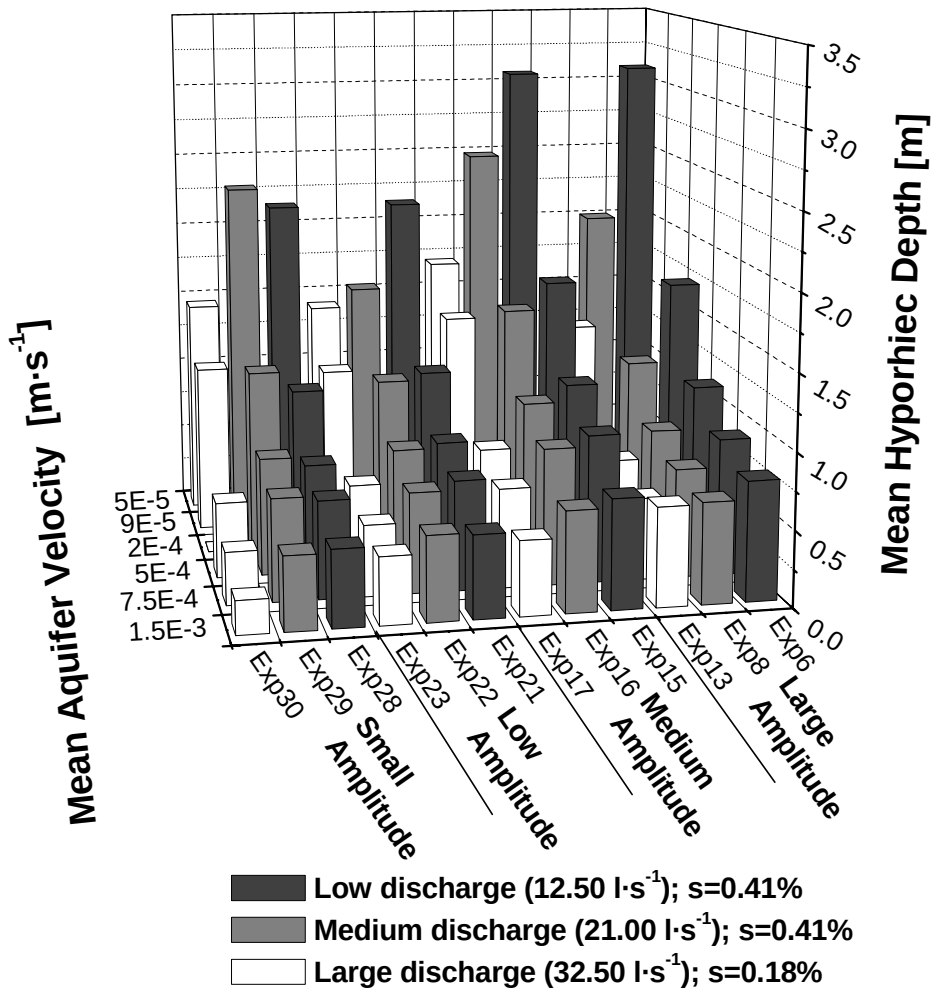

Figure 3.6: Mean hyporheic depth as a function of mean groundwater flow velocity, bedform amplitude, and flow regime for 1λ deep homogeneous alluvium.

3.5.2.2. Residence time

Groundwater velocity influences the residence time distribution (*RTD*) (Figure 3.7); the *RTD* is broad for low values of mean groundwater velocity, and narrow for faster velocities. For large bedform amplitudes, the effect of river discharge persists at all mean aquifer velocities, showing a reduction of *RTD* when the discharge becomes larger, probably due to a reduction in mean hyporheic depth (Figure 3.7, BD1 and BD75). The bedform amplitude also influences the *RTD*, and small bed amplitudes exhibit short residence time distributions (Figure 3.7, cf. BD1 and BD75). The smallest bedform amplitude, BD03, shows a very large *RTD* for low groundwater velocity, which may be due to smaller pressure variations and reduced topographic forcing over this lower-amplitude surface.

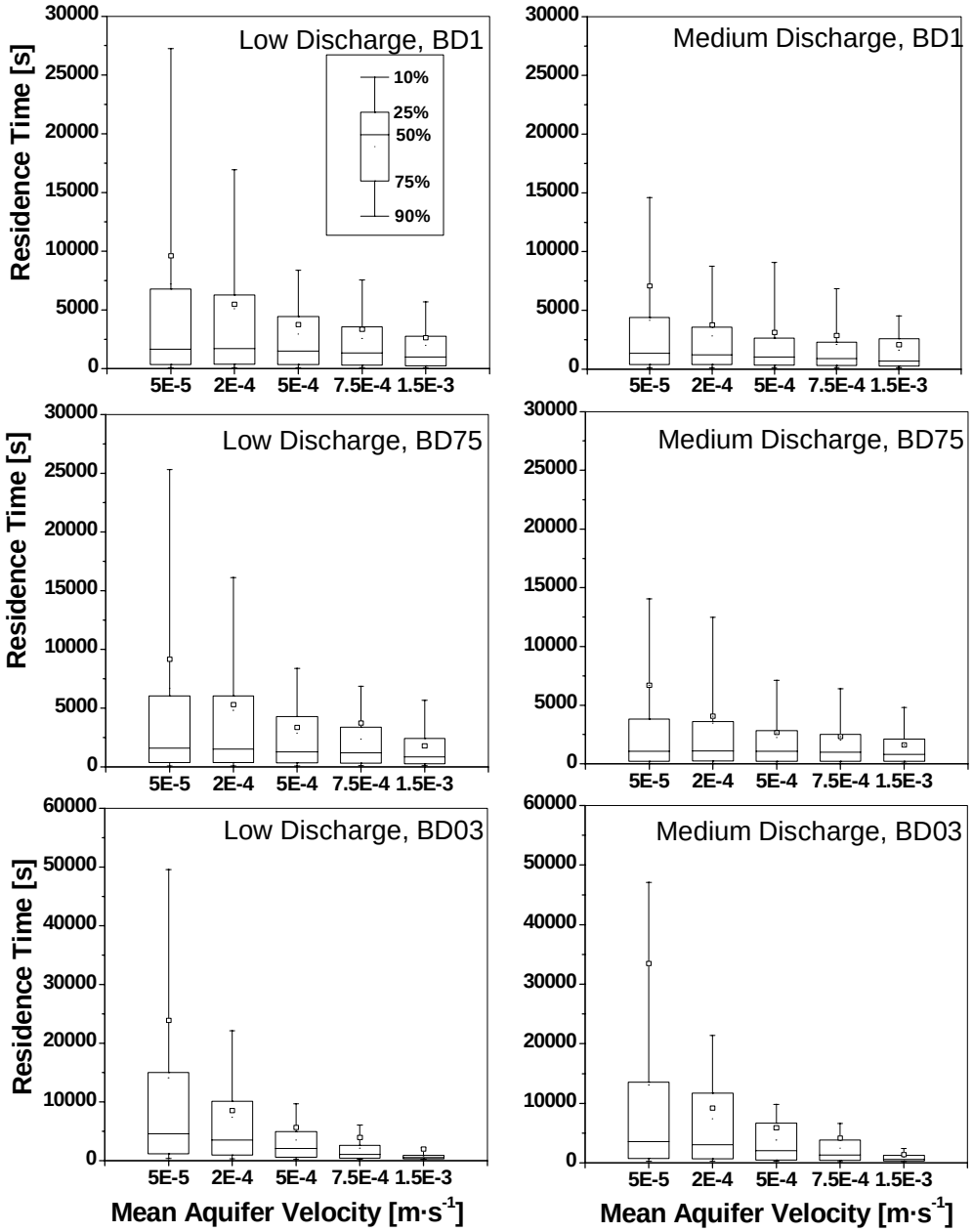

Figure 3.7: Residence time distribution as a function of mean groundwater flow velocity, bedform amplitude, and flow regime for 1λ deep homogeneous alluvium; discharge increases from left to right across the panels, and bedform amplitude decreases from top to bottom (please note the difference in scale for BD03).

In analyzing the data, we observed that the mean residence time varies with the length of the experiment, if we consider all the injected particles when evaluating the residence time distribution. In the model, the pathlines of the particles entrained into the deep aquifer are of infinite length since they do not return to the riverbed surface. The partial loss of solute to the deep aquifer may also happen in real rivers, in which case the

mean residence time is a less valuable measure since it is a function of experiment length, unless it is defined only in terms of the flow re-entering the stream. In this case, the interval is delimited by the residence time of the last particle upwelling in the river. In contrast, the median residence time is not influenced by the small number of particles lost to the deep aquifer and may be a more suitable metric for hyporheic flow.

3.5.2.3. Average downwelling flow

In our simulations, we find that the effect of the mean aquifer velocity on the average downwelling flux is negligible as previously reported by *Storey et al.* [2003] in his one-dimensional pool-riffle simulations. The downwelling flux increases less than 4% when aquifer velocities are increased from $5 \cdot 10^{-5}$ to $1.3 \cdot 10^{-3}$ $m \cdot s^{-1}$ (Figure 3.8). Therefore, the effects of bedform amplitude on downwelling flow are seen at all mean aquifer velocities. The medium-amplitude bedform shows the most intense flux, even though it does not have the largest amplitude. Furthermore, by increasing the discharge from low to medium, while holding the bed slope constant, the average downwelling flux increases (e.g., Figure 8, exp 15-16). This trend is present for lower-amplitude bedforms (medium-, low- and, small-amplitude). However, for the large-amplitude bedform, an increase in discharge results in a decrease of the average downwelling flux. These different responses are likely due to differences in head variations and flow path lengths between the experiments. Increases in downwelling flux with greater discharge over medium- to small-amplitude bedforms could stem from shorter pathlines (supported by shorter residence time distributions as described in the previous section) and a larger bed surface area for hyporheic exchange [*Tonina and Buffington,* submitted (Chapter 2)]. In contrast, for the large-amplitude bedform, the reduction of head variation over the bedform with discharge is not balanced by an adequate reduction in flow path length and/or an increase in bed surface area for hyporheic exchange [*Tonina and Buffington,* submitted]

Analysis of solute decay and temporal changes in concentration can be used to combine the effects of downwelling flux and residence time, and are examined as a function of mean groundwater flow velocity in the next section.

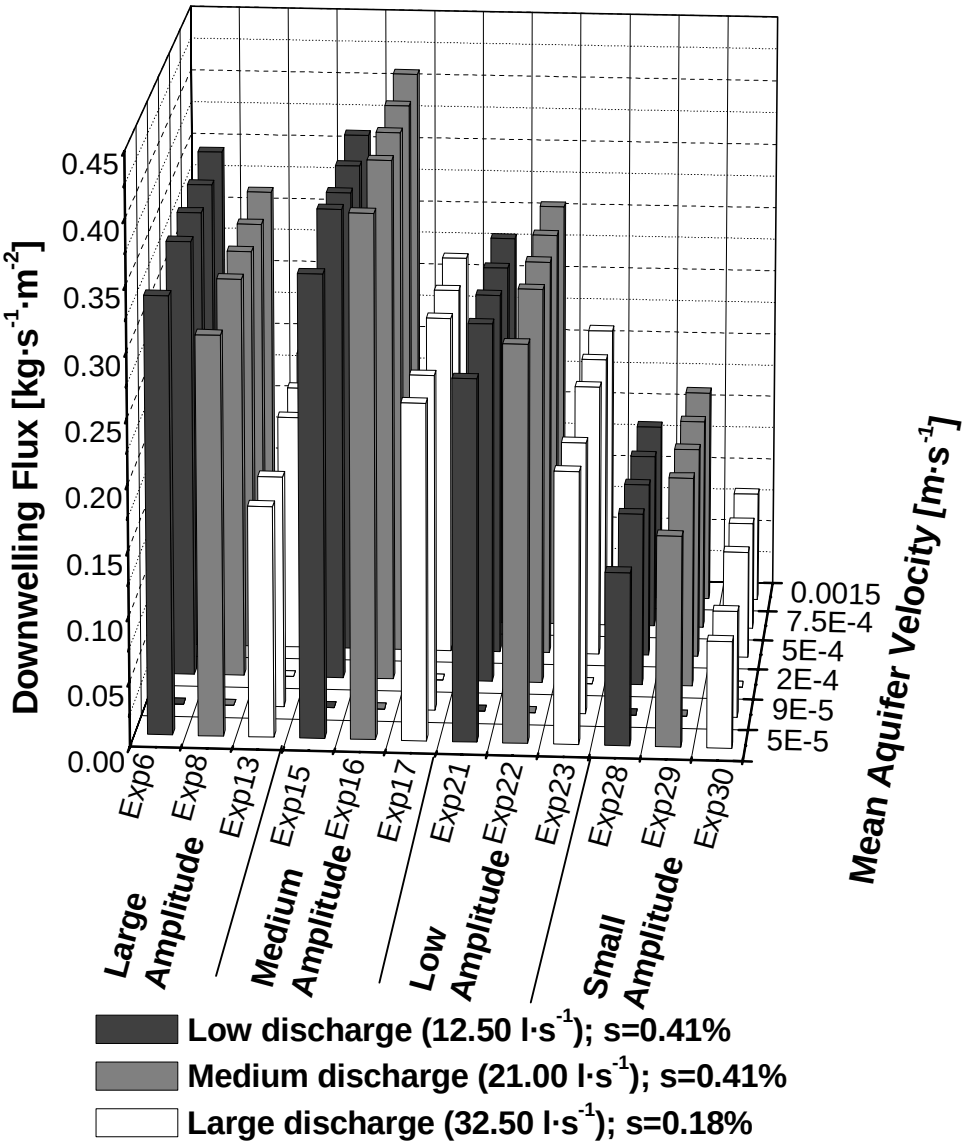

Figure 3.8: Average downwelling flux as a function of mean groundwater flow velocity, bedform amplitude, and flow regime for a 1λ deep homogeneous alluvium.

3.5.2.4. Solute exchange

Hyporheic mixing and solute exchange between the river and aquifer can be quantified through tracer experiments and changes in the solute concentration relative to the initial value at the time of tracer injection (C/C_0). Figure 3.9 shows the solute decay in river water for different groundwater velocities for deep alluvium (1λ).

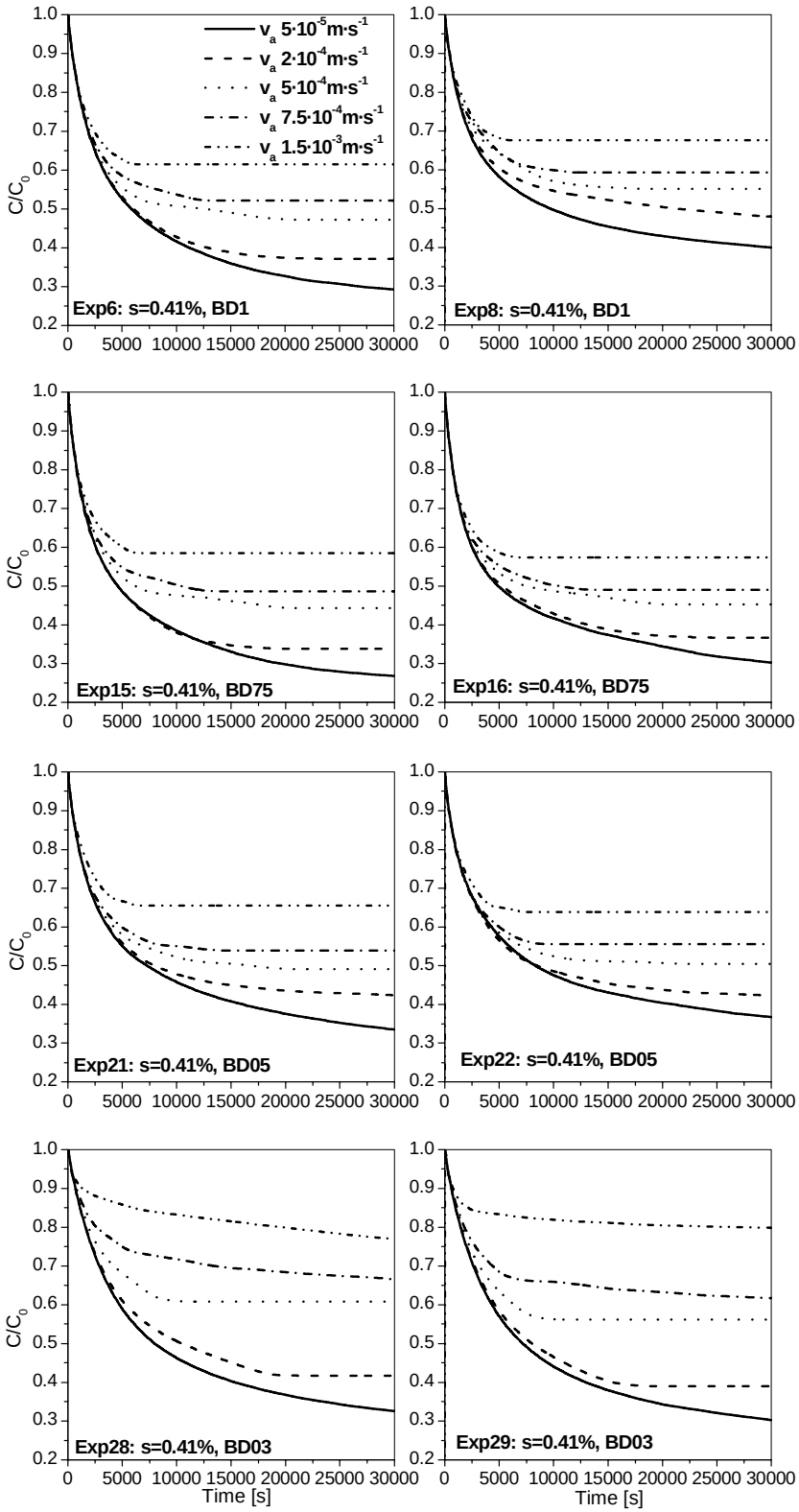

Figure 3.9: Hyporheic solute exchange for 1λ deep homogeneous alluvium for different values of mean groundwater flow velocity (v_a); discharge increases from left to right across the panels, and bedform amplitude decreases from top to bottom.

The mean flow velocity of the aquifer has a strong influence on the exchange. The results show that channels with fast groundwater flow will have less exchange than channels with low groundwater flow, all other factors constant. Fast aquifer flow reduces both the hyporheic volume and the residence time resulting, in less exchange between the river and sediment.

The effects of bedform amplitude and flow regime also are evident on the hyporheic exchange. The steepest exchange rate occurs for the medium-amplitude bedform (BD75) at all groundwater flows and river discharges. Furthermore, this bedform shows a smaller final value of C/C_0, indicating greater total exchange. This bedform amplitude has the best combination of downwelling flux and mean hyporheic depth (analyzed in previous sections), which maximizes the solute exchange, the intensity of which is a function of river discharge, groundwater flow, and channel hydraulics as influenced by bedform geometry. Furthermore, an increase of river discharge results in a lower initial hyporheic exchange rate, which is probably caused by a reduction in pressure gradient for the larger-amplitude bedforms (BD1, BD75 and BD05). The difference in surface-subsurface exchange between discharges diminishes by reducing the amplitude, and eventually for low amplitudes, an increase of discharge results in a negligible variation of surface-subsurface solute exchange at low mean aquifer velocity (Figure 3.9, exp28 and exp29 solid lines). Increasing the mean aquifer velocity, namely changing the upstream and downstream boundary conditions, compresses the vertical extent of the hyporheic zone, resulting in less mass transport between the river and sediment.

3.5.3. Effect of hydraulic conductivity

In a homogeneous medium, a reduction of hydraulic conductivity strongly affects the downwelling flux. Downwelling flow is less intense in more impermeable media (Figure 3.10), while residence time drastically increases with declining hydraulic conductivity (Figure 3.11). The mean hyporheic depth does not change with hydraulic conductivity; k governs the intensity of the process, but not the flow paths. Therefore, the surface-subsurface exchange decreases with less permeable media (Figure 3.12).

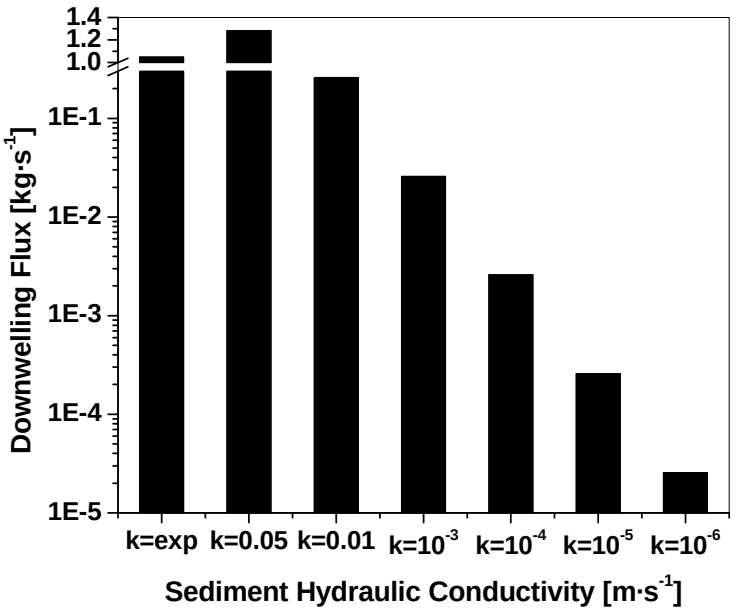

Figure 3.10: Effect of hydraulic conductivity on downwelling flux, example from experiment 6. exp indicates an exponential variation of hydraulic conductivity between 0.05 and 10^{-6} m·s^{-1} (see Section 2.2).

Natural rivers likely show a vertical profile of hydraulic conductivity, possibly with a shallow more permeable layer near the surface of the stream. We analyzed the case of an exponential decay of hydraulic conductivity from 0.05 to 10^{-6} m·s^{-1} in a 0.5λ deep alluvium.

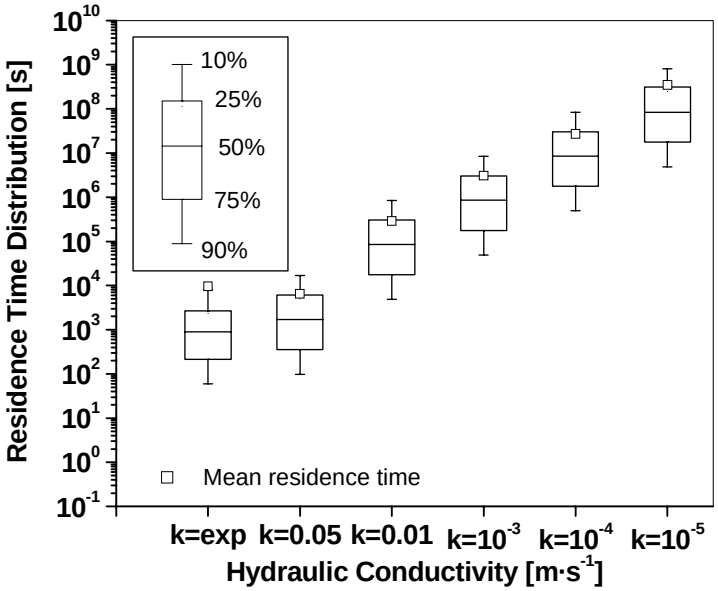

Figure 3.11: Effect of hydraulic conductivity on the residence time distribution, example from experiment 6. See Figure 10 caption for definition of exp.

. Results show an 18% reduction of downwelling flow compared to an equivalent homogeneous case (Figure 10, cf. k=exp and k=0.05 m·s^{-1}), and the *RTD* is slightly shorter (Figure 3.11). The two cases show comparable results because most of the exchange happens close to the surface, where the hydraulic conductivities are similar. Nevertheless, the total solute exchange is less for the case of an exponential conductivity profile (Figure 3.12), because the majority of the pathlines are closer to the surface where more permeable layers are present

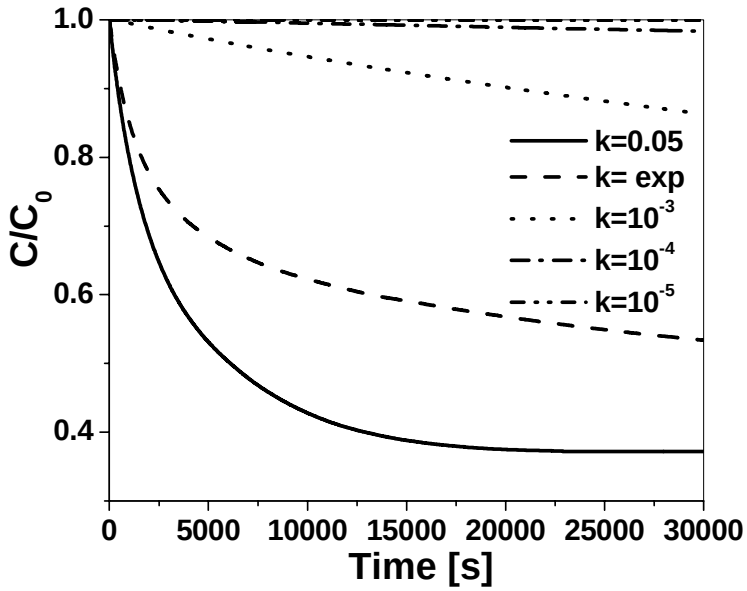

Figure 3.12: Solute exchange for experiment 6, varying hydraulic conductivity (k is in meters per second), for an alluvial depth of 0.5λ. See Figure 10 caption for definition of exp.

3.5.4. Flowpaths

A pathline is the trajectory of a particle injected into a flow field and it is tangent to the local velocity. If the velocity field is steady, each particle leaving from the same injection point follows the same path. We used pathlines to visualize the hyporheic flow inside the porous medium for three different combinations of mean groundwater flow velocity and depth of alluvium: 1) deep alluvium, low velocity (Figure 3.13); 2) deep alluvium, high velocity (Figure 3.14); and 3) shallow alluvium, low velocity (Figure 3.15).

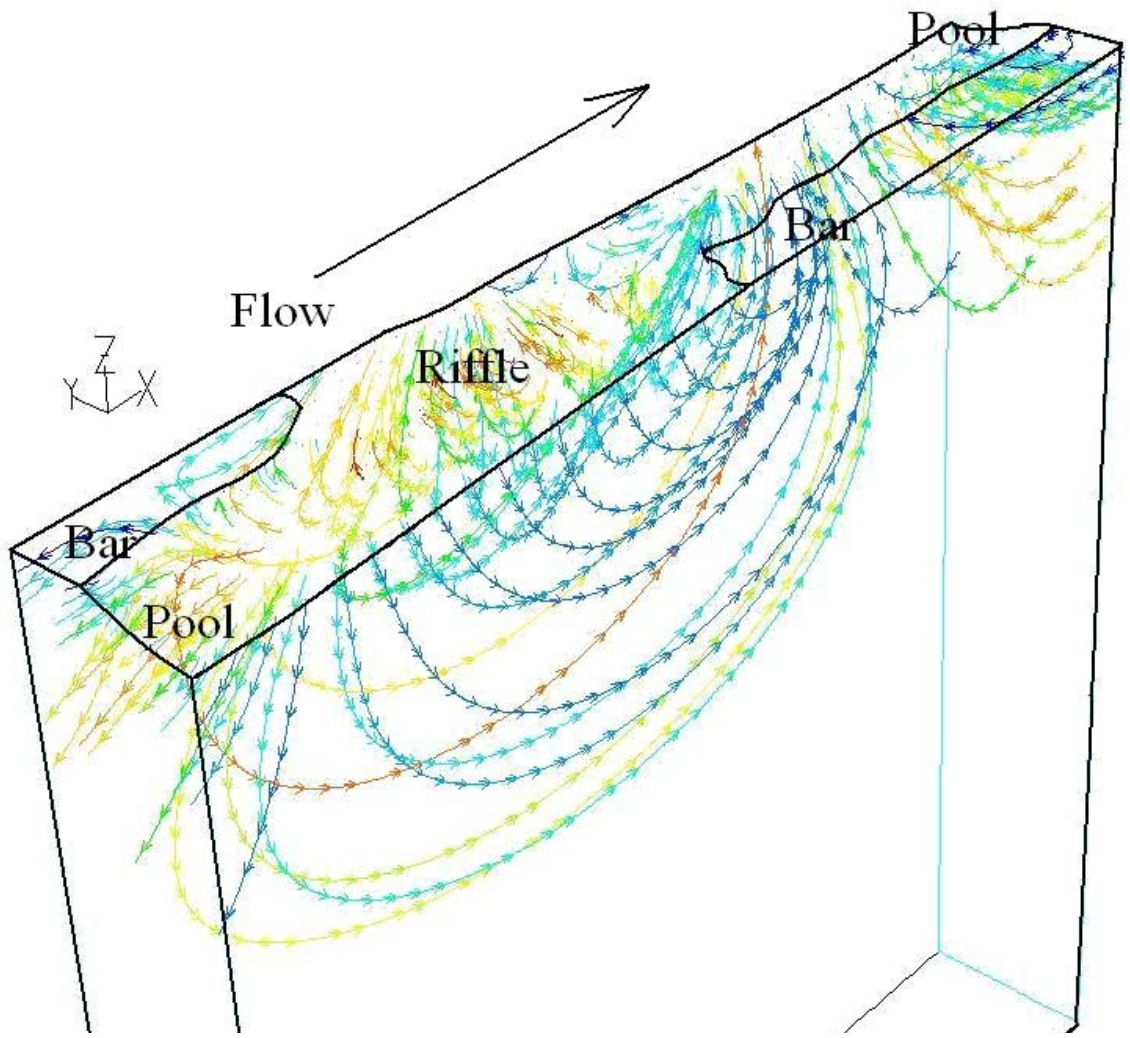

Figure 3.13: Pathlines (colored by particle ID) for pool-riffle morphology, experiment 6 (large amplitude and low discharge), 1λ homogeneous deep aquifer and 0.1% gradient.

For low velocity and deep alluvium, the hyporheic flow is complex (Figure 3.13). There is a near-surface zone where the flow paths cross the riffle crest from one side to the other of the river. This motion follows the surface water flow. Deeper flows are not as three-dimensional as the shallow ones and their direction is more inline with the longitudinal axis of the river, creating a deep hyporheic flow cell. They span the pool-riffle unit morphology and have three-dimensional behavior close to the surface, where low-pressure areas redirect them. This highlights the effect of local topography on river-groundwater interaction, which is usually overlooked in large-scale analysis. Local topography via high- and low-pressure areas determines where groundwater can enter the river and where river water can recharge the aquifer.

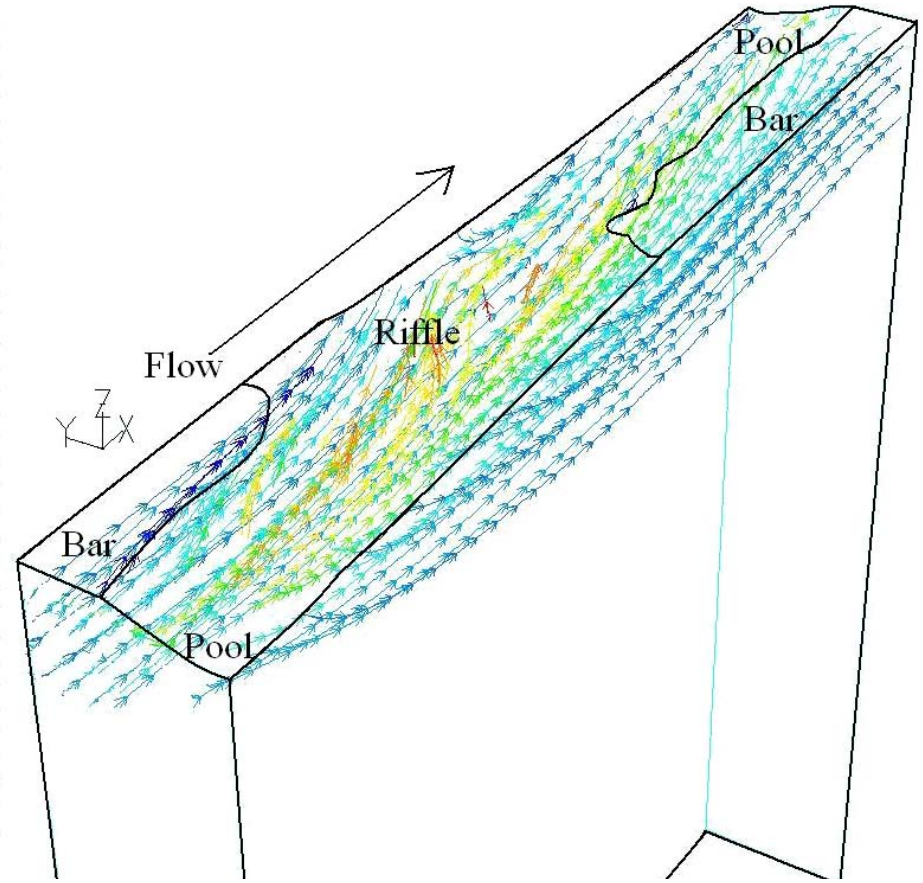

Figure 3.14: Pathlines (colored by particle ID) for pool-riffle morphology, experiment 6 (large amplitude and low discharge), 1λ homogeneous deep aquifer and 3% gradient.

In addition to these downstream fluxes, a secondary recirculating flow goes from downstream to upstream. This flow is visible in Figure 3.13 near the upstream pool, and it conveys river water from the middle of the riffle to the upstream head of the pool. This secondary circulation cell has a shallower depth of penetration than the rest of the hyporheic flow, and is not present in aquifers with high mean velocities ($> 10^{-4}$ m·s^{-1}) (Figure 3.14). When the aquifer has high groundwater velocity, the flowpaths are more two-dimensional and more inline with the downstream direction (Figure 14). They are shallower and span the pool-riffle unit morphology, with few near-surface flow lines that cross the riffle crest.

In contrast, when the aquifer is shallow, with low mean velocity, the hyporheic flow is shallow, but three-dimensional, again, with intense flux at the crest of the riffle (Figure 3.15). There are several strong downwelling areas: at the middle of the stoss side

of the riffle, and at the upstream end of the bar. Strong upwelling areas are located at the middle of the lee side of the riffle and at the pool head, close to the bar side.

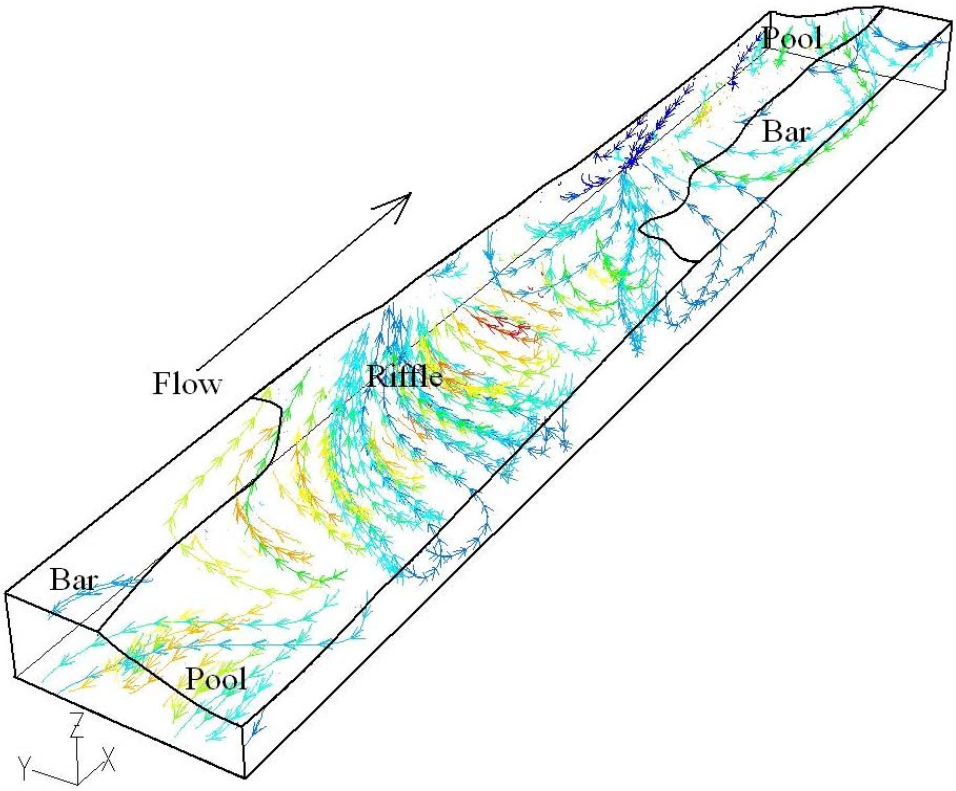

Figure 3.15: Pathlines (colored by particle ID) for pool-riffle morphology, experiment 6 (large amplitude and low discharge), 0.05λ homogeneous deep aquifer and 0.41% gradient.

The fisheries literature indicates that salmonid redds (nests) are typically built in upwelling and downwelling areas [*Geist and Dauble*, 1998; *Baxter and Hauer*, 2000]. Moreover, salmonids usually spawn in pool tails, which are hydraulic transient zones upstream of the riffle, where in-stream water accelerates and downwelling fluxes are present [*Hoopes*, 1972]. When they spawn downstream of the riffle, it is close to the gravel bar side, where the current is less intense than over the riffle. Figures 3.13, 3.14 and 3.15 show abundant upwelling fluxes in this area. These observations support the idea that spawning site selection may depend not only on surface hydraulics (water depth and flow velocity), but also on the intensity of the hyporheic fluxes and how long the upwelling water resides in the sediment, which influences water quality (temperature, dissolved oxygen content, etc.). Areas with intense upwelling and downwelling, around the two bar ends and at the two sides of the riffle, might offer strong hyporheic fluxes

with short *RTD* that will preserve oxygen concentrations and provide a more appealing environment for spawning.

3.5.5. Mean hyporheic depth and mean hyporheic residence time

The surface and subsurface waters that are exchanged through the hyporheic zone are essential components in river solute transport. *Bencala and Walters* [1983] developed a first-order model based on transient storage, which uses two parameters to characterize the hyporheic exchange: the storage area A_S, and the exchange rate, α. This model is a one-dimensional approach in two equations:

$$\frac{\partial C}{\partial t} + \frac{Q}{A_W}\frac{\partial C}{\partial x} = \frac{1}{A_W}\frac{\partial}{\partial x}\left(A_W\, D\frac{\partial C}{\partial x}\right) + \frac{q_l}{A_W}(C_L - C) + \alpha(C_s - C)$$
$$\frac{\partial C_s}{\partial t} = -\alpha\frac{A_W}{A_S}(C_S - C) \qquad \textbf{(3.4)}$$

where C is the in-stream solute concentration, Q the discharge, A_W the river cross sectional area, D the dispersion coefficient, q_l the lateral inflow, and C_L the solute concentration of the lateral inflow. The last term in the first equation and the second equation link the river flow with the storage volume, which we envision as the hyporheic zone, with solute concentration C_S.

The model is widely used, but the storage area and the exchange rate require calibration [*Wagner and Harvey*, 1997]. These values are derived from breakthrough curve analysis of tracer experiments. Thus, they are site specific and applicable only for the flow conditions present during the test. Here, we use our results to develop equations for predicting these values from relevant physical characteristics of river regime, bedform topography, and sediment properties.

We envision the storage zone as the hyporheic volume and we define the cross-sectional hyporheic area, A_H, as the product between the wetted perimeter, P_H, and the mean hyporheic depth:

$$A_S = A_H = d_H \cdot P_H \qquad \textbf{(3.5)}$$

Furthermore, we can employ the relation presented in the work of *Wörman et al.* [2002] to predict the exchange rate based on the cross-sectional area of the river, A_W, the hyporheic area and the mean hyporheic residence time:

$$\alpha = \frac{1}{T_H}\frac{A_H}{A_W} \quad \textbf{(3.6)}$$

We used our findings to develop empirical equations for predicting the mean average depth, d_H, and the mean residence time, T_H, allowing determination of A_H and α. The mean average depth expresses the vertical extent of the hyporheic flow, while the mean residence time combined with the average hyporheic depth describes the retention property of the hyporheic zone.

3.5.5.1. Mean hyporheic depth

We assumed that the mean hyporheic depth is a function of mean flow velocity, v, average water depth, d, water density, ρ, dynamic viscosity of the water, μ, gravity, g, bed slope, s, alluvial depth d_a, hydraulic permeability of the aquifer, K, groundwater gradient, defined as the ratio between mean groundwater flow and hydraulic conductivity of the aquifer, $s_a=v_a/k$, bedform amplitude, Δ, and bedform wavelength, λ.

From the aforementioned results, we observed that the hyporheic depth is not dependent on the sediment permeability and, furthermore, this depth is meaningful only if it is shallower than the impervious layer, which would otherwise constrain and define the hyporheic depth. Consequently, k and d_a are dropped from our prediction of mean hyporheic depth.

To reduce the number of variables, we applied the Buckingham π theorem by using mean flow velocity, water density and mean water depth as governing variables. This operation simplifies the problem from nine variables to six dimensionless groups, which are Reynolds number, *Re*, Froude number, *Fr*, bed slope, aquifer gradient, the ratio of bedform amplitude to water depth, and the ratio of bedform wavelength to water depth.

$$\Pi_1' = \frac{\rho v d}{\mu}; \quad \Pi_2' = \frac{v}{\sqrt{g\,d}}; \quad \Pi_3' = \frac{\Delta}{d}$$
$$\Pi_4' = \frac{\lambda}{d}; \qquad \Pi_5' = s; \qquad \Pi_6' = s_a \quad \textbf{(3.7)}$$

$$\frac{d_H}{d} = \exp\left(\sum_{i=1}^{6} A_i \ln\left(\Pi_i'\right)\right) \quad \textbf{(3.8)}$$

We performed a linear regression analysis on the natural log of the dimensionless numbers to determine the six coefficients, A_i, of equation (3.8) (Table 3.3). Figure 3.16 compares expected and observed values, with a zero intercept imposed for the regression line. The slope of this line is close to one, suggesting a correlation between observed and expected values, supported by a high correlation coefficient, R (Figure 3.16).

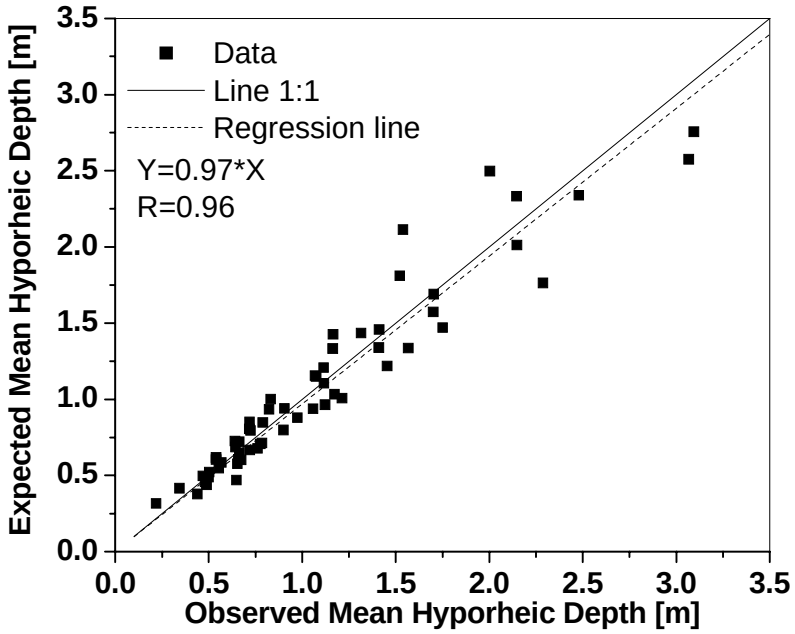

Figure 3.16: Observed versus predicted mean hyporheic depth.

3.5.5.2. Mean hyporheic residence time

In contrast to the above analysis, the mean hyporheic residence time is a function of all the aforementioned variables. The aquifer permeability and depth of alluvium are key factors in evaluating the hyporheic residence time. In applying the Buckingham π theorem, we defined a new set of governing variables: the mean flow velocity, water density and hydraulic permeability. We attained the following non-dimensional numbers

$$\Pi_1 = \frac{\rho v \sqrt{K}}{\mu}; \qquad \Pi_2 = \frac{v^2}{g\sqrt{K}}; \quad \Pi_3 = \frac{d}{\sqrt{K}}; \quad \Pi_4 = s$$
$$\Pi_5 = \frac{\Delta}{\sqrt{K}}; \quad \Pi_6 = \frac{\lambda}{\sqrt{K}}; \quad \Pi_7 = \frac{d_a}{\sqrt{K}}; \quad \Pi_8 = s_a \qquad \textbf{(3.9)}$$

The above dimensionless parameters were used to estimate the mean hyporheic residence time using the following expression:

$$\frac{T_H\, v}{\sqrt{K}} = \exp\left(\sum_{i=1}^{8} B_i \ln(\Pi_i)\right) \qquad \textbf{(3.10)}$$

A linear regression procedure of the logged values similar to the one described in the previous section was used to determine the eight coefficients, B_i,(Table 3.3). Predicted versus observed values, again, show good agreement (Figure 3.17).

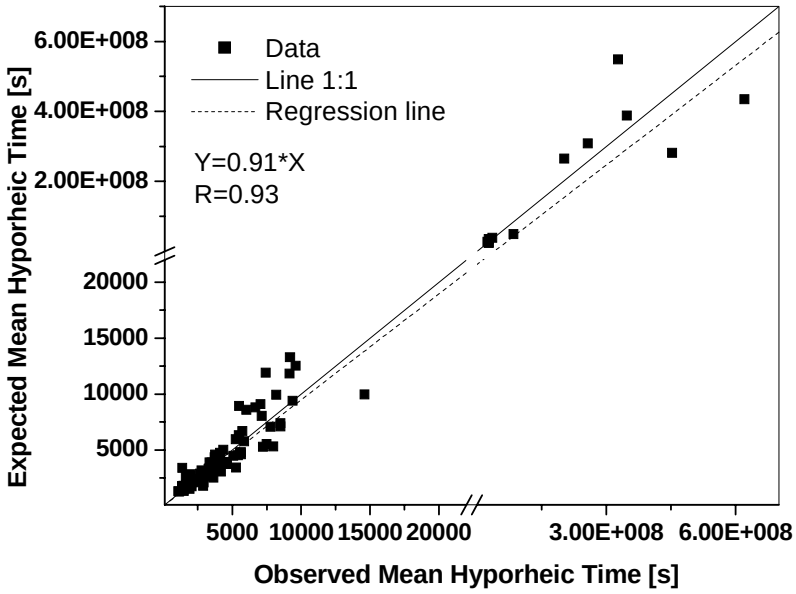

Figure 3.17: Observed versus predicted mean hyporheic residence time.

3.5.5.3. Hyporheic storage area and solute exchange rate

Inserting equations (3.8) and (3.10) into equations (3.5), and (3.6), we obtain a new set of equations for predicting the storage area and exchange rate in the Transient Storage Model, without the need for tracer tests and/or site-specific calibration of the model:

$$A_H = d \cdot \exp\left(\sum_{i=1}^{6} A_i \ln(\Pi_i')\right) \cdot P_H \qquad \textbf{(3.11)}$$

$$\alpha = \frac{1}{\frac{\sqrt{K}}{v}\exp\left(\sum_{i=1}^{8} B_i \ln(\Pi_i)\right)} \frac{A_H}{A_W} \qquad \textbf{(3.12)}$$

Table 3.3: Coefficients for the mean hyporheic depth and the mean hyporheic residence time relationships

i		1	2	3	4	5	6	7	8
Mean hyporheic depth	A_i:	0.36	-0.139	-0.244	0.277	0.850	-0.397		
Mean hyporheic residence time	B_i:	0.014	-1.144	1.315	0.552	-1.027	1.233	0.417	-0.486

3.6. Conclusion

Topographically-induced hyporheic flow is an important mechanism that maintains an aerobic environment within the streambed. Many factors are involved in hyporheic exchange, including flow regime, bedform amplitude, depth of alluvium, mean groundwater flow velocity, and hydraulic conductivity. We investigated their importance in controlling the hyporheic residence time distribution, hyporheic volume, downwelling flux, and hyporheic exchange.

River discharge is a significant factor since it controls the pressure distribution at the sediment interface, and it remains important for different combinations of all the other factors. However, mean hyporheic depth becomes less sensitive to river flow regime when groundwater velocities are greater than $7.5 \cdot 10^{-4}$ m·s^{-1}. Our experiments were mostly for low flow, when bedforms are not entirely submerged yet, and when discharge strongly affects water surface elevation and flow depth. Bedform amplitude provides significant control on channel hydraulics and hyporheic exchange, but its effect is minor when mean groundwater flow velocity is greater than $7.5 \cdot 10^{-4}$ m·s^{-1}.

The depth of alluvium is not a controlling factor for hyporheic exchange as long as it is deeper than the hyporheic flow paths, which in our experiments correspond to depths of 0.5λ meters (one half of the pool-riffle wavelength). When the alluvium is shallower than 0.5λ, as may be common in confined headwater channels, the hyporheic flow is confined by an impervious layer (bedrock), causing a reduction of the residence time distribution (*RTD*) and downwelling rates. In such channels, depth of alluvium is the primary control on the character of hyporheic flow.

Mean groundwater flow velocity is not a key factor when velocities are less than 10^{-4} m·s^{-1}, similar to what has been observed in sand-bed channels [*Packman et al.,* 2000]. Sand-bed rivers have very low permeability and low valley gradients, therefore

mean groundwater velocity is low or negligible. In contrast, gravel-bed rivers can have high groundwater flow velocities due to steeper valley slopes and more porous alluvium. Although high groundwater flow velocities do not affect downwelling flux, they strongly reduce the *RTD*, and hence the hyporheic exchange.

The hydraulic conductivity plays a major role in the advective transport of solutes between surface and subsurface water due to the linear proportion between specific velocity and hydraulic conductivity stated by Darcy's law. When the hydraulic conductivity drops below 10^{-4} $m \cdot s^{-1}$, the hyporheic flow is almost negligible in our experiments. Moreover, the presence of a permeable layer is essential for the occurrence of an intense and significant hyporheic flow. We investigated the case of an exponential decrease in hydraulic conductivity with depth, which showed that as long as there is a permeable near-surface layer, the hyporheic flow remains intense.

The location and extent of upwelling and downwelling is primarily controlled by the surface pressure distribution, not by the depth of alluvium, groundwater flow velocity, or hydraulic conductivity of a homogenous medium. These factors mainly affect either the residence time distribution or the hyporheic flux, while the spatial pattern of hyporheic flow is controlled by bed topography and flow regime.

We also developed an empirical relationship to predict the mean hyporheic depth and mean residence time based on flow regime, channel geometry and substrate characteristics. These relationships can be used in confined rivers with homogeneous and isotropic alluvium to predict the storage area and exchange rate for the Transient Storage Model. This approach does not require calibration and it is not site- or flow-regime specific. It is, however, limited to the range of conditions examined in our experiments and numerical simulations.

Further studies are necessary to evaluate the importance of these factors for different bedform wavelengths. In our work, we changed the amplitude, but kept the wavelength constant due to laboratory constraints. Deeper pools and shorter wavelengths are common in many Pacific Northwest gravel-bed rivers where pool-riffle topography is forced by frequent wood obstructions, and may show different behavior than those presented herein.

Acknowledgements: This work was supported in part by the STC Program of the National Science Foundation under Agreement Number EAR-0120914, by the USDA Forest Service Yankee Fork Ranger District (00-PA-11041303-071), by the US Department of Education Fund for the Improvement of Postsecondary Education (P116Z010107), and by the USDA Forest Service Rocky Mountain Research Station (03-JV-11222014-060). We appreciate the insightful reviews provided by Alberto Bellin, Peter Goodwin and Klaus Jorde.

References

Baxter, C. V., and R. F. Hauer (2000), Geomorphology, hyporheic exchange, and selection of spawning habitat by bull trout (*Salvelinus confluentus*), *Can. J. Fish. Aquat. Sci*., *57*, 1470-1481.

Bencala, K. E., and R. A. Walters (1983), Simulation of solute transport in a mountain pool-and-riffle stream: a transient storage model, *Water Resources Research*, *19*(3), 718-724.

Buffington, J. M., and D. R. Montgomery (1999), Effects of sediment supply on surface textures of gravel-bed rivers, *Water Resources Research*, *35*(11), 3523-3530.

Dagan, G. (1979), The Generalization of Darcy's Law for Nonuniform flow, *Water Resources Research*, *15*(1), 1-7.

Edwards, R. T., (1998), The Hyporheic Zone, in *River Ecology and Management: Lessons from the Pacific Coastal Ecoregion*, edited by R. J. Naiman and R. E. Bilby, Springer-Verlag, New York, 399-429.

Elliott, A., and N. H. Brooks (1997a), Transfer of nonsorbing solutes to a streambed with bed forms: Laboratory experiments, *Water Resources Research*, *33*(1), 137-151.

Elliott, A., and N. H. Brooks (1997b), Transfer of nonsorbing solutes to a streambed with bed forms: Theory, *Water Resources Research*, *33*(1), 123-136.

Geist, D. R., and D. D. Dauble (1998), Redd site selection and spawning habitat use by fall Chinook salmon: the importance of geomorphic features in large rivers, *Environmental management*, *22*(5), 655-669.

Grimm, N. B., and S. G. Fisher (1984), Exchange between interstitial and surface water: implication for stream metabolism and nutrient cycling, *Hydrobiologia*, *111*, 219-228.

Harvey, J. W., and K. E. Bencala (1993), The effect of streambed topography on surface-subsurface water exchange in mountain catchments, *Water Resources Research*, *29*, 89-98.

Hassanizadeh, M. S., and W. G. Gray (1979), General conservation equations for multi-phase systems: 1. Averaging procedure, *Advances in Water Resources*, *2*, 131-144.

Hoopes, D. T. (1972), Selection of spawning sites by sockeye salmon in small streams, *Fishery Bulletin*, *70*(2), 447-457.

Kasahara, T., and S. M. Wondzell (2003), Geomorphic controls on hyporheic exchange flow in mountain streams, *Water Resources Research*, *39*(1), 1005, doi:10.1029/2002WR001386.

Leopold, L. B., M. G. Wolman, and J. P. Miller (1964), *Fluvial Processes in Geomorphology*, Freeman, W.H., San Francisco.

Levine, J. B., and G. D. Salvucci (1999), Equilibrium analysis of groundwater-vadose zone interactions and resulting spatial distribution of hydrologic fluxes across a Canadian prairie, *Water Resources Research*, *35*(5), 1369-1383.

Lisle, T. E., and S. Hilton (1992), The volume of fine sediment in pools: an index of sediment supply in gravel-bed streams, *Water Resources Bulletin*, *28*(2), 371-382.

Marion, A., M. Bellinello, I. Guymer, and A. I. Packman (2002), Effect of bed form geometry on the penetration of nonreactive solutes into a streambed, *Water Resources Research*, *38*(10), 1209, doi:10.1029/2001WR000264.

Packman, A. I., N. H. Brooks, and J. J. Morgan (2000), A physicochemical model for colloid exchange between a stream and a sand streambed with bed forms, *Water Resources Research*, *36*(8), 2351-2361.

Reeves, G. H., P. A. Bisson, and J. M. Dambacher, (1998), Fish Communities, in *River Ecology and Management: Lessons from the Pacific Coastal Ecoregion*, edited by R. J. Naiman and R. E. Bilby, Springer-Verlag, New York.

Rus, D. L., V. L. McGuire, B. R. Zurbuchen, and V. A. Zlotnik (2001), Vertical profiles of streambed hydraulic conductivity determined using slug tests in Central and Western Nebraska, *Water-Resources Investigations*, Report 01-4212, U.S. Geological Survey, Lincoln, Nebraska.

Savant, A. S., D. D. Reible, and L. J. Thibodeaux (1987), Convective Transport Within Stable River Sediments, *Water Resources Research*, *23*(9), 1763-1768.

Storey, R. G., K. W. F. Howard, and D. D. Williams (2003), Factor controlling riffle-scale hyporheic exchange flows and their seasonal changes in gaining stream: A three-

dimensional groundwater model, *Water Resources Research*, *39*(2), 17, doi:10.1029/2002WR001367.

Tonina, D., and M. J. Buffington (submitted), A three-dimensional model for hyporheic exchange in gravel-bed rivers with pool-riffle morphology, *Water Resources Research*.

Triska, F. J., V. C. Kennedy, R. J. Avanzino, G. W. Zellweger, and K. E. Bencala (1989), Retention and transport of nutrients in a third-order stream: Channel processes, *Ecology*, *70*, 1894-1905.

Vittal, N., K. G. Ranga Raju, and R. J. Garde (1977), Resistance of two-dimensional triangular roughness, *Journal Hydraulic Research*, *15*(1), 19-36.

Wagner, B. J., and J. W. Harvey (1997), Experimental design for estimating parameters of rate-limited mass transfer: Analysis of stream tracer studies, *Water Resources Research*, *33*(7), 1731-1741.

Wörman, A., A. I. Packman, H. Johansson, and K. Jonsson (2002), Effect of flow-induced exchange in hyporheic zones on longitudinal transport of solutes in streams and rivers, *Water Resources Research*, *38*(1), 15, doi:10.1029/2001WR000769.

Chapter 4.

EFFECTS OF SALMON REDDS ON RIVER HYDRAULICS AND HYPORHEIC FLOW IN GRAVEL-BED RIVERS[3]

In this paper we analyze the effects of a salmon nests (redds) on river hydraulics and hyporheic flow in a gravel pool-riffle channel. We focus on determining whether the redd formation enhances hyporheic flow through the egg pocket, thereby increasing the chance of embryo survival. We use a computational fluid dynamics model to simulate channel hydraulics and shallow hyporheic flow for a pool-riffle channel having characteristics typical of Idaho rivers. The simulations were repeated superimposing redd topography at the pool tail. Results show that the salmon nests change not only the river hydraulics, but also the local areas of upwelling and downwelling, enhancing the flow velocity through the egg pocket. Furthermore, a newly built redd affects the average hyporheic exchange rate, but when the hydraulic conductivity of the redd is similar to that of the surrounding sediment, the effect on the exchange rate is negligible.

---

[3] Co-authored paper by Daniele Tonina and John M. Buffington, to be submitted to *Canadian Journal of Fisheries and Aquatic Sciences.*

4.1. Introduction

The hyporheic zone is a saturated band of sediment that surrounds alluvial rivers and forms a link between the river and the aquifer. It is a rich ecotone where benthic, hyporheic, and groundwater species temporarily or permanently reside [*Reeves et al.*, 1998]. The hyporheic zone is a particularly important environment for salmonids (*Oncorhychus*, *Salmo*, and *Salvelinus*), which construct their nests (redds) in riverbed gravels and lay their eggs to incubate within the hyporheic zone. After hatching, the alevins live in the hyporheic zone for some time before emerging into the stream [*Levine and Salvucci*, 1999].

During spawning, a female salmonid uses her tail to direct and accelerate river water toward the streambed by turning on her side and undulating her body, excavating a depression in which she lays her eggs. She then digs another pit in front of the first and covers the eggs that have been fertilized by one or more males; after which, she may lay another cluster of eggs in the new pit. The process might take several days, and multiple redds can be located in the same area. The depth of the egg pocket depends on many factors: size of the fish, diameter of the sediment, depth of the water, depth of alluvium, and velocity of flow. During the construction, the female typically winnows fine material out of the nest, leaving relatively coarse, porous sediment [*Chapman*, 1988; *Montgomery et al.*, 1996], with higher hydraulic conductivity than the surrounding sediment.

Salmonids are large enough to alter bed topography during redd construction (*Bjornn and Reiser*, 1991; *Shuett-Hames et al.*, 2000). Mass spawning and/or repeated spawning at the same location over many years may create persistent bedforms with heights as much as 1.5 m [*DeVries*, 1997]. Macro-scale changes in bed topography caused by spawning activity have the potential to alter channel hydraulics and consequent hyporheic flow, which in turn may affect the success of buried salmonid embryos.

Hyporheic flow is driven by spatial variation of pressure along the streambed that is caused by topographically-forced advective accelerations, changes in water depth, and associated divergence of the water-surface slope [*Tonina and Buffington, submitted, in prep*, (Chapters 2 and 3)]. Surface and subsurface water is exchanged across the streambed interface by this spatial variation of pressure, creating zones of downwelling

(river water forced into the subsurface) in high pressure zones, and upwelling (hyporheic water expelled into the river) in low pressure zones. This exchange of surface and subsurface water is known as hyporheic exchange and is an important mechanism for delivering nutrients [*Triska et al.,* 1993b], oxygen [*Coble,* 1961b], and other solutes into the sediment, and for washing away waste products to support the hyporheic ecotone. Moreover, it is an essential component of the carbon and nitrogen cycles [*Triska et al.,* 1993a], and it controls in-stream contaminant transport [*Bencala and Walters,* 1983]. An adequate concentration of dissolved oxygen, *DO,* in the water is essential to maintain an aerobic environment in the sediment, and hyporheic exchange brings *DO* into the riverbed more efficiently than molecular diffusion.

Gravel-bed rivers are common among headwater streams, which constitute an important ecological habitat for salmonids and many benthic species, in part, because of the hyporheic environment that they offer. These channels typically have a pool-riffle morphology [e.g., *Montgomery and Buffington,* 1997] characterized by large bedforms that alternate from one side of the channel to the other and create macro-scale flow obstructions and strongly three-dimensional flow. Because of the permeable sediment and strong head variations along the streambeds of these channels, the upwelling and downwelling hyporheic fluxes are intense. These streams are preferred spawning sites and rearing locations for salmonids [*Montgomery et al.,* 1999; *Buffington et al.,* 2003], many of which are currently at risk in North America [*Nehlsen et al.,* 1991]. These anadromous fish hatch and live the first part of their lives in fresh water. Then they migrate to the ocean, where they spend their adult lives, returning only to spawn at their natal ground, in small gravel-bed reaches, preferably having a pool-riffle morphology [*Montgomery et al.,* 1999]. They tend to spawn in hydraulic transitional zones of the riverbed at the tails of the pools, where downwelling hyporheic fluxes occur [*Baxter and Hauer,* 2000].

Survival of salmonid embryos has been correlated with intra-gravel velocity [*Coble,* 1961a; *Cooper,* 1965]. There are several methods to measure this velocity in the field by using standpipes [*Coble,* 1961a], vertical hydraulic gradients (VHG) [*Terhune,* 1958; *Geist et al.,* 2002], ion adsorption methods [*Clayton et al.,* 1996], and Darcy's law coupled with reach-averaged quantities [*Lapointe et al.,* 2004]. These methods either give

point measurements that are then extrapolated to the entire redd formation, or they provide average properties over the study area that may not represent local variability. The method that we present has the capability to resolve the flow field in detail and is a non-intrusive approach; we use a numerical model coupled with field measurements of channel and redd topography to predict the flow field around and through the redd.

Earlier laboratory studies showed the effects of topographic variations of the riverbed in generating intragravel flow [*Cooper,* 1965]. In his work, *Cooper* [1965] qualitatively visualized the hyporheic flow paths with dyes for different bed topographies in two-dimensional flume experiments. Furthermore, previous research shows the importance of hydraulic conductivity of the sediment and spatial variation of the water profile (and thus the pressure head) in hyporheic exchange [*Vaux,* 1962]. For example, *Geist* [2000] used VHG (a pressure head approach) to identify upwelling and downwelling areas. However, most of these studies were conducted at reach scales, providing little information about local-scale effects of redds on river hydraulics and hyporheic flow. Additionally, it has been suggested that subsurface flow generated by macro-bedforms may mask hyporheic flow generated by redds [*Edwards,* 1998]. In contrast, we hypothesize that redd formation creates localized changes in near-bed pressure distribution that generate local hyporheic flow that is superimposed on the larger-scale effects of bedforms [*Baxter and Hauer,* 2000]. *Alonso et al.* [1988] examined local-scale effects of redds, but used only a two-dimensional model. Their model for surface flow does not take into account either the redd topography or the lateral changes in river topography typical of pool-riffle channels. Furthermore, in their approach the pressure profile over the redd is approximated using a linear decrease of water depth and a constant slope. This limits the ability of the model to examine the effects of local topography on hyporheic flow within the redd, and the effect of redd topography on larger-scale river hydraulics and hyporheic flow.

In recent years, there has been an increasing interest in studying three-dimensional flow in open channels using computational fluid dynamics, *CFD,* [*Hodskinson,* 1996; *Nicholas and McLelland,* 1999a; *Ma et al.,* 2002]. These studies demonstrate the potential for this tool in studying rivers with complex topography, although there are problems in dealing with averaged Reynolds stresses and in choosing

an appropriate turbulence closure. Furthermore, gravel-bed rivers have complex boundaries with high roughness that require application of special near-wall treatments to accurately solve the flow near the river bed [*Nicholas,* 2001]. Nevertheless, with appropriate analysis of the problem, a *CFD* framework can be used to investigate flow characteristics of pool-riffle channels.

We used a three-dimensional *CFD* model coupled with the hyporheic flow model proposed by Tonina and Buffington [submitted, (Chapter 2)] to examine how redds modify both in-stream flow and hyporheic flow, and whether these changes enhance the velocity and dissolved oxygen content through the egg pocket. To address this issue, we first explored the effect of redd topography on river hydraulics. We created a pool-riffle reach having characteristics typical of Idaho rivers, to which we applied a finite element *CFD* model to study the river hydraulics. Next, a simplified salmon nest was designed from a surveyed Chinook salmon (*O. tshawytscha*) redd and was superimposed on the pool-riffle morphology. We then compared two hyporheic flow scenarios, with and without redds. Additionally, we explored the effects of redd topography versus the combined effects of topography and hydraulic conductivity on intra-gravel flow, *DO* profile and hyporheic exchange through the redd.

4.2. Methods

4.2.1. Pool-riffle topography

Using field data from Idaho rivers [*Whiting et al.,* 1999], we simulated a natural pool-riffle channel as a sequence of alternate bars in a single straight channel. We chose a bankfull channel width of six meters and applied the following geometric relationships developed by *Whiting et al.* [1999] to determine width and depth of the channel at bankfull:

$$\begin{aligned} w_B &= 4.680\,Q_B^{0.446} \qquad r^2 = 0.913 \\ D_B &= 0.256\,Q_B^{0.328} \qquad r^2 = 0.93 \end{aligned} \tag{4.1}$$

where w_B is the bankfull channel width, D_B is bankfull depth, and Q_B is bankfull discharge.

Table 4.1: Channel Characteristics

Channel characteristics*		Field values (Whiting et al. 1999)	Prototype	Numerical model
w_B	[m]	6.37	6	0.91
D_B	[m]	0.32	0.35	0.053
Q_B	[$m^3 \cdot s^{-1}$]	2	2	0.018
Δ	[m]		0.35	0.053
λ	[m]		36	5.46

* where w_B is the bankfull width, D_B the bankfull depth, Q_B bankfull discharge, Δ and λ are, respectively, the amplitude and wavelength of the bedform.

Self-formed pool-riffle channels typically have a mean pool wavelength (λ) of five to seven bankfull widths [*Leopold et al.*, 1964; *Keller and Melhorn,* 1978], although shorter values have been reported [*Carling and Orr*, 2000]. Bedform amplitude (Δ) is defined here by the residual pool depth, which is the difference in elevation between the riffle crest and the pool bottom [*Lisle and Hilton,* 1992]. We used a ratio of bedform amplitude to wavelength (Δ/λ) equal to 0.01, which is low, but reasonable for Idaho channels, which tend to have subdued topography compared to other mountain channels. Table 4.1 summarizes the geometric characteristics of the reach.

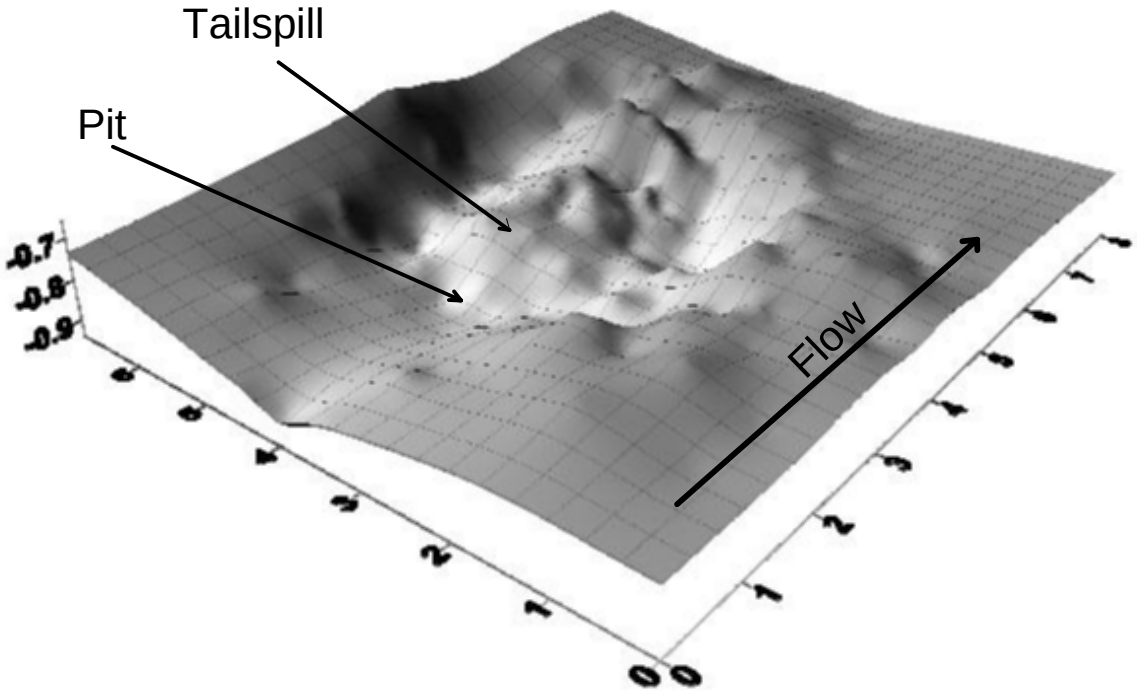

Figure 4.1: Redd topography surveyed at Cape Horn Creek, all dimensions in meters.

4.2.2. Redd topography

Redds are three-dimensional features characterized by a pit followed by a downstream hump, called a tailspill; these features are topographically below and above the original riverbed, respectively. The redd used in our analysis is based on a Chinook salmon redd surveyed in Cape Horn Creek, a tributary to the Middle Fork Salmon River, central Idaho, USA. The redd had a complex form (Figure 4.1) that we simplified for analysis, maintaining the pit depth and tailspill height (Figure 4.2).

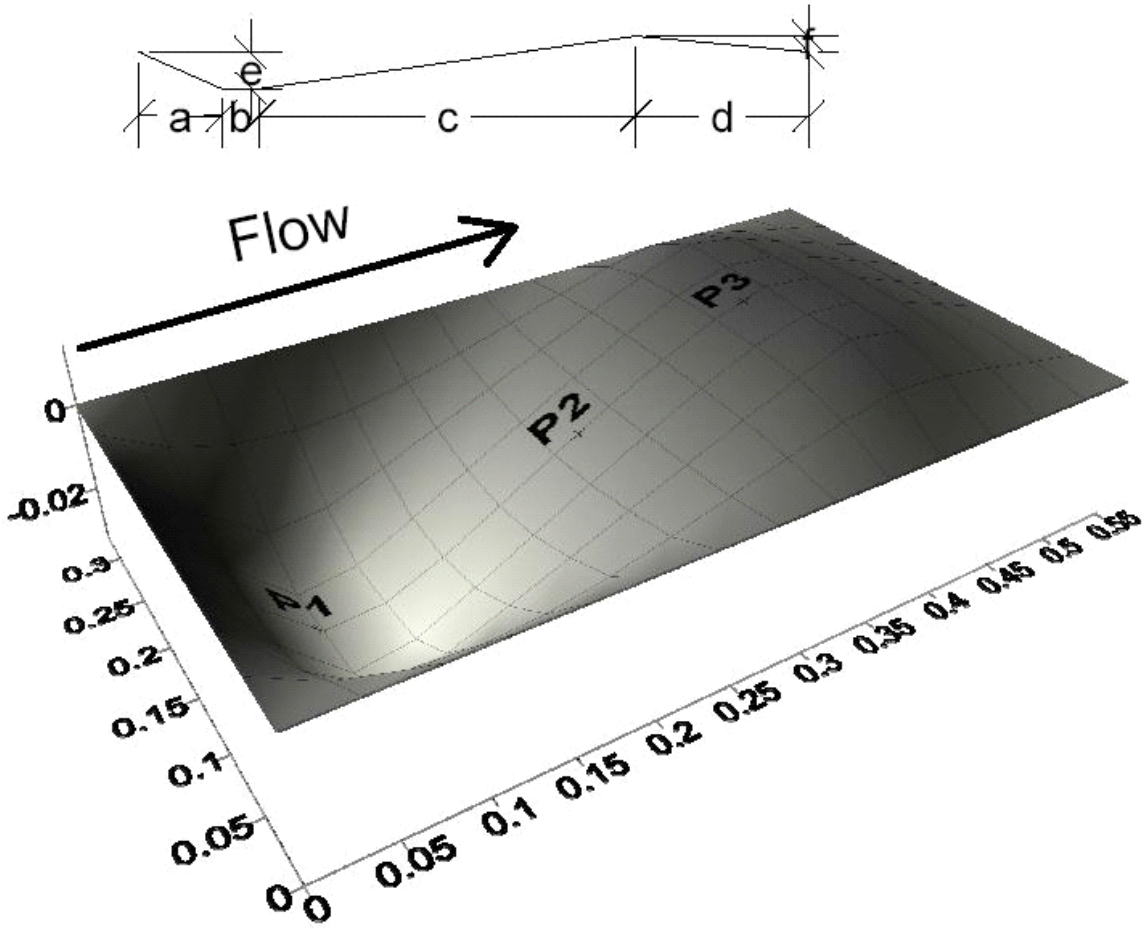

Figure 4.2: Simplified redd topography, showing locations of velocity profiles discussed in section 4.2 (P1 within the redd pit, P2 within the middle of the tailspill, and P3 within the tailspill crest) and redd dimensions along the longitudinal axis (a=0.48, b=0.22, c=2.18, d=1, e=0.21, f=0.09). Redd width is 2.15 and pit width is 0.82. All dimensions are in meters.

Figure 4.2 shows the dimensions of the simplified redd, which are typical values for Chinook salmon [*Alonso et al.*, 1988]. Salmonids orient their redds parallel to the current, and when they spawn in pool tails, the tailspill of the redd typically extends to

the riffle crest [*Hoopes*, 1972]. In our simulations, the redd is inserted at the pool tail, with its longitudinal axis oriented with the flow.

4.2.3. Numerical model of the channel

The reach used in the numerical simulation was a 1:6.59 scale model of the original reach, where the geometric length scale, L_L, is 6.59 m. This was done in order to have a fine mesh size for the numerical model. Since the Reynolds numbers are large both in the prototype and in the model, the model was dynamically scaled by matching the Froude numbers, *Fr*. This method is widely used for design of scale models [*Chadwick and Morfett*, 1997]. All of the geometric dimensions are scaled by L_L:

$$\frac{(w_B)_p}{(w_b)_m} = \frac{(D_B)_p}{(D_B)_m} = \frac{(\Delta)_p}{(\Delta)_m} = \frac{(\lambda)_p}{(\lambda)_m} = L_L \qquad \textbf{(4.2)}$$

where the subscripts *m* and *p* denote the model and the prototype, respectively. The redd prototype was also scaled by the geometric factor L_L when inserted into the numerical model. To satisfy the undistorted Froude model conditions, the following relation, in which *g* is the gravitational acceleration, was applied:

$$Fr = \frac{U_B}{\sqrt{g\,D_B}}$$
$$\frac{(Fr)_p}{(Fr)_m} = 1 \qquad \textbf{(4.3)}$$

which requires that

$$\frac{(U_B)_p}{(U_B)_m} = \sqrt{L_L} \qquad \textbf{(4.4)}$$

Since discharge is a function of flow velocity and cross-sectional area, the model discharge can be assessed by the following relation:

$$\frac{(Q_B)_p}{(Q_B)_m} = L_L^{\,5/2} \qquad \textbf{(4.5)}$$

The simulations were carried out with FLUENT 6.1 (Fluent Inc.), a *CFD* package that solves the Reynolds equations for unsteady and incompressible flow. The turbulence closure chosen was the Realizable κ–ε model [*Shih et al.*, 1995], which performs well in simulating three-dimensional flows with large rates of strain and boundary curvature

[*Fluent Inc.,* 2003]. We treated the near-wall flow with the standard wall function [*Fluent Inc.,* 2003]. To simulate an open channel flow, we used the volume of fluid, VOF, option that models a two-phase system: water and air [*Hirt and Nichols,* 1981]. The presence of air enabled the software to determine the water surface position by simultaneously solving water and air flow fields. This method gives a more accurate representation of the flow field than the commonly used fixed-lid approach in which the water surface is specified a priori. If the water surface is not accurately assigned for the latter approach, an incorrect mass and momentum distribution in the fluid may occur, leading to errors in the solution of flow velocity and near-bed pressure.

The study reach was a sequence of three pools and two riffles, with two planar reaches at the beginning and at the end. The planar entrance and exit were to ensure that the flow was completely developed both in approaching the pool-riffle reach and in leaving the numerical domain. This allowed us to set the water outlet and inlet as a pressure outlet and a velocity inlet, respectively. The riverbed was set up as a wall and decoupled from the groundwater because of the small momentum and mass transfer between surface and subsurface flows (i.e. groundwater flux does not effect the surface flow), while the bed surface was modeled as a pressure inlet for coupling the surface and subsurface domains (discussed in the next section). We set up a pressure inlet boundary for the upstream and downstream inlets for the air. The volume was meshed with dimensions 0.045 and 0.024 m in the horizontal plane along x and y directions, respectively. This grid provided enough accuracy for the computational capability of our computer. The water depth was meshed with 16 uniformly spaced nodes, and boundary layers with finer mesh were used near the bed surface and sides of the channel to solve the flow close to these boundaries. Because of the mesh size, it was possible to capture the bedform roughness, but not the grain roughness, which was represented by the standard wall functions for turbulent flow [*Fluent Inc.,* 2003].

4.2.4. Numerical model of hyporheic flow

Fluent 6.1 (FLUENT Inc.) was also used to model the hyporheic flow. The first pool-to-pool sequence was chosen as the study section and was meshed with hexahedral elements with three-centimeter sides. We selected this dimension to satisfy Darcy's law,

which requires that the size of the volume on which it is applied is larger than the scale of the microscopic quantities governing the flow (i.e., the diameter of the porous medium) [*Hassanizadeh and Gray,* 1979]. The diameter of the medium is on the order of a fraction of a millimeter, which is smaller than the mesh size. At the same time, the chosen dimension provides sufficient resolution of the flow field. Application of Darcy's law additionally requires low Reynolds number flow and negligible convective accelerations [*Hassanizadeh and Gray,* 1987].

To solve the flow field six boundary conditions are needed, plus a seventh for the exposed part of the bars. The sides of the groundwater model, which correspond with the sides and bottom of the channel, and the exposed sections of bar were modeled as wall boundaries. The submerged riverbed surface was modeled as a pressure inlet, and the pressure distribution obtained by the surface flow simulations (Section 2.3) were used as boundary values. The upstream and downstream ends of the domain were set as periodic boundaries, which in FLUENT creates the same conditions at both ends, ensuring that what is going out from one boundary is going into the other one, forming an infinite reach of pool-riffle sequences. Since we investigated one pool-riffle unit, the periodic boundary was set in such a way that what was exiting one periodic boundary was entering the domain in the other periodic boundary on the opposite side.

Once the flow field was solved, the particle tracking method was applied to evaluate flow paths and residence times for each particle. This method consists of injecting particles into the bed surface, following their trajectories, and recording the time to pass through the aquifer before reentering the river, excluding the particles which are lost to the deep aquifer and do not reemerge into the river within the model domain.

To investigate the dissolved oxygen profile within the sediment, we analyzed the oxygen dispersion as if it were driven primarily by an advective mechanism. Dissolved oxygen, *DO*, is brought into the sediment by the downwelling flux of river water and is used by the micro-invertebrates, biofilms, and other animals that dwell in the sediment interstices. The oxygen uptake by these organisms is referred to as sediment oxygen demand, *SOD*. We applied a constant value of *SOD* equal to 2.64 $g \cdot m^{-3} \cdot d^{-1}$ [*Huang et al.,* 2001] throughout the sediment domain. To scale the groundwater model, we matched the Reynolds numbers in the model and prototype

$$\frac{(Re)_p}{(Re)_m} = 1$$
$$\frac{SOD_m}{SOD_p} = L_{SOD} = L_L^5 \qquad \textbf{(4.6)}$$

where L_{SOD} is the scale for the rate of oxygen uptake within the sediment. Since the *SOD* is a function of time and volume (volume scale is L_L^3), L_{SOD} can be obtained knowing the geometric scaling factor of the model (L_L) and the time scale factor, which is equal to the square of the geometric scale for an undistorted Reynolds model. Thus, L_{SOD} is the length scale raised to the fifth power, and the SOD_m becomes 0.38 g·m^{-3}·d^{-1}.

Furthermore, we assumed that the oxygen is a passive tracer transported by the hyporheic flow, and the diffusive process is conservatively represented solely by molecular dispersion, D_m. The D_m value for oxygen in water was estimated from the *Wilke and Chang* [1955] formula:

$$D_m = 7.4 \cdot 10^{-8} \frac{T \sqrt{\psi M}}{\mu V} \qquad \textbf{(4.7)}$$

where T is the absolute temperature of the water in degrees Kelvin, ψ is a parameter for the solvent capacity of the water, 2.26, M is the molecular weight of the water (18 g·mole^{-1}), μ is the water viscosity in centipoises, and V is the molar volume of oxygen, 25.6 cm^3·g^{-1}. The oxygen transport equation used in the model becomes:

$$\frac{\partial DO}{\partial t} + v_i \frac{\partial DO}{\partial x_i} = D_m \nabla^2 C - SOD \qquad \textbf{(4.8)}$$

where v is the local velocity inside a cell and i identifies the three principal directions. Additionally, the boundary conditions were set by imposing constant values of 10 mg·l^{-1} and 2 mg·l^{-1} of *DO* at the bed surface and bottom of the alluvium, respectively. The former is a typical value of *DO* in well-oxygenated rivers at 15 °C [*Wetzel*, 1983, Table 9-1].

4.3. Experiments

We ran two simulations, one with a gravel pool-riffle morphology, and the second with a redd superimposed on this channel. A constant discharge of 1 m^3·s^{-1} (scaled value) was used to simulate a low flow discharge. The pressure distribution predicted at the

riverbed was then applied as the boundary condition for the groundwater model to generate the hyporheic flow.

Two scenarios were examined for the pool-riffle morphology: one with deep alluvium (0.5λ, where λ is the bedform wavelength), and one with shallow alluvium (0.05λ). In the first case, the depth of alluvium does not interfere with hyporheic flow, while in the second case it significantly alters hyporheic volume [*Tonina and Buffington,* in prep. (Chapter 3)]. A constant hydraulic conductivity of 10^{-3} m·s^{-1} was used for both cases, a value that is typical of mixed gravel and sand [*Das,* 1998, Table 5.1].

Four scenarios were simulated for the pool-riffle reach with the redd. We ran two scenarios for each case of deep and shallow alluvium: one with a constant hydraulic conductivity of 10^{-3} m·s^{-1}, to analyze the effect of redd topography only, and a second with the redd having a higher hydraulic conductivity (0.05 m·s^{-1} typical of clean gravel [*Das,* 1998, Table 5.1]) than the surrounding sediment, to examine the combined effects of redd topography and the winnowing of fines that occurs during spawning. The vertical location of the redd depends on the depth at which the females lay the eggs. In a recent paper, *DeVries* [1997] reported that the average depths of the top and bottom of the egg pocket for Chinook salmon are approximately 15 and 50 cm below the original bed surface, respectively. Consequently, we assumed an egg pocket depth of 50 cm.

4.4. Results

4.4.1. River hydraulics

As expected, our simulations predict that at low discharge, parts of the bars are dry, and the flow meanders around them, plunging into the pool and accelerating over the riffle (Figure 4.3a). The high velocity core swings from the left to the right riverbank, remaining in the outer side of the pool. Downstream of the riffle crest on the inner side of the pool is a large eddy that creates a dead zone where the water moves slowly. The same recirculating zone was observed in flume experiments conducted at the Saint Anthony Falls Laboratory for the same bed topography, but at a slightly higher discharge [*Tonina and Buffington,* submitted (Chapter 2)]. The water surface elevation increases as it

approaches the riffle and then decreases downstream of the riffle crest. A super-elevation effect is visible at the outer side of the pool where the flow bends upon entering the pool.

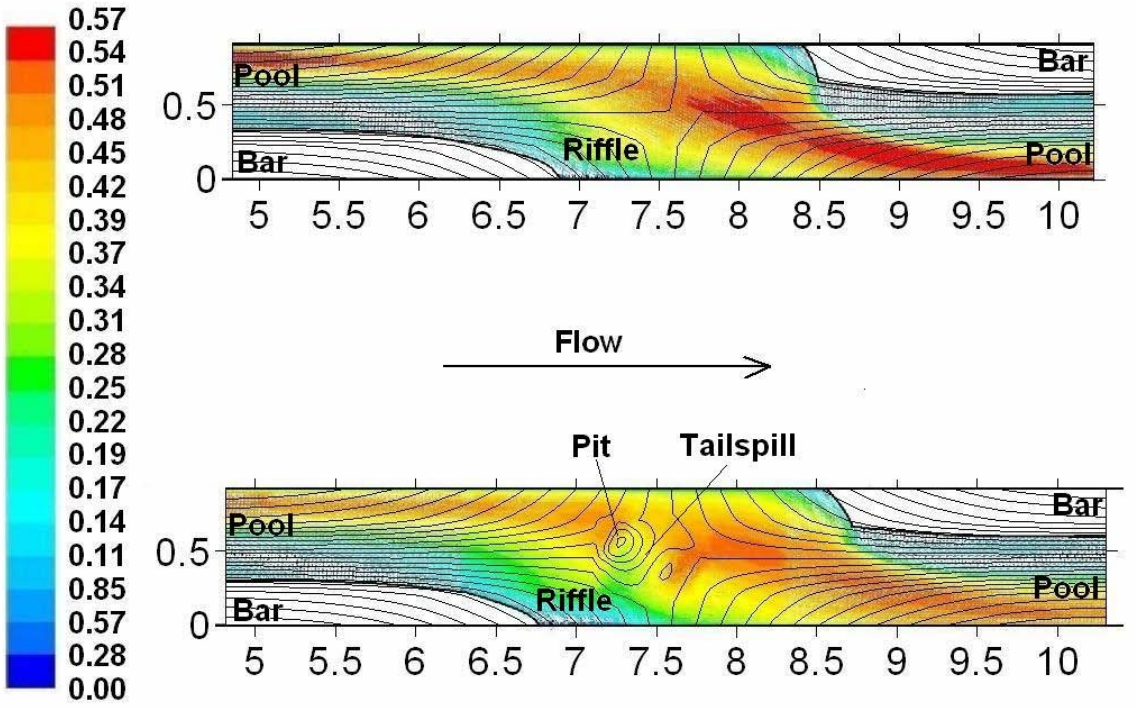

Figure 4.3: Velocity vectors colored by magnitude ($m \cdot s^{-1}$) at the water surface in a pool-riffle channel (*a*) without and (*b*) with redd topography (all dimensions in meters). Contour lines represent bed topography.

The velocity distribution of the flow changes when a redd is built at the end of the pool (Figure 4.3b). The redd is oriented parallel to the current, which accelerates as it approaches the riffle, but the presence of the redd pit retards the acceleration, and the velocity suddenly drops. The water then accelerates again as the flow is forced to shallow over the tailspill of the redd, but the main high velocity core remains close to the bar. The flow separates at the upstream edge of the pit (Figure 4.4), creating a recirculating vortex characterized by low pressure, similar to what happens on the lee side of a dune [e.g., *McLean and Smith*, 1986]. Additionally, the presence of the pit and the tailspill affect the water surface elevation, which falls at the beginning of the pit, rises again, and eventually lowers over the tailspill.

The pressure distribution over the riverbed in the vicinity of the redd is strongly influenced by the change in river hydraulics caused by the presence of the redd (Figure

4.5). Without the redd, high pressure areas are located in the outer part of the pool tail, while lower pressure areas occur in the inner part of the pool downstream of the riffle.

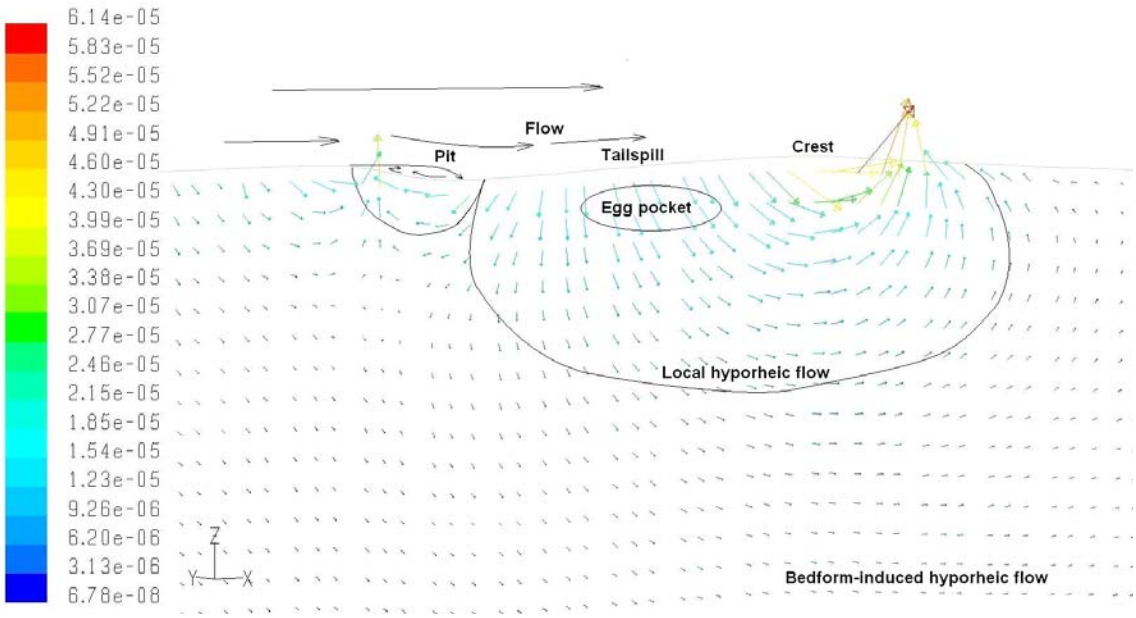

Figure 4.4: Hyporheic flow along the longitudinal axis of the redd, with velocity vectors colored by magnitude ($m \cdot s^{-1}$), and scales of hyporheic flow indicated (local, induced by redd topography versus bedform, induced by pool-riffle topography). All dimensions in meters.

The redd alters these patterns, creating a high-pressure area before the tailspill and a low-pressure zone both within the pit and downstream of the tailspill. As discussed above, the low-pressure zone in the pit stems from the flow separation at the upstream lip of the pit. A complimentary high-pressure zone occurs just downstream where the boundary layer reattaches as the flow climbs the tailspill (Figures 6.4 and 6.5b). We observe that the pressure distribution in the pool remains largely unchanged with or without the redd. Consequently, the effects of the redd are localized at the riffle. These changes in the pressure distribution have corresponding effects on the hyporheic flow through the streambed and redd, as discussed in the next section.

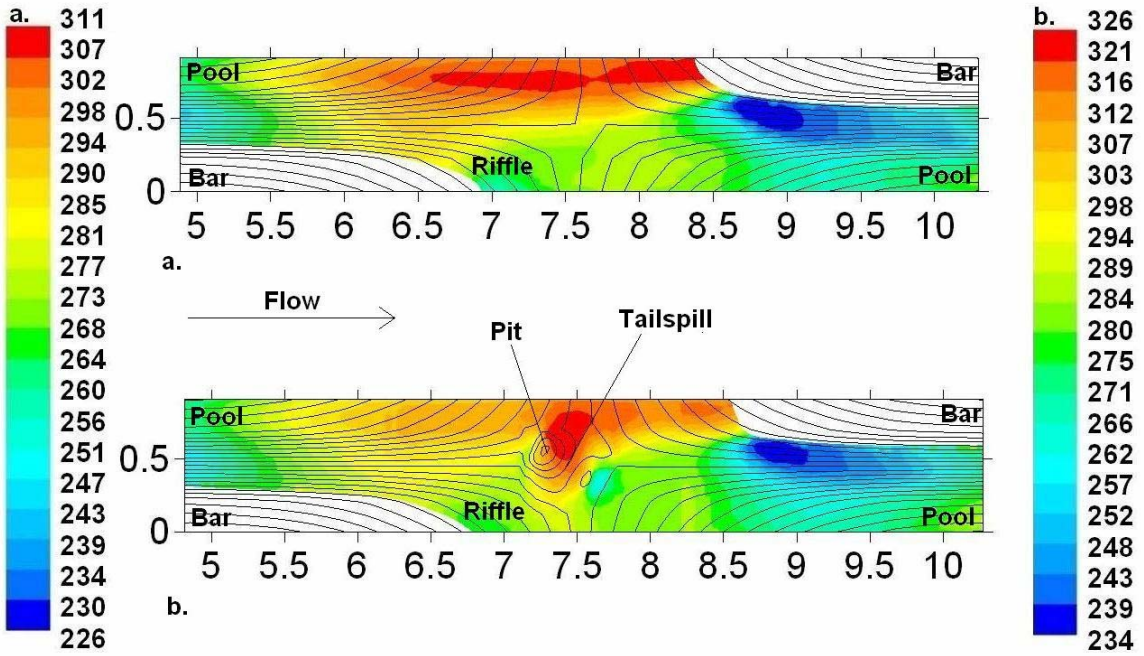

Figure 4.5: Near-bed pressure distribution (Pascal) in a pool-riffle channel (a) without and (b) with redd topography (all dimensions in meters). Contour lines represent bed topography.

4.4.2. Hyporheic flow

Figure 4.6a shows the upwelling and downwelling areas for the case without a redd. The upwelling areas are located downstream of the riffle crest and in the recirculating zone close to the bar. The depth of alluvium does not affect the location and extent of upwelling and downwelling areas, which are functions of the near-bed pressure distribution as influenced by bed topography and channel hydraulics [*Tonina and Buffington*, submitted (Chapter 2)]. The pressure distribution over the sediment surface generates a three-dimensional hyporheic flow within the sediment. With deep alluvium, hyporheic flow paths cross the riffle and then bend from the pool bottom toward the bar slope where areas of low pressure are present (Figure 4.7). The flow can be divided into a primary flow that moves longitudinally, and a secondary flow, which brings water from the outer side of the pool to the inner side, creating an elliptical current similar to the in-stream flow. The hyporheic pathlines are three-dimensional close to the surface, while deeper pathlines show a more two-dimensional behavior. In contrast, when the depth of alluvium is shallow, the hyporheic flow is strongly three-dimensional and interacts with the impervious layer. The flow paths penetrate down into the sediment until they reach

the impervious layer, and then they travel parallel to the bottom to emerge at a low-pressure zone on the streambed (Figure 4.8).

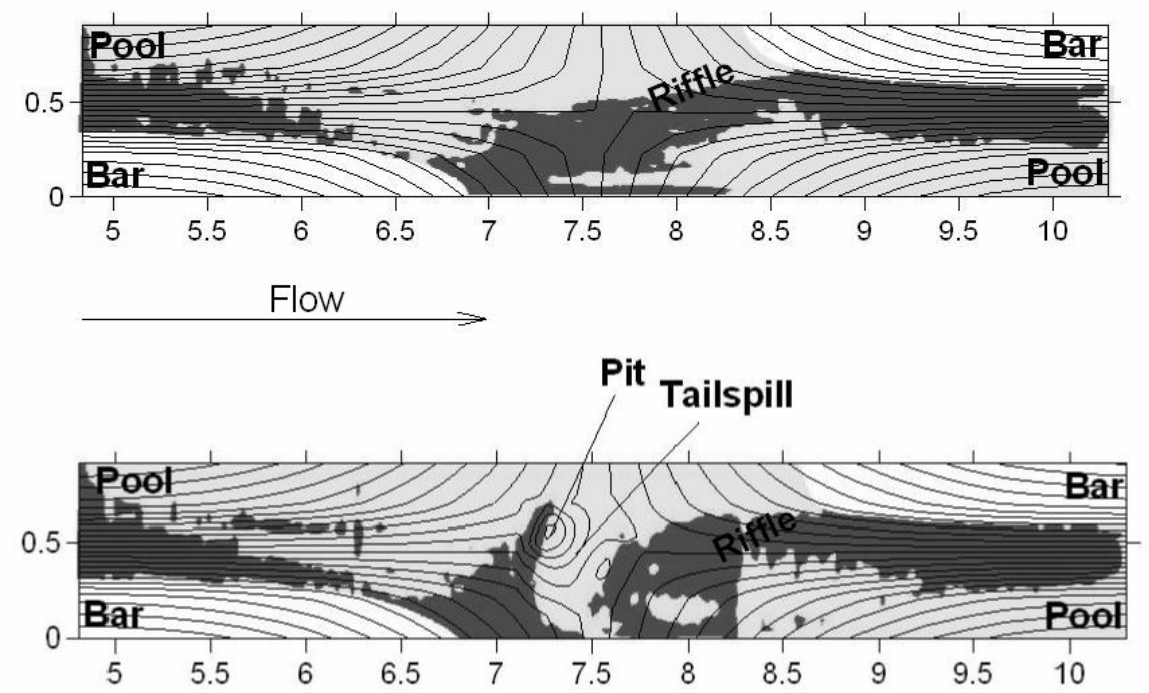

Figure 4.6: Upwelling (dark gray) and downwelling (light gray) areas in a pool-riffle channel with shallow alluvium (0.05λ) (*a*) without and (*b*) with redd topography (all dimensions in meters). Contour lines represent bed topography.

At the riffle crest, the flow is downwelling on the upstream side of the riffle and upwelling on the downstream side (Figures 4.6a and 4.7). This pattern of hyporheic flow is forced by the gradient of high to low pressure across the riffle (cf. Figures 4.5a and 4.6a). There are also some downwelling vectors heading upstream, present in both deep and shallow aquifer, because of the low groundwater gradient used in our simulation (0.2%) (Figures 4.7 and 4.8). Steeper groundwater gradients would produce faster mean groundwater flow, which would in turn prevent hyporheic flow from moving upstream and would compress the hyporheic flow close to the riverbed surface [*Tonina and Buffington,* in prep. (Chapter 3)].

Figure 4.6b shows the upwelling and downwelling areas for the pool-riffle unit with a redd placed at the pool tail. The redd changes the pattern of hyporheic exchange, imposing upwelling in areas where downwelling would have otherwise occurred. Recirculating eddies in the redd pit and downstream of the tailspill crest create low-pressure zones that force upwelling downstream of the tailspill and in the downstream

half of the redd pit (Figure 4.4 and 6b). In contrast, the high-pressure zone over the tailspill (Figure 4.5b) forces downwelling through the tailspill, where the eggs are located (Figure 4.4 and 6b). The redd also receives in-stream water laterally because of the presence of the bar. As flow exits the pool and is topographically forced over the riffle, the water surface rises approaching the bar head, therefore intensifying the pressure over the sediment. This high-pressure zone drives river water toward the redd.

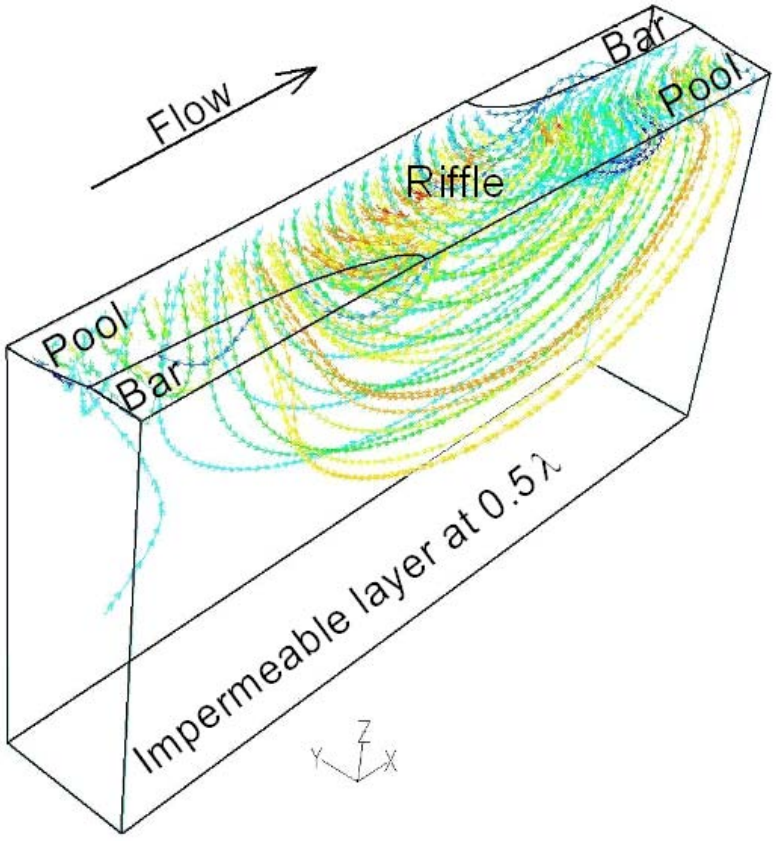

Figure 4.7: Hyporheic pathlines (colored by particle ID) for pool-riffle morphology with deep alluvium (0.5λ).

We also assessed the intra-gravel (hyporheic) velocity at three locations within the redd (Figure 4.2, P1-3), and at the same coordinates for the case without the redd. Redd formation incorporates both the effects of redd topography and the change of hydraulic conductivity from winnowing of fine particles and re-packing of the gravel during spawning. Consequently, we explored the effects of redd topography versus the combined effects of topography and altered hydraulic conductivity on intra-gravel velocity through the redd. To isolate the effects of topography, we assumed a hydraulic conductivity of the redd equal to that of the surrounding sediment, or “aquifer”

($k_{redd}=k_{aq}=10^{-3}$ m·s^{-1}). For the combined effects of topography and altered hydraulic conductivity, we assumed a hydraulic conductivity of 0.05 m·s^{-1} within the redd. We also examined two cases of alluvium depth (0.05λ versus 0.5λ).

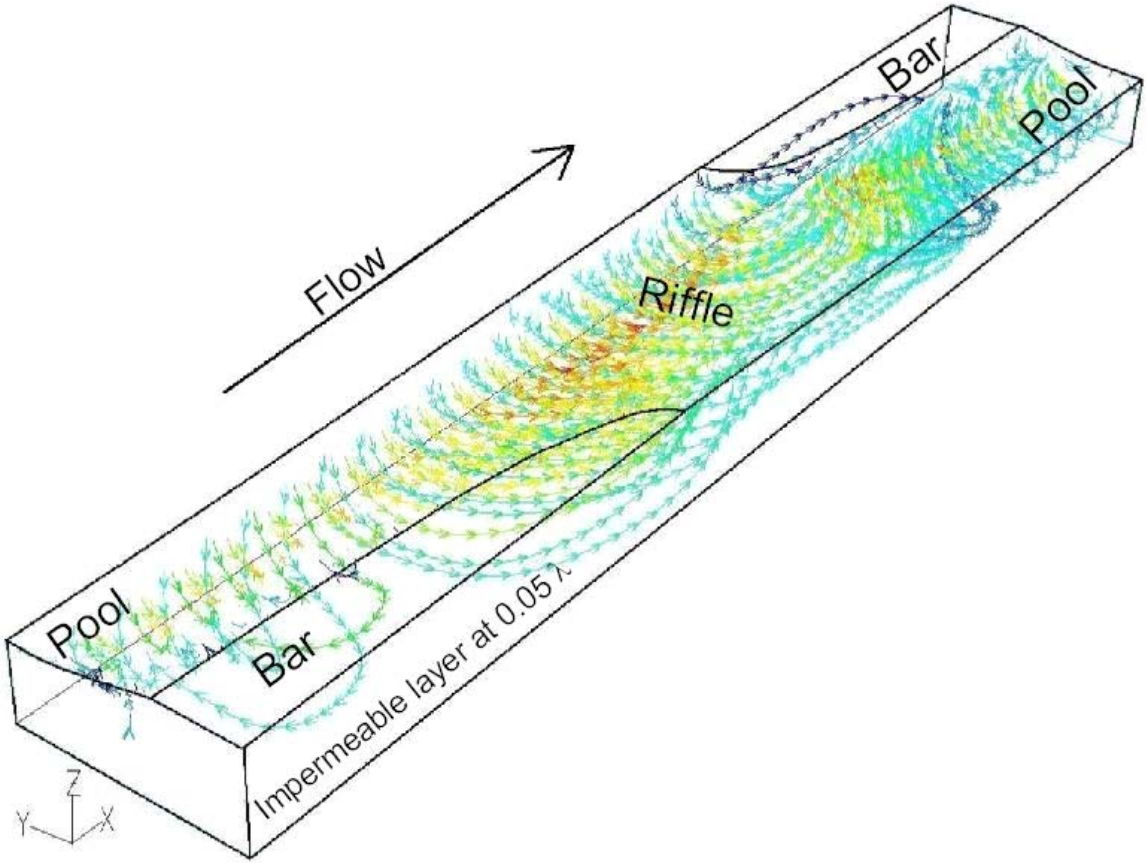

Figure 4.8: Hyporheic pathlines (colored by particle ID) for pool-riffle morphology with shallow alluvium (0.05*λ*).

We find that redd topography alone causes a 3-4 fold increase in velocity within the egg pocket (Figure 4.9a, P2-3). In contrast, the combined effects of redd topography and altered hydraulic conductivity cause the velocity to increase by two orders of magnitude (Figure 4.9b, P2-3). We also find that the depth of alluvium does not significantly change the velocities within the redd (cf. Figures 4.9a-b to Figures 4.9c-d). However, for shallow alluvium, the velocities for a given location are slightly lower than for the case of deep alluvium. It is important to note that depth of alluvium influences the hyporheic flow and, therefore, affects the intra-gravel velocities [*Tonina and Buffington*, in prep. (Chapter 3)], but we suggest that shallower and less intense hyporheic flows,

which should have less interaction with the impervious layer, would be less affected by a decrease in alluvial depth than would deeper and more intense flows.

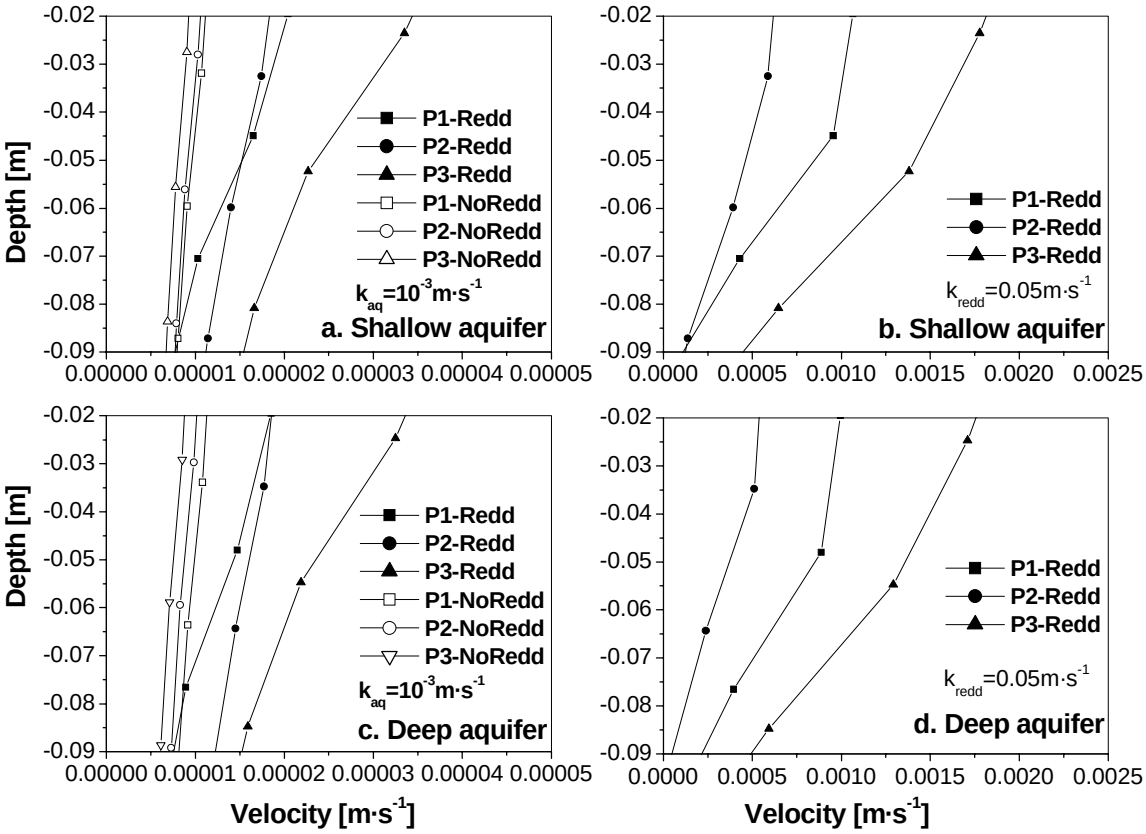

Figure 4.9: Vertical profile of hyporheic velocity at three locations along the longitudinal axis of the redd (at the pit (P1), at the middle of the tailspill (P2), and at the tailspill crest (P3)) for redd topography with: (*a*) shallow alluvium (0.05λ) and hydraulic conductivity of the redd equal to that of the surrounding sediment, $k_{redd}=k_{aq}=10^{-3}$ m·s^{-1}, (*b*) shallow alluvium and hydraulic conductivity of the redd greater than that of the surrounding sediment, k_{redd} = 0.05 m·s^{-1} and k_{aq} = 10^{-3} m·s^{-1}; (*c*) deep alluvium (0.5λ) and $k_{redd}=k_{aq}=10^{-3}$ m·s^{-1}, and (*d*) deep alluvium, k_{redd} = 0.05 m·s^{-1} and k_{aq} = 10^{-3} m·s^{-1}. All values are model-scaled, and depth is relative to the bed surface, with -0.02 and -0.09 m indicating the top and bottom of the egg pocket, respectively.

The hyporheic exchange is influenced by the presence of the redd and by the spawning-related change in hydraulic conductivity within the redd. Figure 4.10 shows the downwelling flux at 90, 75, 50, 25, and 10% of the residence time, which corresponds to the amount of downwelling flux that remains in the riverbed at a given time after it enters the sediment. Biological uptakes and chemical transformations, such as nitrification and denitrification, require a certain amount of time to take place, and these flux magnitudes correspond with the amount of river water that is present within the sediment and,

therefore, undergoing those biochemical processes in the groundwater environment. Results show that both the downwelling flux and the residence time are affected by the presence of the redd (Figure 4.10), but the change in hydraulic conductivity causes more substantial changes than the redd topography alone. In addition, the depth of alluvium does not affect the average downwelling flux, although the shallower alluvium shows less intense flux. However, shallow depths of alluvium than those modeled here might change the intra-gravel flow more appreciably

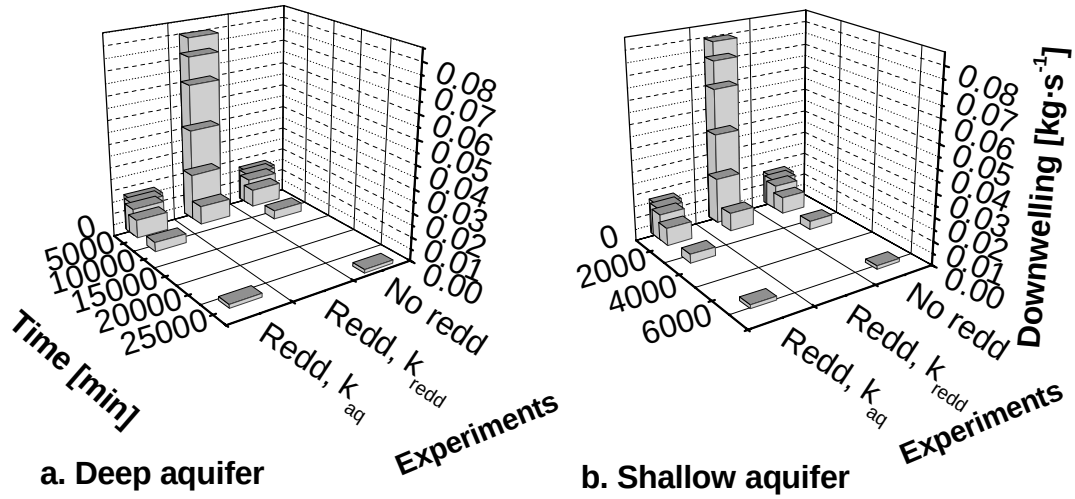

Figure 4.10: Downwelling flux per time quartiles for deep (0.5λ) and shallow alluvium (0.05λ).

In Figure 4.11, we show the decay of solute concentration (magnitude of hyporheic exchange) over one pool-riffle unit. The redd does not affect the solute decay in the river as long as the hydraulic conductivity of the redd is the same as the surrounding sediment. When the conductivity of the redd is higher, there is an initial strong exchange, after which the curves have similar shape. This suggests that redds tend to affect only the near-bed hyporheic exchange (i.e., that with the shortest residence times).

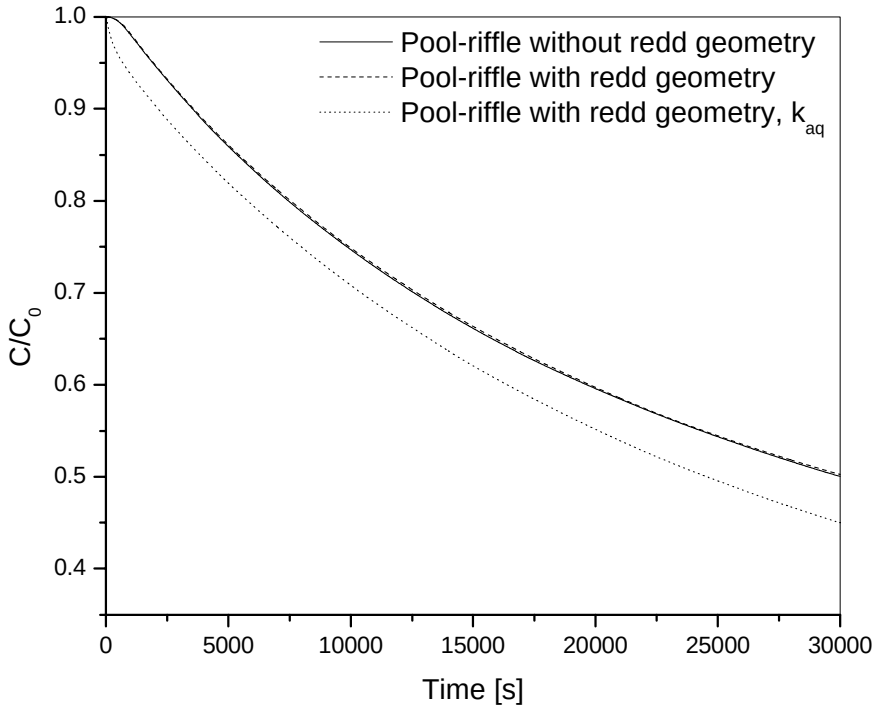

Figure 4.11: In-stream decay of solute concentration for deep alluvium (0.5λ). *C* is the solute concentration at a given time, and C_0 is the initial solute concentration.

4.4.3. Oxygen distribution

Dissolved oxygen (*DO*) concentration is a critical factor for the growth and development of salmonid embryos incubating within eggs buried in the streambed, and later for the alevins that will dwell among the gravel interstices before emerging into the stream [*Chapman*, 1988]. The *DO* value is a function of temperature; in cold water, dissolved oxygen has a higher saturation value. We applied equation (4.8) to assess the importance of redds on the *DO* distribution within the sediment.

Figure 4.12a shows the profile of *DO* along the center axis of the redd. When the hydraulic conductivity of the redd is higher than the surrounding sediment, the egg pocket has a *DO* concentration equal to that of the in-stream water. To isolate the effect of redd topography, we set the hydraulic conductivity of the redd equal to that of the surrounding gravel. In this case, the *DO* concentration within the redd is lower than the in-stream value of 10 mg·l^{-1}, and it decreases to 4.5 mg·l^{-1} at the bottom of the egg pocket (50 cm below the original riverbed) (Figure 4.12b). However, most of the redd is still above the threshold of deprivation (6 mg·l^{-1}) [*Levy and Slaney*, 1993]. Figure 4.12c corresponds to the reference case for which there is no redd formation at the tail of the

pool, with hyporheic flow caused by bedform topography only. This case shows a strong reduction in *DO* concentration in the zone where the egg pocket would be present. The *DO* concentration drops to around 5 $mg \cdot l^{-1}$ in the zone where the middle of the egg pocket would be located, and below 2 $mg \cdot l^{-1}$ at the bottom of the pocket under the riffle crest.

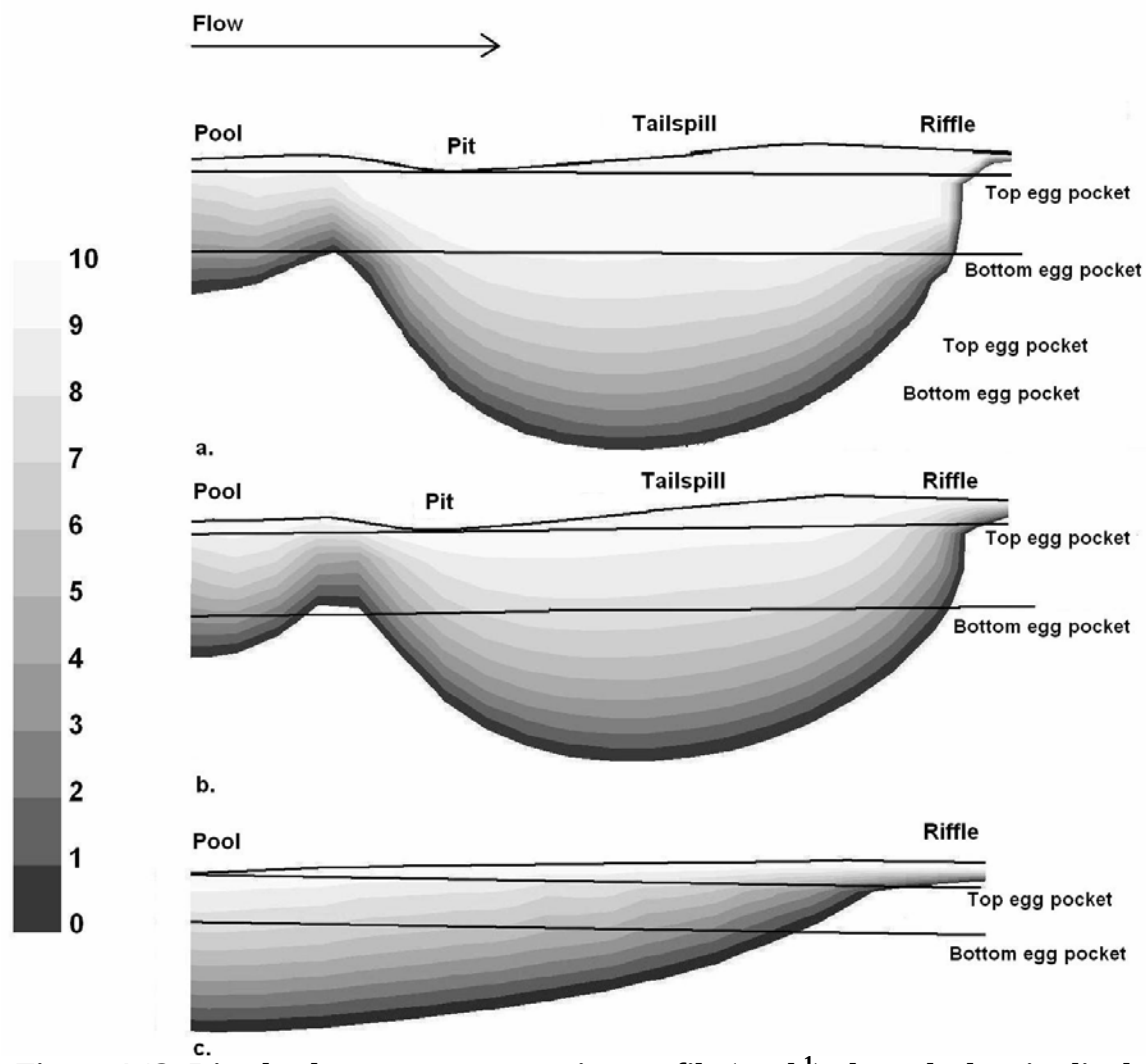

Figure 4.12: Dissolved oxygen concentration profile ($mg \cdot l^{-1}$) along the longitudinal axis of the redd for three cases: (*a*) with redd topography and altered hydraulic conductivity (k_{redd}= 0.05 $m \cdot s^{-1}$); (*b*) with redd topography alone (same hydraulic conductivity of the surrounding sediment); and (*c*) without redd (reference conditions before spawning). The upper and lower horizontal lines denote the top and bottom position of the egg pocket at 14 and 59 cm below the bed topography.

4.5. Discussion

In this paper, we investigated whether redd formation influences river and hyporheic flows and if the magnitude of these changes would affect the habitat quality within the sediment by increasing surface-subsurface water exchange and intra-gravel velocity at the redd location. Unlike previous studies, we analyzed the process with a detailed three-dimensional model, which integrates the most important physical and hydraulic characteristics of pool-riffle and redd morphologies. One limitation of the model is the impervious sides assumed in the groundwater domain, conditions that best apply to confined rivers [e.g. *Montgomery and Buffington*, 1997]. However, our results likely would still hold in scenarios where lateral groundwater fluxes are not too intense, since the modeled redd is located at the pool tail, which is far from the riverbanks, and as we found in this work, redd formation affects hyporheic flow at local scales, which is less influenced by lateral boundary conditions. Therefore, our observations likely have wider application than for confined channels only.

The model results indicate that redd topography can affect river hydraulics by changing the flow field and water depth. This interaction between redds and river hydraulics has been overlooked in previous models that did not capture the three-dimensional bed topography and detailed channel hydraulics. We find that these biophysical interactions at the redd scale may be an essential component in forming successful spawning environments.

The changes in river flow momentum and velocity caused by redds alters the near-bed pressure profile, which in turn modifies the location and intensity of the upwelling and downwelling areas. Redd topography generates local hyporheic flow that downwells along the tailspill and upwells downstream of the tailspill crest. Downwelling also occurs within the redd pit. These results show that reach-scale hyporheic flow does not mask the exchange induced by redds. On the contrary, it is the redd topography that imposes new distributions of upwelling and downwelling areas, creating upwelling areas at the redd pit, where downwelling would otherwise occur. However, these changes in hyporheic flow occur at the redd scale and do not propagate to larger scales. Although, our results show that the presence of one redd does not influence the average hyporheic

exchange, we believe that multiple redd formations could influence the reach-average exchange, since the pressure profile would be more variable and more sediment would have higher permeability because of spawning activity.

If the spatial variability of upwelling and downwelling around redds is not recognized, local measurements, such as vertical hydraulic gradients (VHG), may yield misleading results. For example, a single local measurement near the lip of a redd pit might yield the erroneous conclusion that redds are located in upwelling zones. Consequently, we recommend a higher sampling density for those approaches to better represent local conditions and local variability.

The magnitude of the hyporheic flow governs intra-gravel velocity, which has a multiple effects on embryo survival; it keeps gravel interstices clear of fine particles and waste products, and brings oxygen into the sediment. The redd-induced hyporheic flow, which is locally more intense than that due to bedforms, causes a four-fold increase in hyporheic flow velocity through the egg pocket compared to the same channel without a redd. In addition, redd construction increases the hydraulic conductivity within the redd, enhancing the intra-gravel velocities by about two orders of magnitude. Moreover, the redd shape creates a heterogeneous flow field with the fastest flow located underneath the tailspill where the eggs are laid. Hyporheic flow converges underneath the redd tailspill because of the three-dimensional shape of the redd and its location close to the upstream head of the bar.

Our results confirm that pool tails, where redds are commonly constructed, are areas of high pressure and downwelling. The hyporheic flow in pool tails that is generated by pool-riffle topography creates a marginally suitable subsurface habitat for salmonid eggs even without the effects of redds; there is sufficient downwelling with adequate hyporheic velocity and oxygen content for egg survival at depths where egg pockets would be located. However, we find that oxygen levels may decrease below the deprivation limit (6 $mg \cdot l^{-1}$) near the bottom of where egg pockets would be located, emphasizing that the hyporheic flow generated by pool-riffle topography alone creates only marginal habitat. Redd construction in pool tails significantly enhances the hyporheic velocity and oxygen concentration, increasing the potential for embryo survival. However, a redd located in an upwelling area (for instance downstream the

riffle close to the bar side) would experience a more intense mixing between in-stream and groundwater. River water would be driven into the sediment by the redd shape and it would mix with the upwelling flux of groundwater that is preferentially directed toward the pit or tailspill end. The mixing will provide warmer water during the winter [*Garrett et al.,* 1998], and cooler water during the summer depending on the amount of groundwater present and the residence time of the hyporheic flow. However in this location, if the redd morphology was removed by fluvial erosion, embryo survival would depend on the intensity of the upwelling hyporheic flow generated by the bedform, which may have a low oxygen content by the time it reaches the eggs, due to a longer flow path through the subsurface compared to that of the pool tail.

We used a simple *DO* transport model based on convective transport that relies on a constant sink of oxygen, *SOD,* within the sediment volume. *SOD* depends on oxygen concentration and varies with depth, as well as organic and inorganic transformations, but because of the uncertainty of the magnitude of this variability, we assumed a constant value. Our results support the importance of the redd formation in enhancing and developing a suitable environment for embryos and fry in the gravel interstices. Redds locally affect the downwelling flux, enhancing the *DO* exchange between in-stream water and pore water. River water is driven into the tailspill and through the egg pocket to exit at the tailspill crest. This mechanism keeps the redd oxygenated with a constant water flow. *Geist* [2000] reported that dissolved oxygen concentrations were higher in areas in which spawning had occurred, confirming our finding that redd formation enhances hyporheic exchange.

The higher hydraulic conductivity of the material present within the redd ensures that well-oxygenated river water fills the pore interstices. Consequently, salmonid spawning activities likely have a positive influence on survival of their offspring. Moreover, salmonids actively modify their environment and are not passive inhabitants of it. However, the same activities that enhance embryo survival may make the eggs vulnerable to pollutants that are present in the stream; redd-induced hyporheic flow will direct pollutants into egg pockets that are easily penetrated because of their coarse, open structure and high hydraulic conductivity.

Understanding the physical and biological interactions associated with salmonid spawning is important for conservation and restoration efforts. Hyporheic fluxes generate physical and chemical gradients within the stream that can be detected by salmonids. Salmonids preferentially use areas with strong hyporheic fluxes for spawning [*Baxter and Hauer,* 2000; *Geist,* 2000], probably because of the associated physiochemical gradients and higher water quality. Consequently, coupled surface and subsurface flow models, such as the one presented here, could be used to provide maps of upwelling and downwelling areas that can be incorporated into salmon habitat models to predict spawning zones, or to guide stream and habitat restoration efforts. Our findings indicate that such models need to represent the detailed three-dimensional topography and hydraulics of the channel to accurately map hyporheic habitat and the biophysical interactions associated with salmonid spawning activities. Although Chinook salmon redds form macro-scale topography comparable in size to that of bar and pool topography, the size of redds and their consequent influence on surface and subsurface flow will vary with salmonid species. Smaller fish typically build smaller redds.

Acknowledgements. This work was supported by the USDA Forest Service Yankee Fork Ranger District (00-PA-11041303-071), by the US Department of Education Fund for the Improvement of Postsecondary Education (P116Z010107), and by the USDA Forest Service Rocky Mountain Research Station (03-JV-11222014-060). We thank Bruce Rieman for thoughtful comments on an earlier draft of this manuscript, Russ Thurow for his advice on redd characteristics, and Nick Scheidt for field assistance.

References

Alonso, C. V., F. D. Theurer, and D. W. Zachmann (1988), *Tucannon River Offsite Study: Sediment intrusion and dissolved-oxygen transport model*, U.S. Department of Agriculture, Agricultural Research Service Hydro-Ecosystem Research Group, Fort Collins.

Baxter, C. V., and R. F. Hauer (2000), Geomorphology, hyporheic exchange, and selection of spawning habitat by bull trout (*Salvelinus confluentus*), *Canadian Journal of Fisheries and Aquatic Sciences, 57,* 1470-1481.

Bencala, K. E., and R. A. Walters (1983), Simulation of solute transport in a mountain pool-and-riffle stream: a transient storage model, *Water Resources Research, 19*(3), 718-724.

Bjornn, T. C., and D. W. Reiser (1991), Habitat requirements of salmonids in streams, *American Fisheries Society, Special Publication*(19), 83-138.

Buffington, J. M., D. J. Isaak, and R. F. Thurow (2003), Hydraulic Control on the Spatial Distribution of Chinook Salmon Spawning Gravels in Central Idaho: Integrating Reach-Scale Predictions via Digital Elevation Models, in Proc. *AGU Fall Meeting*, edited by EOS, AGU, 84, San Francisco.

Carling, P., and H. G. Orr (2000), Morphology of Riffle-Pool Sequences in the River Severn, England, *Earth Surface Processes and Landforms, 25*, 369-384.

Chadwick, A., and J. Morfett (1997), *Hydraulics in civil and environmental engineering*, E & FN Spon, London.

Chapman, D. W. (1988), Critical Review of Variables Used to Define Effects of Fines in Redds of Large Salmonids, *Transaction of the American Fisheries Society, 117*(1), 1-21.

Clayton, J. L., J. King, and R. F. Thurow (1996), Evaluation of an Ion Adsorption Method to Estimate Intragravel Flow Velocity in Salmonid Spawning Gravel, *North American Journal of Fisheries Management, 16*, 167-174.

Coble, D. W. (1961a), Influence of Water Exchange and Dissolved Oxygen in Reddes on Survival of Steelhead Trout Embryos, *Transaction of the American Fisheries Society, 90*, 469-474.

Coble, D. W. (1961b), Influence of Water Exchange and Dissolved Oxygen in Redds on Survival of Steelhead Trout Embryos, *Transaction of the American Fisheries Society, 90*, 469-474.

Cooper, A. C. (1965), The effect of transported stream sediments on the survival of sockeye and pink salmon eggs and alevin, in *Bulletin 18*, International Pacific Salmon Fisheries Commission, New Westminster, B.C., Canada.

Das, M. B. (1998), *Principles of Geotechnical Engineering*, PWS Publishing Company, Boston.

DeVries, P. (1997), Riverine salmonid egg burial depths: review of published data and implications for scour studies, *Canadian Journal of Fisheries and Aquatic Sciences, 54*, 1685-1698.

Edwards, R. T. (1998), The Hyporheic Zone, in *River Ecology and Management: Lessons from the Pacific Coastal Ecoregion*, edited by R. J. Naiman and R. E. Bilby, pp. 399-429, Springer-Verlag, New York.

Fluent Inc. (2003), *Fluent User's Guide*, Distributor: Fluent US, Lebanon. NH.

Garrett, J. W., D. H. Bennett, F. O. Frost, and R. F. Thurow (1998), Enhanced incubation success for kokanee spawning in groundwater upwelling sites in a small Idaho stream, *North American Journal of Fisheries Management, 18*, 925-930.

Geist, D. R. (2000), Hyporheic discharge of river water into fall Chinook salmon (*Oncorhynchis tshawytscha*) spawning areas in the Hanford Reach, Columbia River, *Canadian Journal of Fisheries and Aquatic Sciences, 57*, 1647-1656.

Geist, D. R., T. P. Hanrahan, E. V. Arntzen, G. A. McMicheal, C. J. Murray, and Y.-J. Chien (2002), Physicochemical Characteristics of the Hyporheic Zone Affect Redd Site Selection by Chum Salmon and Fall Chinook Salmon in the Columbia River, *North American Journal of Fisheries Management, 22*, 1077-1085.

Hassanizadeh, M. S., and W. G. Gray (1979), General conservation equations for multi-phase systems: 1. Averaging procedure, *Advances in Water Resources, 2*, 131-144.

Hassanizadeh, M. S., and W. G. Gray (1987), High velocity flow in porous media, *Transport in porous media, 2*, 521-531.

Hirt, C. W., and B. D. Nichols (1981), Volume of fluid (VOF) method for the dynamics of free boundaries, *J. Comput. Phys.*, 201-225.

Hodskinson, A. (1996), Computational fluid dynamics as a tool for investigating separated flow in river bends, *Earth surface processes and landforms, 21*, 993-1000.

Hoopes, D. T. (1972), Selection of spawning sites by sockeye salmon in small streams, *Fishery Bulletin, 70*(2), 447-457.

Huang, G., N. Tamai, and H. Ishida (2001), Characterization of dissolved oxygen depletion in Lake Yanaka, in Proc. *Proceedings of the 29th Congress of IAHR*, Theme B, 747-752.

Keller, E. A., and W. N. Melhorn (1978), Rhythmic spacing and origin of pools and riffles, *Geological Society of American Bulletin, 89*, 723-730.

Lapointe, M. F., N. Bergeron, and F. Bérubé (2004), Interactive effects of substrate sand and silt contents, redd-scale hydraulic gradients and interstitial velocities on egg to emergent survival of Atlantic salmon (*Salmo salar*), *Canadian Journal of Fisheries and Aquatic Sciences, 61*, 2271-2277.

Leopold, L. B., M. G. Wolman, and J. P. Miller (1964), *Fluvial Processes in Geomorphology*, Freeman, W.H., San Francisco.

Levine, J. B., and G. D. Salvucci (1999), Equilibrium analysis of groundwater-vadose zone interactions and resulting spatial distribution of hydrologic fluxes across a Canadian prairie, *Water Resources Research, 35*(5), 1369-1383.

Levy, D. A., and T. L. Slaney, 1993, *A review of Habitat Capability for Salmon Spawning and Rearing*, B.C. Resources Inventory Committee (RIC) c/o Habitat Management Division Dept. of Fisheries and Oceans, Vancouver B.C.

Lisle, T. E., and S. Hilton (1992), The volume of fine sediment in pools: an index of sediments supply in gravel-bed streams, *Water Resources Bulletin, 28*(2), 371-383.

Ma, L., P. J. Ashworth, J. L. Best, L. Elliott, D. B. Ingham, and L. J. Whitcombe (2002), Computational fluid dynamics and the physical modelling of an upland urban river, *Geomorphology, 44*, 375-391.

McLean, S. R., and D. J. Smith (1986), A model for flow over a two-dimensional bed form, *Journal of Hydraulic Engineering, 112*, 300-317.

Montgomery, D. R., E. M. Beamer, G. R. Pess, and T. P. Quinn (1999), Channel type and salmonid spawning distribution and abundance, *Canadian Journal of Fisheries and Aquatic Sciences, 56*, 377-387.

Montgomery, D. R., and J. M. Buffington (1997), Channel-reach morphology in mountain drainage basins, *Geological Society of American Bulletin, 109*, 596-611.

Montgomery, D. R., J. M. Buffington, N. P. Peterson, D. Schuett-Hames, and T. P. Quinn (1996), Stream-bed scour, egg burial depths, and the influence of salmonid spawning on bed surface mobility and embryo survival, *Canadian Journal of Fisheries and Aquatic Sciences, 53*, 1061-1070.

Nehlsen, W., J. E. Williams, and J. A. Lichatowich (1991), Pacific salmon at the crossroads: stocks at risk from California, Oregon, Idaho, and Washington, *Fisheries, 16*(2), 4-21.

Nicholas, A. P. (2001), Computational fluid dynamics modelling of boundary roughness in gravel-bed rivers: an investigation of the effects of random variability in bed elevation, *Earth surface processes and landforms, 26*, 345-362.

Nicholas, A. P., and S. J. McLelland (1999a), Hydrodynamics of floodplain recirculation zone investigated by field monitoring and numerical simulation, in *Floodplain: Interdisciplinary Approaches*, edited by S. B. Marriott and J. Alexander, pp. 15-26, Geological Society, London.

Reeves, G. H., P. A. Bisson, and J. M. Dambacher (1998), Fish Communities, in *River Ecology and Management: Lessons from the Pacific Coastal Ecoregion*, edited by R. J. Naiman and R. E. Bilby, Springer-Verlag, New York.

Shih, T. H., W. W. Liou, A. Shabbir, Z. Yang, and J. Zhu (1995), A new κ-ε eddy-viscosity model for high Reynolds Number Turbulent Flow - Model development and validation, *Computers Fluids, 24*(3), 227-238.

Terhune, L. D. B. (1958), The Mark VI Groundwater Standpipe for Measuring Seepage through Salmon Spawning Gravel, *J. Fish. Res BD. Canada, 15*(5), 1027-1063.

Tonina, D., and M. J. Buffington (in prep.), Effects of physical characteristics on hyporheic flow in pool-riffle channels, *Water Resources Research*.

Tonina, D., and M. J. Buffington (submitted), A three-dimensional model for hyporheic exchange in gravel-bed rivers with pool-riffle morphology, *Water Resources Research*.

Triska, F. J., J. H. Duff, and R. J. Avanzino (1993a), Patterns of hydrological exchange and nutrient transformation in the hyporheic zone of a gravel bottom stream: examining terrestrial-aquatic linkages, *Freshwater Biology, 29*, 259-274.

Triska, F. J., J. H. Duff, and R. J. Avanzino (1993b), The role of water exchange between a stream channel and its Hyporheic zone in nitrogen cycling at the terrestrial-aquatic interface, *Hydrobiologia, 251*, 167-184.

Vaux, W. G. (1962), *Interchange of stream and intragravel water in a salmon spawning riffle, Special Scientific Report--Fisheries*, No. 405, United States Fish and Wildlife Service, Washington D.C.

Wetzel, R. G. (1983), *Limnology*, second edition, Hart Brace Jovanovich Collage Publishers.

Whiting, P. J., J. F. Stamm, D. B. Moog, and R. L. Orndorff (1999), Sediment-transporting flows in headwater streams, *Geological Society of American Bulletin, 111*(3), 450-466.

Wilke, C. R., and P. Chang (1955), Correlation of diffusion coefficients in dilute solutions, *AIChE Journal, 1*, 264-270.